2020-12-10

Effect of non-condensable gases (NCG) on Effective Thermal Conductivity of oil sands

Dutta, Shuvolaxmi

UNIVERSITY OF CALGARY

Effect of non-condensable gases (NCG) on Effective Thermal Conductivity of oil sands

by

Shuvolaxmi Dutta

A THESIS

SUBMITTED TO THE FACULTY OF GRADUATE STUDIES

IN PARTIAL FULFILMENT OF THE REQUIREMENTS FOR THE

DEGREE OF MASTER OF SCIENCE

GRADUATE PROGRAM IN CHEMICAL ENGINEERING

CALGARY, ALBERTA

DECEMBER, 2020

Abstract

Effective thermal conductivity (ETC) of oil sands is a key parameter affecting the distribution of heat in the thermal enahnced oil recovery, especially in Steam-Assisted Gravity Drainage (SAGD) operations. ETC depends on the the size and distribution of sand grains and also fluids filling the pore space. The co-injection of non-condensable gases (NCG) with steam, as a technique to improve the oil sand production, also significantly affects ETC. There is very limited experimental data for thermal conductivity of oil sands when it is saturated with bitumen, steam condensate and NCG. The objective of this research is to measure the thermal conductivity of oil sands at varying saturations of NCG and operating conditions using a rapid unsteady state technique. A needle probe emitting heat as a line source is used to determine the effect of NCG saturation on ETC of oil sands at different temperatures and pressures. The experimental data is later fitted into existing ETC models to develop modified correlations of ETC of oil sands incorporating gas saturation, temperature, and pressure. The intricacy of this work thus lies in determining ETC of a porous medium containing three-phase saturations. A part of the study also includes the estimation of ETC of oil sands in the presence of a surfactant in conjunction with NCG. The experimental correlations developed from this study can be used for simulating SAGD process involving NCG co-injection.

Preface

This research work was a part of the Industrial Research Chair (IRC) program of China National Offshore Oil Corporation (CNOOC). This thesis is original, unpublished, independent work by Ms. Shuvolaxmi Dutta under the guidance of Dr. Brij Maini and Dr. Hossein Hejazi. All the experiments for this research were conducted in the Porous Media Lab (ENG 424) and Hydrocarbon Production Lab (CCIT 015) of University of Calgary. The thermal conductivity needle probe used in the experiments was acquired from Huskeflux Thermal Sensors and Campbell Scientific (Canada) Corporation.

Acknowledgements

My sincere gratitude goes to Dr. Brij Maini and Dr. Hossein Hejazi, Department of Chemical and Petroleum Engineering, Schulich School of Engineering, University of Calgary, for supervising this research work and guiding me to obtain a good understanding of the subject. I am also grateful to the department of Chemical and Petroleum Engineering, Schulich School of Engineering, University of Calgary, NSERC/NEXEN and CNOOC for sponsoring this project.

I will like to thank Dr. S. A. (Raj) Mehta and Dr. Pedro Pereira Almao, for being a part of my thesis examination committee and reviewing my thesis.

I will like to acknowledge with gratitude the help and support I received from Mr. Richard Then, with the laboratory set-up and troubleshooting the problems that came in the way.

Lastly, I am indebted to my family, friends and colleagues for their constant support, motivation and feedbacks.

Dedicated to my family….

Table of contents

Abstract ii

Preface iii

Acknowledgements iv

Table of contents vi

List of figures x

List of tables xii

List of symbols and abbreviations xiii

Abbreviations xv

Chapter 1: Introduction 1

Chapter 2: Technical Background 5

2.1. Structure and composition of oil sands 5

2.2. SAGD process and co-injection of NCG with steam 6

2.3. Heat transfer process in porous media and oil sands 9

2.3.1. Heat conduction process 9

2.3.2. Heat conduction process in solid, gases and liquids 10

2.3.3. Heat transfer mechanisms in porous medium and oil sands 14

2.3.4. Factors affecting heat conduction of a porous medium 15

2.3.5. Mathematical form of unsteady state or transient heat conduction process 17

2.4. Measuring the thermal conductivity of a medium using unsteady state or transient method 17

2.5. Models for estimation of effective thermal conductivity (ETC) of a porous medium 22

2.5.1. Mixing Rule models 23

2.5.2. Percolation model 30

2.5.3. Temperature and Pressure dependant models 30

Chapter 3: Previous Experimental Measurements 33

3.1. Previous works on thermal conductivity measurements with the transient method 33

3.2. Previous works on developing effective thermal conductivity models of multiphase porous/packed structures and oil sands 36

Chapter 4: Experimentation 43

4.1. Method Overview 43

4. 2. Experimental set-up 43

4.2.1. Needle-probe (TP02) 44

4.2.2. Vessel containing the specimen 48

4.2.3. Data Acquisition System (DAS) 49

4.3. Equipment/Apparatus and Materials used in the experiments 50

4.4. Experimental set-ups used for measurements 52

4.4.1. Setup 1: Measuring thermal conductivity of dry sand 53

4.4.2. Setup 2: Measuring thermal conductivity of water saturated sand 53

4.4.3. Setup 3: Measuring thermal conductivity of sands saturated with water and bitumen 55

4.4.4. Setup 4: Measuring thermal conductivity of sands saturated with water, bitumen and NCG 56

4.4.5. Setup 5: Measuring thermal conductivity of sand saturated with bitumen, NCG and a surfactant Solution..... 58

4.5. Calibration of the needle-probe TP02 59

4.6. Data analysis..... 59

4.7. Experiment set points and parameters 59

4.8. Dean-Stark extraction method 60

4.9. Possible errors in the measurements. 61

Chapter 5: Results and Discussions 63

5.1. Experimental Results..... 63

5.1.1. Effective thermal conductivity of evacuated sand pack..... 65

5.1.2. ETC of Sand pack saturated with water 66

5.1.3. Sand pack saturated with bitumen and water 68

5.1.4. Sand pack saturated with bitumen-water-nitrogen..... 71

5.1.5. Sand pack saturated with bitumen-water-nitrogen-surfactant..... 74

5.2. Correlations on effective thermal conductivity of the sand pack 76

5.2.1. Estimating thermal conductivity of pure sand..... 77

5.2.2. Estimating thermal conductivity of sands saturated with bitumen and water..... 79

5.2.3. Estimating thermal conductivity of sands saturated with bitumen, water and nitrogen 81

Chapter 6: Conclusions and Recommendations 89

6.1. Conclusions 89

6.2 Recommendations for Future Work 91

References 92

Appendix 1: Experimental data for water saturated and bitumen-water saturated sand pack: ... 100

Appendix 2: Experimental data for bitumen, nitrogen and saturated sands: 105

Appendix 3: Correlations 107

Appendix 4: Calculation sheet from the LoggerNet software data 109

Appendix 5: Porosity calculation 112

Appendix 6: Glycerol calibration calculation 114

Appendix 7: Saturation calculation for bitumen-water saturated sand pack. 117

Appendix 8: Saturation calculation for bitumen, water and nitrogen saturated sands 121

Appendix 9: Saturation calculation for bitumen, nitrogen and surfactant saturated sands. 125

Appendix 10: LoggerNet software raw file 134

List of figures

Figure no.	Name of the figure	Page no.
1.	How Oil and Natural Gas contribute to Canada's Economy.	1
2.	Mining versus in-situ extraction	2
3.	In-situ process overview.	3
4.	Structure of oil sands.	5
5.	Schematic diagram of SAGD process	5
6.	Cumulative recovery curve for 25 days predicted by Alnoaimi.	7
7.	Heat transfer processes in a porous medium.	11
8.	Experimental set-up of the transient needle-probe method to calculate the thermal conductivity of a system.	14
9.	A graph showing rise in temperature with logarithm of time to calculate the ETC of the medium.	16
10.	Thermal conductivity variation of natural oil sand samples, pure bitumen and pure sand with temperature.	26
11.	Thermal conductivity variation of artificially prepared oil sand samples with temperature.	26
12.	ETC of bimodal distribution of Al_2O_3 filler in a polyethylene matrix predicted by different models and compared with experiments conducted by Pietrak and Winiewski.	30
13.	Basic experimental set-up.	34
14.	Diagram of TP02.	34
15.	A typical wiring diagram of TP02.	36
16.	The vessel used to contain the specimen.	38
17.	Process flow diagram for Setup 1.	41
18.	Process flow diagram for Setup 2.	42
19.	Process flow diagram for Setup 3.	43
20.	Process flow diagram for Setup 4.	44
21	Process flow diagram for Setup 5.	45

22.	Dean–Stark apparatus setup for an azeotrope with a solvent whose density is less than that of water.	47
23.	Effective thermal conductivity of evacuated sand pack.	51
24.	Effective thermal conductivity of water saturated sand pack.	52
25.	Effect of temperature on effective thermal conductivity of bitumen and water saturated sand pack.	54
26.	Effect of bitumen saturation on effective thermal conductivity of bitumen and water saturated sand pack.	54
27.	Effect of temperature on effective thermal conductivity of bitumen, water and nitrogen saturated sand pack.	57
28.	Effect of nitrogen saturation on effective thermal conductivity of bitumen, water and nitrogen saturated sand pack.	58
29.	Effect of surfactant on ETC of the sand-pack saturated with bitumen-nitrogen-surfactant solution.	60
30.	Predicted vs Observed effective thermal conductivity of evacuated sands using “Parallel model”.	61
31.	Predicted vs Observed effective thermal conductivity of bitumen and water sands using “Maxwell Eucken” model.	63
32.	Predicted vs Observed effective thermal conductivity of bitumen, water and nitrogen saturated sands using “Maxwell Eucken” model.	64

List of tables

Table no.	Name of the table	Page no.
1.	Composition of oil sands.	4
2.	The effective thermal conductivity data for evacuated sands system	50
3.	Effective thermal conductivity data for water saturated sands	51
4.	Effective thermal conductivity data for bitumen and water saturated sands	53
5.	Effective thermal conductivity data for bitumen, water and nitrogen saturated sands	56
6.	Effective thermal conductivity data for bitumen, nitrogen and surfactant solution saturated sands	59

List of symbols and abbreviations

Symbols:

a: distance reached by the molecules after last collision; particle radius (μm)

α: Thermal diffusivity $(k/\rho.Cp)$ (m^2/s)

β: Thermal expansion coefficient (K^{-1})

Bi: Biot number

C_p: Specific heat at constant pressure (W/m^2K)

C_v: Specific heat at constant volume (W/m^2K)

d_p: Pore diameter

Dp: Diameter of the solid particle in the medium

D: Dimensionless distance parameter

E_n: Integral constants

E_{sen}: Sensitivity of the thermocouple joints (μV/K)

F: Electrical resistivity formation factor

g: Acceleration due to gravity (m/s^2)

I: Current to the heater wire (Amps)

k: Thermal conductivity (W/mK)

k_{SB}: Boltzman constant $(1.3806*10^{-23}\ m^2kg/s^2.K)$

k_{cont}: Thermal conductivity of continuous phase (W/mK)

k_{disp}: Thermal conductivity of dispersed phase (W/mK)

Keff: Effective thermal conductivity of the medium (W/mK)

k_f: Thermal conductivity of the fluid phase of medium (W/mK)

k_s: Thermal conductivity of the solid phase of medium (W/mK)

k_{sand}/k_s: Thermal conductivity of sand (W/mK)

k_{H2O}: Thermal conductivity of water (W/mK)

k_{Bit}: Thermal conductivity of bitumen (W/mK)

k_{Nitro}: Thermal conductivity of nitrogen gas (W/mK)

k_p: Permeability of the porous medium

Kn: Knudsen number

λ: Mean free path of gas molecules

λn: Intergral constants

l: Domain size

m: Mass (kg)

n: Number of gas molecules per unit volume

η: Dynamic viscosity of the fluid (Pa-s)

π: Pi (3.14159)

ρ: Density (kg/m^3)

ϕ: Porosity

Ra: Rayleigh-Darcy number

R: Distance from the heated needle

$R_{current}$: Resistance across heater wire (Ω)

R_{wire}: Resistance/per unit length of the heater wires

$\theta(r,t)$: Dimensionless temperature parameter

Ω_k : Collision integral

τ: Fourier's number, Dimensionless time parameter

ΔT: Temperature gradient across distance l

T_i: Initial temperature (C)

T_f: Final temperature (C)

T_{hot}: Temperature at the hot junction (ºC)

T_{cold}: Temperature at the cold junction (ºC)

T_{Pt1000}: Temperature at the RTD junction (ºC)

μ: Dynamic viscosity of the gas

$V_{current}$: Voltage across the sensor resistance (Volts)

V_{sen} : Voltage difference between the hot and cold joints (μV)

v: mean molecular speed of gas molecules (m/s)

V: Volume (m^3)

q: Heat transferred to a system (kJ)

Q: Heat from heat source (W/m)

$q_{x,y,z}$: Heat flux (W/m^2)

x_{water}: Water saturation in pore space

Z: Wall collision frequency of gas molecules per unit area

Abbreviations

AFS: The American Foundry Society

API: The American Petroleum Institute

ASTM: The American Society for Testing and Materials

DAS: Data Acquisition System

CSS: Cyclic Steam Stimulation

EMT: Effective Medium Theory

EOR: Enhanced Oil Recovery

ETC: Effective thermal conductivity

GHG: Green-house gas

NCG: Non-condensable gas

IEEE: Institute of Electrical and Electronics Engineers

ITR: Interfacial Thermal Resistance

OOIP: Original oil in place

RTD: Resistance Temperature Detector

SAGD: Steam-Assisted Gravity Drainage

SOR: Steam to oil ratio

VDC: Voltage Direct Current

Chapter 1: Introduction

Alberta's oil sands industry has played a significant role in developing the economy of Canada since its inception in early 20th century. At present, Canada is the fifth largest producer of natural gas and sixth highest producer of crude oil [1]. Figure 1 [1] shows the contribution of oil and natural to Canada's Economy. The oil sands industry not only generates substantial revenues for the government, but also helps in creating jobs and in developing the regions surrounding the oil deposits.

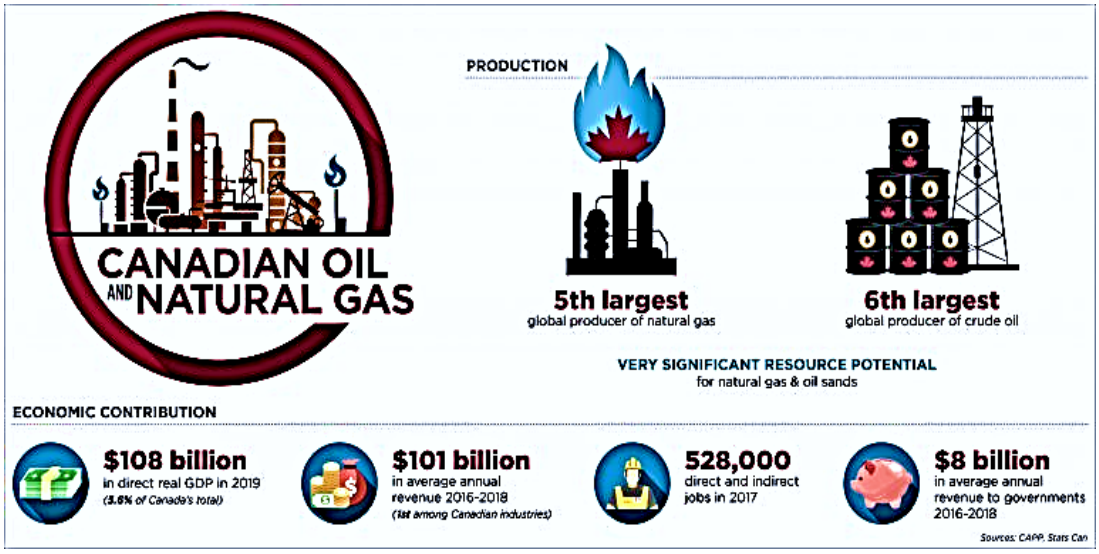

Fig.1: How Oil and Natural Gas contribute to Canada's Economy [1].

These oil deposits were formed millions of years ago from the remains of dead marine organisms. The residuals of these organisms shifted to the sea bed and were pressurized by layers of sediments accumulating on top of them. This pressure concurrently with the change in temperature of the earth, converted the organic matters into oil. With the course of time, oil migrated and trapped in reservoir rocks which led Canada to have one of the biggest deposits of crude oil in the world. Canadian oil sands are mainly located in the provinces of Alberta and Saskatchewan in the regions of Athabasca, Cold Lake and Peace River [1].

The oil sands are mainly comprised of solids (sands and clay), water and bitumen. Bitumen in oil sands is extracted and upgraded to acquire the final crude oil. Bitumen is an extra heavy oil (API gravity 8°) which is very viscous (nearly solid-like at room temperature) and contains a complex mixture of many thousand hydrocarbons [1]. Generally, based on the extraction techniques any oil can be classified into two main categories:

a. Conventional Oil: The oil which is liquid at ambient conditions and can be extracted using conventional drilling and pumping techniques. The recovery methods of these kinds of oils are usually much easier and involve less cost.
b. Unconventional Oil: The oil which cannot be extracted using traditional methods and which requires advance extraction methods. Bitumen present in oil sands is a type of unconventional oil which were formed from geological phenomena and advance recovery methods are required to extract this oil.

Based on the depth of the oil sands reservoir, bitumen can be recovered through surface mining and in-situ extraction. Surface mining is possible only when the reservoir depth is less than 75 m. In general, oil sands reservoirs of less than 50 m of depth contain poor grade oil. The surface mining account for only 20% of the total reserve [2].

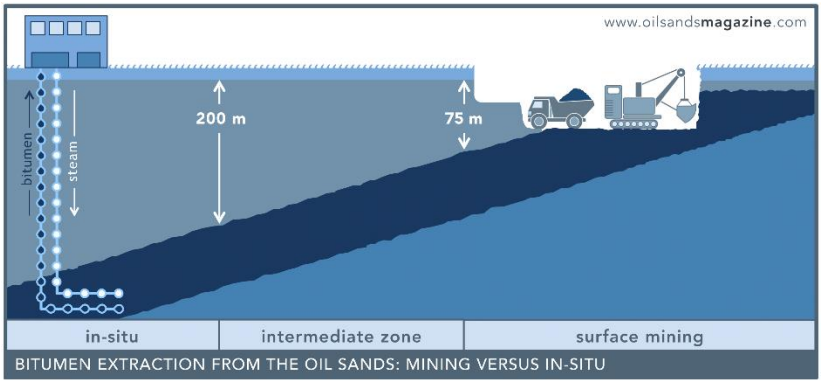

Fig. 2: Mining versus in-situ extraction [2].

The other 80% of the recoverable oil is present is deeper oil reservoirs and require advanced techniques, known as in-situ methods. During surface mining lumps of oil sands are shoveled and transported to the extraction unit of the oil sands industry through haul trucks. At the extraction unit, the lumps of oil sands are first crushed down and then mixed with hot water. The heavier solids settle at the bottom and bitumen is then pumped to the upgrading section for further refining. In the in-situ method, steam is injected into the oil sands reservoir to heat the bitumen and reduce its viscosity so that it can flow into a production well. The surface mining requires huge amount of water whereas in-situ process demands enormous volumes of steam. Numerous researchers and scientists are working to reduce the steam and water required in these processes.

One in-situ method used for oil extraction is the Cyclic Steam Stimulation (CSS). In this method certain amount of steam is injected though a vertical well to heat and mobilize the bitumen. The heated bitumen is then pumped to the surface through the same well. However, the most common type of in-situ method that is used in oil sands reservoirs is the Steam-assisted Gravity Drainage (SAGD) process. In this process a pair of horizontal wells, one injection well and one production well, are drilled one above the other to extract bitumen by gravitational drainage. Steam is injected through the injection well (top well) which helps in reducing the viscosity of bitumen by increasing its temperature. The bitumen then flows to the production well (bottom well) by gravity and is conveyed to the plant.

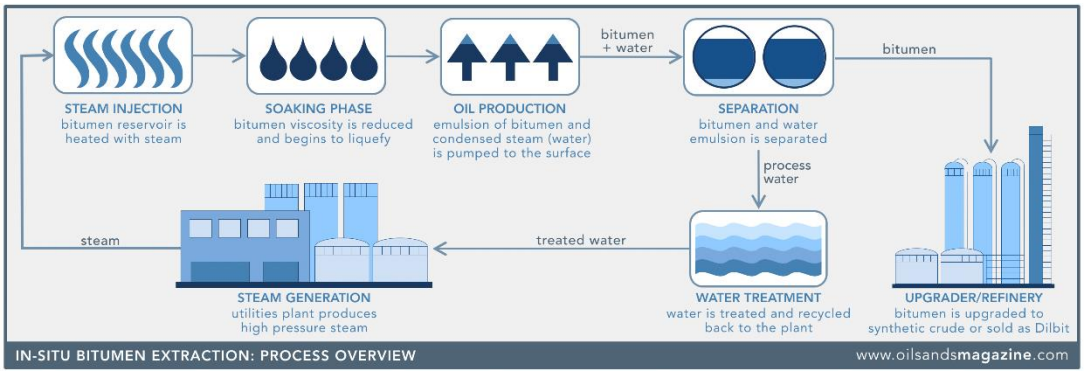

Fig. 3: In-situ process overview [2].

The SAGD process is able to economically recover bitumen from deeper oil deposits but the enormous steam requirement of the process has always been a matters of concern. The high volume of steam used in this process is associated with high greenhouse gas (GHG) emission and huge cost. Many researchers are working to decrease the steam-to-oil ratio (SOR) and increase the oil recovery rate during SAGD operations. One of the suggested method to increase the average oil recovery rate is to co-inject non-condensable gases (NCG) along with steam. The injected NCG accumulates near the top of the pay zone and acts like an insulating blanket for reducing the heat loss to the overburden, thus increasing the thermal efficiency of the system [3]. The NCG also helps in generating excess pressure gradient in the reservoir which also improves the recovery efficiency.

The addition of NCG with steam affects the thermal properties of oil sands. The experimental data of thermal properties of oil sands under these conditions are still very limited. In this study, experiments were conducted on oil sands at different temperatures, pressure and gas concentrations to examine the effect of NCG on thermal conductivity. In some tests, surfactants were added to the water present in the sand to examine the variation of thermal conductivity of the system in the presence of foam. The main objective of this project is to develop correlations on thermal conductivity of oil sands as a function of three phase saturation (oil, water and gas), temperature and pressure based on the experimental findings. The results and outcomes from this project will be a useful for predicting the oil recovery rate during simulation of SAGD reservoirs where NCG is added with steam.

Chapter 2: Technical Background

This chapter provides background information on the basic structure and composition of oil sands; the process of addition of NCG with steam in the SAGD reservoirs; the heat transfer processes in oil sands and the transient heat conduction equation used to calculate the thermal conductivity of a medium.

2.1. Structure and composition of oil sands

Oil sands has a compact porous structure comprising of solids (sand and fine clay), bitumen and water. Although the composition of oil sands considerably varies based on geological location and reservoir depth, it is approximately comprised of 85% solids, 10% bitumen and 5% water by weight [2]. The detailed composition of oil sands is provided in Table 1.

Table 1: Composition of oil sands [2].

Main components	Detailed components	Approximate (weight %)
Bitumen	Asphaltenes (14-18%)	10-20%
	Maltenes	
	Sulphur (4-5%)	
Solids	Quartz Silica sand	Over 80%
	Potassium feldspar and fine clays (Kaolinite, illite, chlorite and smectite)	5%
Water		0-9%

The solids present in oil sands is mainly silica sand along with some proportions of potassium feldspar and fine clays. The oil sands that have higher percentages of fine clays (kaolinite, illite, chlorite and smectite), have lower percentage of bitumen and are generally considered as low grade ore. The fine clays are mainly associated with the water phase of oil sands. Thus when the oil sands possess higher percentage of water, the fines percentage also increases and correspondingly bitumen fraction decreases. The water that is found inside the oil sands is called connate water and generally has dissolved ions of potassium, sodium, chloride and sulphite. The bitumen inside the oil sands is an extremely viscous,

complex hydrocarbon which is practically immobile at room temperature and pressure. The bitumen found in Alberta oil sands also has 4-5% of sulphur and traces of heavy metals like vanadium and nickel. Bitumen can be segregated into two classes of organic compounds, Asphaltenes and Maltenes. The viscous and dense properties of bitumen are mainly contributed by Asphaltenes which also carries the heavy metals and sulphur in bitumen. The rest of the fraction in bitumen is Maltenes which can be separated into resins, aromatics and saturates.

Each sands grains of oil sands are wrapped around by a thin layer of water which in turn is enclosed by a layer of bitumen. The sand grains have an angular shape and they tend to stick to one another giving the oil sands a very coarse structure. Figure 4, given below, reveals the basic structure of oil sands.

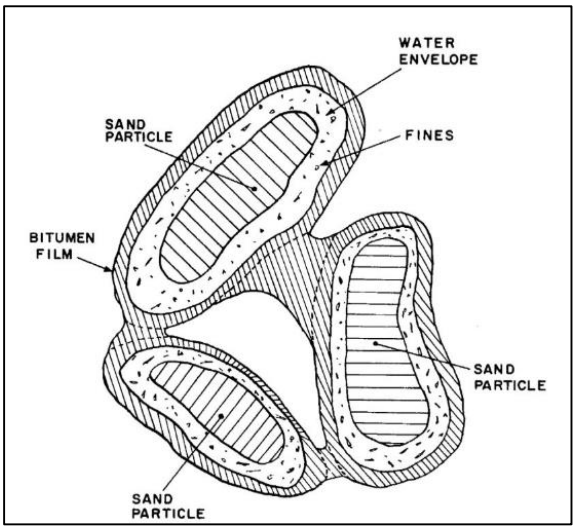

Fig. 4: Structure of oil sands [5].

2.2. SAGD process and co-injection of NCG with steam

SAGD is an oil recovery process invented by Dr. Roger Butler in 1970s, in which steam is injected to an oil sands reservoir to heat up the bitumen and reduce its viscosity so that it can flow into a production well and pumped to the surface. A typical SAGD configuration is comprised of a pair of parallel horizontal wells, which are drilled to lie one above the other with a vertical distance of 4 to 6 meters between them.

The highly pressurized steam is injected through the upper well and the heated oil and condensate are gravitationally drained through the lower well.

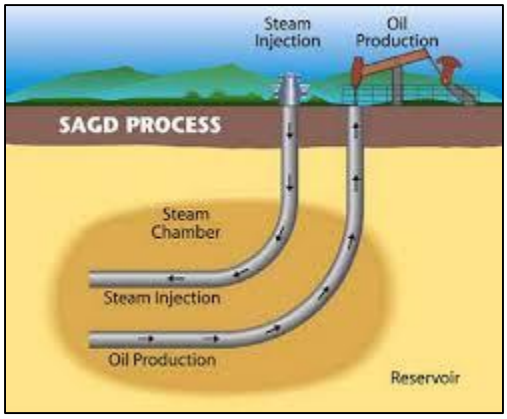

Fig. 5: Schematic diagram of SAGD process [3].

During the start-up phase of SAGD process, steam is circulated in both the top and bottom wells to heat the reservoir lying in between the wells. Such steam circulation for around 2-4 months ensures that bitumen temperature in the region between the two wells increases and its viscosity gets reduced. After the bitumen becomes mobile, steam is injected only from the injector well. When the steam is continuously injected through the injection well, it ascends towards the top of the formation and forms a "steam chamber" that propagates vertically and horizontally inside the reservoir. The boundary of the steam chamber acts as an interface of heat transfer between steam and the surrounding reservoir oil sands. The heated bitumen and condensate water flows counter-currently against the ascending steam by gravity, towards the horizontal well at the end of the reservoir. The SAGD process is found to boost the heavy oil recovery factor to 50-60% of the original oil in place (OOIP) [6]. The heat injected into the reservoir gets consumed by three mechanisms. The first portion is lost to the cap rock, the second portion remains contained in the steam chamber and only the third portion is used for oil heating. Thus, huge amount of energy is used for steam generation, which is associated with substantial green-house gas (GHG) emission and high cost.

To reduce the loss of energy to the cap rocks, one of the used methods is to co-inject a non-condensable gas (NCG) (like nitrogen) along with steam. This enhanced oil recovery (EOR) method is being used since 1970s. The NCG serves the following purposes [4]:

a. It reduces the heat loss to the cap rock by reducing the temperature near the top of the steam chamber.
b. It imparts a gas drive by carrying the pressure ahead of steam which improves the sweep in the reservoir.
c. NCG is soluble in bitumen and thus it increases the volume of the oil which further increases its mobility.

As NCG is injected with steam at the steam temperature and pressure, it decreases the steam partial pressure and temperature. Due to decrease in steam pressure, the steam volume also increases which gives an additional sweep in the system. The gas which is co-injected with steam in the reservoir, reaches the upper part of the reservoir very rapidly and starts diffusing to form a very thin layer [7]. This gives rise to gas fingering at the top of the reservoir and oil is displaced counter-currently in the reservoir. The gas has low thermal conductivity and thus as the gas accumulates at the top, it decreases heat loss to the cap rock. The gas also helps to carry the pressure swiftly to the top of the reservoir. A numerical and physical modeling study by Alnoaimi [4], showed that the cumulative oil recovery was around 0.125 bbl in 25 days for steam alone injection and was around 0.138 bbl for steam/N_2 injection in 25 days as shown in Figure 6.

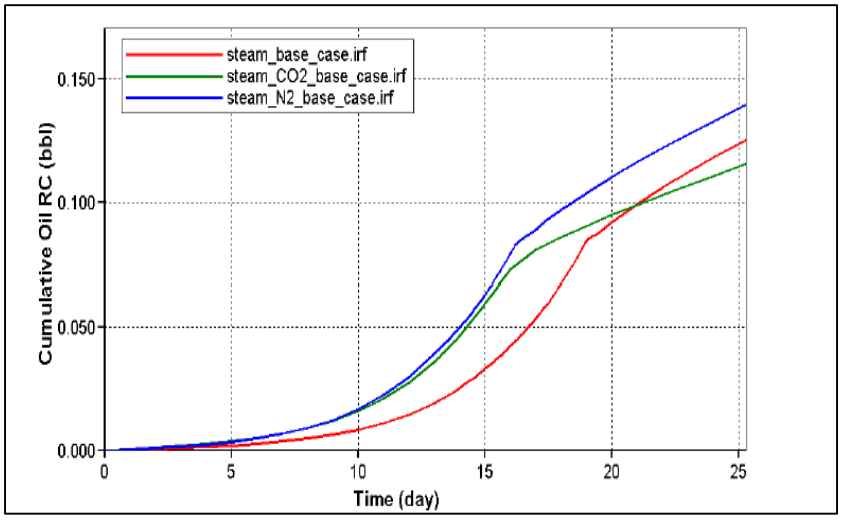

Fig. 6: Cumulative recovery curve for 25 days predicted by Alnoaimi. [4]

2.3. Heat transfer process in porous media and oil sands

2.3.1. Heat conduction process:

The basic steady state heat conduction equation comes from the **Fourier's Law** of heat conduction which states that the heat flux (rate of heat flow per unit area) in a particular direction is proportional to the temperature gradient [10]:

$$q_x = -k\frac{\partial T}{\partial x} \qquad q_y = -k\frac{\partial T}{\partial y} \qquad q_z = -k\frac{\partial T}{\partial z} \qquad \text{Equation 2.1.}$$

If all the three equations are multiplied by a suitable unit vector and then added then the following equation is obtained [10]:

or, $$q = -k.\nabla T \qquad \text{Equation 2.2.}$$

Equation 2.2 is the three dimensional form of Fourier's law, where, q is the three dimensional heat flux vector, k is the thermal conductivity of the medium and ∇T is the three dimensional temperature gradient vector. Equation 2.1 represents the Fourier's Law of heat conduction in an isotropic medium. The negative sign of the equation implies the direction of heat flux is opposite to the direction of temperature gradient. Thus the thermal conductivity of a medium can be defined as the heat conducted by the medium

across a temperature gradient. Though thermal conductivity is broadly classified as a second order tensor but it can be considered a scalar property in case of an isotropic medium where the physical properties of the system remains constant in all directions.

2.3.2. Heat conduction process in solid, gases and liquids:

Thermal conduction in solids:

In solids, thermal conduction may occur due to two processes: lattice vibrations and free electrons diffusion. With the increase in lattice vibrations, the heat transfer through the medium gets enhanced. Also, when the flow of free electrons increases, it results in an increased electrical conductivity of the system. Thus it escalates the heat conduction through the medium by diffusion. The overall thermal conductivity of the system is the combined effect of these two phenomena. In metals, the diffusion of free electrons play a significant role for heat conduction as metals possess free electrons. In non-metals, the lattice vibration effect lead the heat conduction process as they don't have free electrons [63].

The lattice vibration effect mainly depends on the arrangement of the molecules in the medium. As for example, in wood, which can be classified as an amorphous solid (i.e. it has random and disordered arrangement of molecules), the thermal conductivity is very low and it acts as a thermal insulator. Metals have highly ordered arrangement of molecules and also have free electrons, thus metals are good conductor of heat and electricity. Non-metals like diamonds, are also good conductor of heat [63].

For solids, with the increase in temperature, the number of free electrons and lattice vibrations increase, but the increased vibrations obstruct the diffusion of free electrons in the medium, thus the overall thermal conductivity of the substances decrease in most cases. As the solids are incompressible in nature, the thermal conductivity does not show a significant change with pressure.

The determination of thermal conductivities of heterogeneous solids like a composite and granular substances, are based on several factors such as arrangement of the components, percentage composition

of the components, thermal conductivity of individual components or the porosity of the solid. These factors will be discussed later in detail.

Thermal conduction in gases:

The thermal conductivity of gases at low densities can be explained by kinetic theory of gases [10]. To estimate the thermal conductivity of a gas, a non-equilibrium condition was considered along a temperature gradient of dT/dy. The average kinetic energy of the gas molecules was taken as the energy that the molecules obtained from their last collision in a temperature region of T. A hypothetical plane y was assumed and the heat flux q_y was calculated by taking the difference of total kinetic energies of the molecules in positive y-direction and negative y-direction, crossing the y plane.

$$q_y = Z(\frac{1}{2}mv^2|_{y-a} - \frac{1}{2}mv^2|_{y+a}) = \frac{3}{2}\text{kZ}(T|_{y-a} - \frac{1}{2}T|_{y+a}) \qquad \text{Equation 2.3.a.}$$

Where, a=2/3λ , a is the distance travelled by the molecules after last collision and λ is the mean free path. λ is given by $\lambda=1/(2^{0.5}\pi d^2 n)$. d is the diameter of the rigid sphere molecule, n is the number of molecules per unit volume. v in Equation 2.3.a is the mean molecular speed and $v= (8kT/\pi m)^{0.5}$. k_{SB} is the Boltzman constant and m is the mass of the molecule. Z is the wall collision frequency per unit area and Z=1/4nv.

Equation 2.3.a is based on the assumption that all the molecules obtain the velocities from their last collision and the temperature gradient is linear for several mean free paths. So, based on the last assumption it can be written:

$$T|_{y-a} = \frac{1}{2}T|_y - \frac{2}{3}\lambda\frac{dT}{dy} \qquad \text{Equation 2.3.b.}$$

$$T|_{y+a} = \frac{1}{2}T|_y + \frac{2}{3}\lambda\frac{dT}{dy} \qquad \text{Equation 2.3.c.}$$

By organizing equation 2.3. a, b, and c the following equation can be obtained:

$$q_y = -\frac{1}{2}nk_{SB}v\lambda\frac{\partial T}{\partial y} \qquad \text{Equation 2.3.d.}$$

Equation 2.3.d corresponds to Fourier's law of heat conduction as given in Equation 2.1 and the thermal conductivity for a monoatomic gas can be written as:

$$k_{eff} = \frac{1}{2} n k_{SB} v \lambda = \frac{1}{3} \rho C_v v \lambda \qquad \text{Equation 2.3.e.}$$

In Equation 2.3.e., $\rho = nm$, is the gas density and $C_v = \frac{3}{2} k_{SB}/m$ is the specific heat at constant volume. If we substitute the values of v and λ, as given above in Equation 2.3.e., we get [10]:

$$k_{eff} = \frac{\sqrt{(\frac{mkT}{\pi})}}{\pi d^2} \frac{k_{SB}}{m} = \frac{2}{3\pi} \frac{\sqrt{(\pi m k_{SB} T)}}{\pi d^2} C_v \qquad \text{Equation 2.3.f.}$$

Equation 2.3.e. states that thermal conductivity of gases is directly proportional to λ and ρ. But λ or the mean free path is inversely proportional to pressure and ρ is directly proportional to pressure. So, as a whole, thermal conductivity of gases is independent of pressure as is evident from Equations 2.3.e and 2.3.f. As per Equation 2.3.f., the thermal conductivity of a dilute gas medium is directly proportional to the square-root of temperature. These equations were found to be accurate only up to 10 atm pressure and for higher pressures Chapman-Enskog equation [10] was found to be more accurate, which is given as below:

$$k_{eff} = \frac{25}{32} \frac{\sqrt{\pi m k_{SB} T}}{\pi \Omega_k \sigma^2} C_v = 1.9891 \times 10^{-4} \frac{\sqrt{(T/M)}}{\Omega_k \sigma^2} \qquad \text{Equation 2.3.g.}$$

The values of the parameters of σ and Ω_k (collision integral) can be found in Bird, Stewart and Lightfoot [10].

In a porous medium the mean free path of the gas is a factor of the pore diameter and the collisions between the solid surface and gas molecules must be considered. So, in that case λ' is the modified mean free path and is given by [23]:

$$\lambda' = \frac{\lambda d_p}{\lambda + d_p} \qquad \text{Equation 2.3.h.}$$

d_p is the pore diameter. At high gas pressures, $\lambda << d_p$, and thus $\lambda' = \lambda$ and at low gas pressures, $\lambda >> d_p$, and thus $\lambda' = d_p$. At very low pressures, the mean free path takes up the size of the gas enclosure for

which λ is no longer inversely proportional to the pressure and conductivity of the gas becomes proportional to the pressure [23].

Equation 2.3.f and Equation 2.3.g are not valid for polyatomic gases. Eucken equation provides reasonable results for polyatomic nonpolar gases and is given by:

$$k_{eff} = (C_p + \frac{5}{4}\frac{R}{M})\mu \qquad \text{Equation 2.3.i.}$$

Where C_p is the specific heat at constant pressure, R is the universal gas constant, M is the molecular weight of the gas and μ is the dynamic viscosity of the gas.

Thermal conduction in liquids:

Same as in gases, heat conduction in liquids also takes place through two different processes. The first mode of conduction is through the collision of the atoms, molecules or ions and the second one is through the molecular diffusion. During heat conduction through particle collisions, as the number of collisions increases, the exchange of energy between molecules also increases. Heat transfer through molecular diffusion occurs when the molecules undergo random motion in a particular medium. Thus with the increase in temperature of liquids the randomness of the molecules increases and this inhibits the heat conduction process. The thermal conductivity of liquid mostly decrease with the increase in temperature with only exception of pure water where the thermal conductivity initially increases (till around 130 ^{o}C) and then decreases with temperature. As in solids, because of the incompressibility nature of liquids, their thermal conductivities change very little with pressure.

Bridgman [10] predicted the thermal conductivity of pure liquids by developing an analogous equation to Equation 2.3.e. He assumed that the liquid molecules are arranged in a cubic matrix with a centre to centre spacing of $(V/N)^{1/3}$, where V/N is the volume per molecule [10]. The mean molecular speed in Equation 2.3.e was replaced by sonic velocity, u and the distance travelled after collision was replaced by centre to centre spacing $(V/N)^{1/3}$. The value of C_v was used as $3(k_{SB}/m)$ from the Dulong and

Petit [10] formula, as the specific heat at constant volume of a monoatomic liquid is nearly equivalent to a solid at high temperatures. Using all the above parameters in Equation 2.3.e, the following equation was obtained, called Bridgman's equation [10]:

$$k_{eff} = 3(\frac{N}{V})^{2/3} k_{SB}.u \qquad \text{Equation 2.3.j.}$$

For polyatomic liquids, when the factor 3 in Equation 2.3.i, was replaced with 2.8, a better match with the experimental data was observed [10]. This equation was limited to densities much above the critical density as the correlation was based on the assumption that the liquid molecules vibrates in an enclosure formed by its nearest neighbouring molecules.

The sonic velocity u, is the velocity of low frequency sound and can be estimated from the relation:

$$u = \sqrt{(\frac{C_p}{C_v}\left(\frac{\partial P}{\partial \rho}\right)_T)} \qquad \text{Equation 2.3.k.}$$

$\left(\frac{\partial P}{\partial \rho}\right)_T$ can be calculated from isothermal compressibility measurements or from equation of state, and $\frac{C_p}{C_v}$ is nearly equal to one for liquids, except around critical point [10].

2.3.3. Heat transfer mechanisms in porous medium and oil sands:

In a porous media, heat transfer can be associated by the combined mechanisms of the following phenomena [8]:

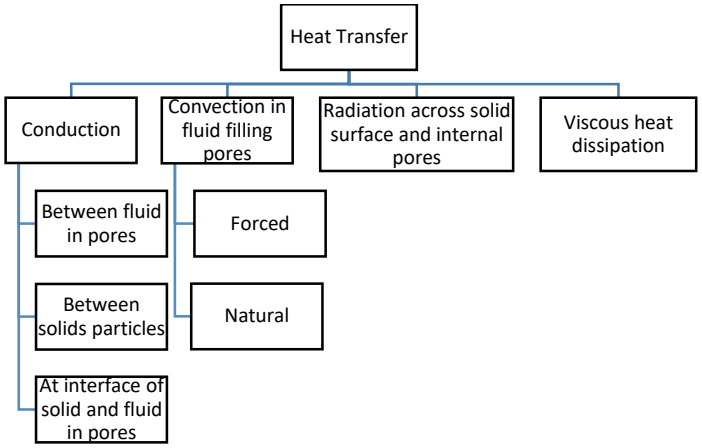

Fig. 7: Heat transfer processes in a porous medium.

The main mode of heat transfer in a porous structure is the heat conduction between the solid grains, between the fluids present in the pores and at the interface of solid grains and fluid. Convective heat transfer can be a result of forced convection or natural convection or a combination of both. The density variations of the fluids inside the pores give rise to a buoyant force which results in natural convective heat transfer whereas external driving forces, such as pressure gradient, are the causes of forced convective heat transfer. The temperature gradient inside the pores results in the uneven thermal expansion of fluids and as a consequence the density gradient is formed leading to natural convective heat transfer. Heat transfer by radiation comes into effect when heat is emitted from the solid surface in the form of electromagnetic waves. Radiative heat transfer process plays an important role at very high temperatures. In case of heat flow through a viscous fluid in pores, the viscosity of fluid results in the conversion of energy from the moving fluid (kinetic energy) into internal energy of the fluid and ends up heating up the fluid. This partially irreversible process is referred to as viscous heat dissipation. This heat dissipation is usually high in regions of large velocity gradients (boundary layers) and in highly turbulent regions.

As discussed in Section 2.1., oil sands has a porous structure, where the pores between the sand grains are saturated with bitumen and water. Due to the presence of bitumen, which is a highly viscous fluid, the Rayleigh-Darcy number (Ra) is generally very low, indicating uniform thermal expansion of the fluids and thus the natural convective heat transfer effects are quite low.

$$Ra = \frac{\rho \beta \Delta T k_p l g}{\eta \alpha} \qquad \text{Equation 2.4.}$$

This research is focussed towards the estimation of effective thermal conductivity (ETC) of oil sands with three phase saturation of bitumen, water and gas.

2.3.4. Factors affecting heat conduction of a porous medium:

The thermal heat conduction in a porous medium occurs through each components present in the system. The effective heat conductivity in porous media depends on the following factors [33]:

- Porosity of the medium.
- Thermal conductivity and volume fraction of individual phases.
- Organisation of pores.
- Contact area between grains and shape of grains.
- Grain size distribution.
- Temperature and pressure of the medium.

According to Carson et al. [9], porosity of a material can be categorized into “internal porosity” or “external porosity”. When the solid phase of the material is in a continuous intersected phase with a diffused or continuous fluid phase, the porosity of the material falls into the internal porosity division, as in the case of a porous sponge. Whereas when the fluid phase is the continuous medium with diffused or continuous solid phase, this type of porosity is in external porosity division, as in case of granular substances like oil sands. Carson et al. also gave an understanding of the effect of different phases on the “optimal heat conduction pathway” in a porous structure. This is the path that the heat flow will follow in a medium. They found that when $k_{cont} > k_{disp}$, the heat flow is mostly through the continuous phase and when $k_{cont} < k_{disp}$, the heat flow is mostly through dispersed phase. The first case explains the “optimal heat conduction pathway” in an internal porosity medium and the second case is that of an external porosity medium. This is to be noted that when the porosity (ϕ) of the medium approaches zero, the effective thermal conductivity of the medium (K_{eff}) is close to the thermal conductivity of the solid phase and when porosity approaches unity, K_{eff} is close to the thermal conductivity of the liquid phase.

Grain size distribution is an important factor that controls the thermal conductivity of a porous medium. This is because grain size not only has a direct effect on the heat transfer area but it also controls other factors in the system such as porosity, pore arrangement and permeability. A work by Midttomme and Roaldset [11] showed that grain size has a significant influence on ETC of finer materials compared

to coarse materials. Pressure and temperature of the system also play a vital role in controlling the ETC of a medium. It is expected that with the increase in temperature kinetic energy of the molecules of a medium increase, which increases the intermolecular distance between the molecules and this leads to a decrease in heat conduction through the medium. The exactly reverse effect is expected if there is rise in pressure of the system which alters the porosity of the system.

Grain contact area is another key factor controlling the heat flow in granular porous media like unconsolidated sands. Grain to grain contact depends on the surface morphology and the loading pressure. Askari et al. [64,65] developed a self-affine fractal stochastic functions to account for the surface roughness in granular porous media which could accurately model the resistance to heat flow resulting from surface roughness and loading pressure. The model was utilized to analyze the effect of anisotropy [66,67] and partial saturation [68] on effective thermal conductivity granular porous media.

2.3.5. Mathematical form of unsteady state or transient heat conduction process:

The unsteady state or transient heat conduction equation, neglecting convective heat transfer, is given as [10]:

$$\rho C_p \frac{\partial T}{\partial t} = (\nabla . k \nabla T) \qquad \text{Equation 2.5.a.}$$

If the thermal conductivity is considered to be independent of the temperature, the equation can be written as [10]:

$$\frac{\partial T}{\partial t} = \alpha(\nabla^2 T) \qquad \text{Equation 2.5.b.}$$

Where α (= k/ρCp) is the thermal diffusivity of the medium.

2.4. Measuring the thermal conductivity of a medium using unsteady state or transient method

To model the heat conduction in a porous medium, the ETC of the medium needs to be determined accurately. The ETC of a medium can be estimated either by performing experiments or by using previous correlations or ETC models. To determine the thermal conductivity of a medium experimentally, the two

classes of applicable methods are: 1) steady state methods and 2) unsteady state (transient) methods. In both methods, an external heat is supplied to the system, but the difference between them is that in the first case the ETC is measured after the system attains steady state and in the second case the ETC is measured before the system reaches steady state. Two most extensively used unsteady state methods are "transient hot wire" method and "transient needle-probe" method. In "transient hot wire" method a vertical, cylindrical wire is used which simultaneously serves as a heating element and as a thermometer [14]. The "transient needle-probe" method involves the use of a needle-probe (equipped with a set of thermocouples), which is inserted into the medium. The needle-probe is connected to an electrical source, which applies a step power at time zero to the medium, after establishing thermal equilibrium between the probe and the medium [12]. The rise in temperature due to the power input is recorded with time through a Data Acquisition System (DAS), for certain period or until the temperature increase levels off.

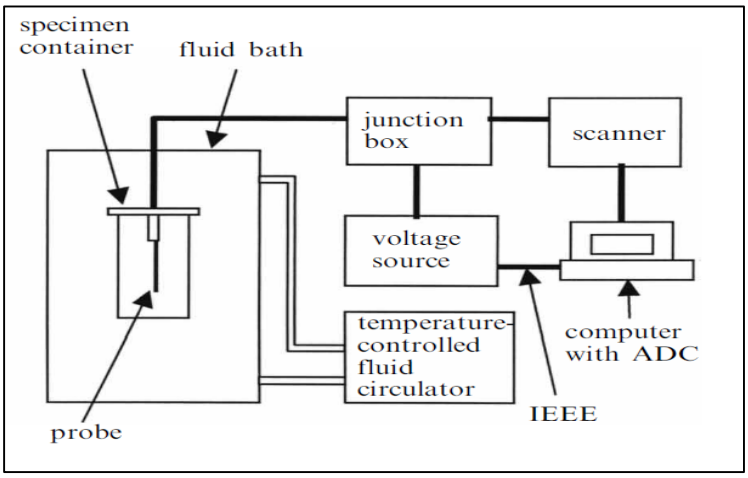

Fig. 8: Experimental set-up of the transient needle-probe method to calculate the thermal conductivity of a system [13].

Figure 8 shows a typical set-up used in the needle probe method. The main advantages of this method over the hot-wire methods are:

- Easy installation: The hot-wire method is sometimes difficult to operate due to physical model constraints [12].

- A small sample can be tested.
- The initial cost requirement is low.
- The time requirement for the experimental run is quite short: As the system works in the unsteady state zone, the time required to run an experiment (excluding the initial set-up and equilibration time) is generally only 20 secs to 1 min.
- The accuracy of measurements is better than ±5% for composites [12].

In this work, the transient needle probe method is used to measure the thermal conductivity of oil sands. The detailed experimental set-up will be discussed in Experimentation Section (Chapter 4). In this section, the mathematical model used to calculate the thermal conductivity of the medium is presented. To determine the effective thermal conductivity (K_{eff}) from unsteady state temperature measurements, we need to start with the transient heat conduction as given in equation 2.5.b, but with a constant heat input q from a source:

$$\frac{\partial T}{\partial t} - \alpha(\nabla^2 T) = q \qquad \text{Equation 2.7.a.}$$

If we consider the heat flows only in radial direction, this equation can be rephrased as:

$$\frac{\partial T}{\partial t} - \alpha\left(\frac{\partial^2 T}{\partial r^2}\right) - \frac{\alpha}{r}\left(\frac{\partial T}{\partial r}\right) = q \qquad \text{Equation 2.7.b.}$$

Where r is the radial distance from the "infinite" line source. As $\alpha = k/\rho Cp$, the above equation can be written as:

$$\rho C_p \frac{\partial T}{\partial t} - K_{eff}\left(\frac{\partial^2 T}{\partial r^2}\right) - \frac{K_{eff}}{r}\left(\frac{\partial T}{\partial r}\right) = q \qquad \text{Equation 2.7.c.}$$

Initial and Boundary condition for this equation are:

1. At the start of time t, the temperature of the medium is T_i, i.e., $T(r,0) = T_i$ Equation 2.8.

   At the end of time t, the temperature of the needle is T_f, i.e., $T(0,t) = T_f$
2. The heat flux far from the needle at the outer boundaries of sample at the radial distance of R will be zero i.e.,

$$\frac{\partial T(R)}{\partial r} = 0 \qquad \text{Equation 2.9.}$$

To solve equation 2.7.c few dimensionless parameters are used which are given below [15]:

$\theta(r,t) = (T(r,t)-T_f)/(T_i-T_f)$ [Dimensionless temperature parameter] Equation 2.10.

$D = r/R$ [Dimensionless distance parameter] Equation 2.11.

$\tau=\alpha t/R^2$ [Fourier's number, Dimensionless time parameter] Equation 2.12.

Rearranging these parameters and incorporating these in Equation 2.7.b.:

$$\frac{\partial \theta}{\partial \tau} - \left(\frac{\partial^2 \theta}{\partial D^2}\right) - \frac{R}{D}\left(\frac{\partial \theta}{\partial D}\right) = \frac{R^2}{(T_i - T_f)K_{eff}} q \qquad \text{Equation 2.13.}$$

The assumptions considered to solve these equations are discussed below [12]:

a. The probe should have an infinite length: The length of the probe should be much longer than the radius of the probe to ensure that an infinitely thin long heat source and heat flow only along radial direction can be considered for the modelling. According to Blackwell [49], the minimum length to diameter ratio of the heat source should be 20 to 30.

b. The probe has an infinite thermal conductivity: This is to ensure that the heat supplied to the needle probe is instantly transferred to the medium.

c. The contact resistance between the probe and the medium is constant: If there is any additional contact resistance between the needle and the medium, then the transient time (10*Probe diameter^2/thermal diffusivity of the medium) will increase, which may impede the accuracy of the measurements.

d. All physical properties of the medium are constant.

e. The medium is extended infinitely: Carslaw and Jaeger [12] estimated that to have a small measurement time, the temperature at the boundary of the medium should be 1% less than that of the probe surface temperature. To make this possible, the radius of the sample should be greater than 30 times of the needle probe radius [12].

f. The energy transfer is only due to one-dimensional radial conduction and there is no influence of convection and radiation: Equation 2.7.a is solved based on the heat transfer along radial direction.

Applying the initial and boundary conditions, replacing the dimensionless parameters, and considering the above assumptions, the solution for the above partial differential equation results in the following equation [23]:

$$\Delta T = \left(T_f - T_{r,t}\right) = -\frac{Q}{2\pi K_{eff}} \mathrm{I}\left(\frac{R}{2\sqrt{(\alpha t)}}\right) \qquad \text{Equation 2.14.}$$

Where, I is an infinite series described as $I(x) = C - lnx + \frac{x^2}{2} - \frac{x^4}{8} + \cdots$

C is the Euler constant =0.5772.

In the above infinite series, $x = \frac{R}{2\sqrt{(\alpha t)}}$. For higher values of t, the higher order terms of the series can be neglected and the equation gets minimized to:

$$\Delta T = \left(T_f - T_{r,t}\right) = -\frac{Q}{2\pi K_{eff}} [\mathrm{C} - \ln\left(\frac{R}{2\sqrt{(\alpha t)}}\right)] \qquad \text{Equation 2.15.}$$

If we consider ΔT is the rise in temperature (T_2- T_1) between times t_1 and t_2, and t_1=1 sec then Equation 2.14.b can be written as:

$$\Delta T = (T_2 - T_1) = -\frac{Q}{4\pi K_{eff}} \ln(t_2) \qquad \text{Equation 2.16.}$$

It is to be noted that, in equation 2.14, Q is the power/unit length that is supplied to the needle-probe and whereas q in Equation 2.13 is the heat flux. Equation 2.16 is the final equation that is applied to calculate the thermal conductivity of the medium. If the rise in temperature is plotted against time, it yields a curve as shown in figure 9.

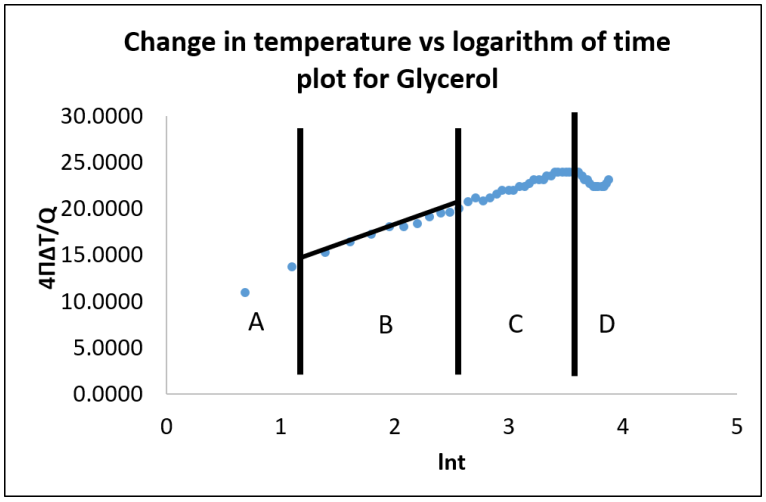

Fig.9: A graph showing rise in temperature with logarithm of time to calculate the ETC of the medium.

The section A of the graph represents the region where heat capacity effects predominate; section B indicates the region of heat conduction when the rise in temperature is linear with time; section C signifies the region where axial conduction and convection effects results in the decrease of temperature with time; and the slope starts to decline; section D denotes the zone when the system is no longer acting as semi-infinite in the radial direction. The inverse of the slope of section B will give the thermal conductivity of the medium. Section B is mainly characterised by the specimen thermal properties and Sections A and C are the thermal regions which are dominated by the probe or boundary conditions of the specimen [13]. In an ideal situation, Section B would have continued indefinitely in an infinitely long probe and in an infinite specimen size, but due to a finite length of the probe and finite volume of the specimen, the straight line starts to change its course resulting in Sections C and D [13].

2.5. Models for estimation of effective thermal conductivity (ETC) of a porous medium

There are numerous ETC models available in the literature for porous media like oil sands, containing multiple fluid phases. The effects of temperature and pressure have been considered in some of these models. Based on the arrangement of the phases, consideration of particle size and shape, porosity

of the medium and Interfacial Thermal Resistance (ITR), the models can be mainly classified as "mixing rules" models or "percolation" models [17].

2.5.1. Mixing Rule models:

The most common ETC models are the "mixing rules" which involves predicting of ETC of the system using the thermal conductivities of individual phases and their composition. Several different mixing rules models have been developed based on the arrangement of the fluid and solid in the system. These include: Parallel model, Series model, Geometric mean model, Maxwell model, Rayleigh, Kunni-Smith model, Krupiczka model, Zehner-Schlunder model etc.

Parallel model:

The Parallel ETC model is based on the hypothesis that fluid and solid phases are arranged in layers which are parallel to the heat flow. The basic equation structure of the parallel model is:

$$K_{eff} = \phi k_f + (1 - \phi) k_s \qquad \text{Equation 2.17}$$

Where k_f and k_s are the thermal conductivities of the fluid and solid phase. This model helps to estimate the maximum ETC of a medium [23].

Series model:

The Series model is based on the hypothesis that the fluid and solid phases are arranged perpendicularly to the heat flow. The basic equation structure of this model is [23]:

$$K_{eff} = \frac{k_s k_f}{\phi k_s + (1-\phi) k_f} \qquad \text{Equation 2.18.}$$

This model gives an estimation of the minimum ETC of a medium.

Geometric mean model:

This model is based on the concept that the ETC of a system should lie somewhere between the harmonic mean ETC and the weighted arithmetic mean ETC of the system [23]. The basic equation structure of this model is:

$$K_{eff} = k_f^{\phi} . k_s^{1-\phi}$$ Equation 2.19.

Maxwell-Eucken model:

Maxwell [18] gave an analytical solution for effective conductivity of a heterogeneous medium in his work on electricity and magnetism. Maxwell model was based on random dilute distribution of spherical particles in a continuous matrix of filler, neglecting thermal resistances between the two phases. It was found that Maxwell model was good in predicting effective thermal conductivity for highly porous medium. The basic equation structure for Maxwell's equation when $k_{cont}>k_{disp}$, i.e. in case of oil sands is:

$$K_{eff} = \left(\frac{2k_s + k_f - (k_s - k_f)\phi}{2k_s + k_f + (k_s - k_f)\phi}\right) . k_f$$ Equation 2.20.

Hashin-Shtrinkman [50] model looks mathematically similar to Maxwell although they had a dissimilar approach. Eucken [16] further extended Maxwell's approach and included the effects of multiple phases.

Rayleigh models:

Rayleigh [51] model was a modified form of Maxwell model where the spherical particles were considered to be arranged in a cubic array, which also reflected the thermal interaction between the particles and fluid. The model predicted the effective thermal conductivity better than Maxwell model for higher filler (solid) volume. The model was in a form of an infinite series in the denominator of the equation. When the higher order terms of filler fractions were ignored, it looked similar to the Maxwell model [18]. The structure of the model is given as below:

$$K_{eff} = k_f . \left(1 + \frac{3\phi}{\frac{k_s - 2k_f}{k_s - k_f} - (1-\phi) + \frac{1.569(k_s - k_f)}{(3k_s - 4k_f)}(1-\phi)^{\frac{10}{3}} + \cdots_{..}}\right)$$ Equation 2.21.

Kunii-Smith model:

This model considered that the thermal conductivity of individual phases and also the void fraction in a medium is independent of each other like that of "cylindrical packed beds of unconsolidated particles".

In this case, the ETC should be a result of amalgamation of the parallel and series models [8, 19]. The solid phase is considered to follow a "series model" and the fluid phase and void phase are to follow a "parallel model". The basic structure of the model is given below:

$$K_{eff} = k_f.(\phi + \frac{(k_s A)(1-\phi)}{Ck_s + Bk_f}) \quad \text{Equation 2.22.}$$

Where A is a function of the diameter of the particles (D_p) in the packed bed and is defined by [19]:

$$A = \frac{1}{3D_p}\left[\frac{2}{3}^{0.5} + 1 + \frac{3}{2}^{0.5}\right]D_p = 0.895 \quad \text{Equation 2.23.}$$

B is a function of the length of the cylinder (l).

$$l = \frac{\frac{\pi}{6} * D_p^3}{\frac{\pi}{4} * D_p^2} = 2/3D_p; B = \frac{l}{D_p} = 2/3 \quad \text{Equation 2.24.}$$

C is the function of packing of the medium and depends on the porosity of most loosely packed medium (ϕ_1) and porosity of most tightly packed medium (ϕ_2). So in any case the porosity of a medium (ϕ) lies between ϕ_1 and ϕ_2, i.e. $\phi_1 >= \phi >= \phi_2$.

$$C = C_2 + (C_1 - C_2).(\phi - \phi_2)/(\phi_1 - \phi_2) \quad \text{Equation 2.25.}$$

$$\phi_1 = 1 - \frac{\pi}{6} = 0.476, \phi_2 = 1 - \sqrt{2}\frac{\pi}{6} = 0.260$$

If the values of ϕ_1 and ϕ_2 are put in the Equation 2.22, it gets reduced to:

$$C = C_2 + (C_1 - C_2).(\phi - 0.260)/0.260 \quad \text{Equation 2.26.}$$

Usually $C=C_1$ for $\phi >= \phi_1$ and $C=C_2$ for $\phi >= \phi_2$.

This model was found to be valid for porosity ranging from 0.26 to 0.476.

Krupiczka model:

Krupiczka [52] model is based on the assumption that the spheres inside the medium are arranged in cubic lattice and is valid for a porosity range of 0.215 to 0.476 [16].

$$K_{eff} = k_f.k_s^{0.280 - 0.7571.\log(\phi) - 0.057.\log\left(\frac{k_s}{k_f}\right)} \quad \text{Equation 2.27.}$$

Hasselman-Johnson model:

Hasselman-Johnson [21] model included the particle size along with the porosity. This model also considered the effect of interfacial gaps between filler and matrix on the thermal diffusivity and correspondingly thermal conductivity of the system, i.e. they included the effects of interfacial thermal resistance (ITR) [21]. Their model is similar to Maxwell [18] model where a matrix of spherical arrangement of particles, and Rayleigh's [51] model where a matrix of cylindrical arrangement of particles, which were perpendicular to heat flow, was considered [17]. The basis equation of the model is given as below:

$$K_{eff} = \frac{k_s}{\left(1+{2k_s}/{k_f}-{k_s}/{k_f}\right)(1-\phi)+\frac{k_s}{k_f}} \qquad \text{Equation 2.28.}$$

Bruggeman model:

Bruggeman [53] model assumed that a composite material can be developed by considering miniscule change in a medium. This resulted in differential equations and thus the model is also called differential effective medium theory or differential effective medium scheme (DEM). This model proved advantageous not only to various type of materials such as composites, porous materials, aerosols etc, but also to multicomponent systems. This model predicted the effective thermal conductivity of composites most accurately for lower porosity among other effective medium theory models. Using the approach of this model, Every and Tzou [22] derived a formulae for effective thermal conductivity which is given as below:

$$\phi^3 = \left(\frac{k_f}{K_{eff}}\right)^{\frac{(1+2\alpha)}{(1-\alpha)}} . \left(\frac{(K_{eff}- k_s(1-\alpha))}{(k_f- k_s(1-\alpha))}\right)^{\frac{3}{(1-\alpha)}} \qquad \text{Equation 2.29.}$$

Where α is a dimensionless parameter and is a function of ITR and $\alpha=a_k/a$ where a_k is the Kapitza radius and a is the particle radius. For particles where a>= 2 μm, α is equal to 0.75 [22].

Zehner-Schlunder model:

Zehner and Schlunder [54] model predicted the ETC of a partially saturated packed bed by considering the medium as a cylindrical shape cell with spherical shaped particles. Their model was formulated using combined effect of thermal conductivity of grains and cavities. They assume two parallel conduits of heat flow, one was between solid and fluid phase in the middle of the cylinder and other one was through the fluid phase at the surface of the cylinder. The equation structure of the model is given below:

$$K_{eff} = 1 - \sqrt{1-\phi} + \frac{2\sqrt{1-\phi}}{1-\frac{Ek_f}{ks}}\left(\frac{\left(1-\frac{k_f}{k_s}\right)E}{\left(1-\frac{Ek_f}{k_s}\right)^2}\ln\left(\frac{k_s}{Ek_f}\right) - \frac{E+1}{2} - \frac{E-1}{1-\frac{Ek_f}{k_s}}\right) \quad \text{Equation 2.30.}$$

$$E = 1.25\left(\frac{1-\phi}{\phi}\right)^{1.11} \quad \text{Equation 2.31.}$$

The Lewis-Neilsen model:

The prediction of the Lewis-Neilsen [55] model was found to be quite accurate till solid fraction of 40% but they didn't include Interfacial Thermal Resistance (ITR). This model didn't work well for higher volume fraction. But the advantage of their equation was its simplicity and inclusion of particle shapes and patterns. The main equation structure of this model is given below:

$$K_{eff} = \frac{1+E_1E_2(1-\phi)}{(1-E_2\delta(1-\phi))} \quad \text{Equation 2.32.}$$

Where,

$$E_2 = \frac{\frac{k_s}{k_f}-1}{\frac{k_s}{k_f}+E_1} \quad \text{Equation 2.33.}$$

$$\delta = 1 + \frac{\phi_m}{(1-\phi_m)^2}(1-\phi) \quad \text{Equation 2.34}$$

ϕ_m is the maximum volume fraction of pores that is achievable and it depends on the shape of the particle in the medium. E_1 is the shape coefficient and is generally 1.5 for spheres where the aspect ratio (length/diameter) is 1. ϕ_m ranges from 0.1 to 0.4 in case of spherical particles [17].

Woodside Messmer model:

Woodside and Messmer [23] estimated the ETC of a two-phase unconsolidated porous medium with gas filled pores, using a modified three-element resistor model. They found that the ETC of the medium is mostly dependent on the conductivity of the saturating fluid compared to the conductivity of the solid medium for an unconsolidated pack and mostly ETC increases with the increase in conductivity of the fluid. The ETC of the packs in vacuum was about 100^{th} times less than that of the thermal conductivity of the solid. The effect of gas pressure on the ETC of the medium was found to be consistent with the kinetic theory of gases. The most important part of gas phase heat conduction was the conduction between the solid particles only to a distance of around one-sixth of the particle radius [23]. This model considered a combination of parallel and series model and has the following three components:

a. First element consist of particles and saturating fluid which were arranged in series (k_1).
b. Second element consist of only solid particles which are very closely packed and thus form a continuous channel (k_2).
c. Third element consist of only electrolyte filling the matrix in between the solid particles (k_3).

They assumed that these three elements were arranged parallel to each other. The main equation structure of this model is given as below [23]:

$$K_{eff} = k_1 + k_2 + k_3 \qquad \text{Equation 2.36.}$$

$$K_{eff} = \frac{ak_s k_f}{dk_f + (1-d)k_s} + bk_s + ck_f \qquad \text{Equation 2.37.}$$

In the above equation a+b+c=1. If the solid particles are not conductive only the third element contributes to the heat conduction.

Also, it is to be noted that, $c = {}^{1}/_{F}$ Equation 2.38.

F is the formation electrical resistivity factor and is the ratio of resistivity of a porous medium fully saturated with an electrolyte to the resistivity of the electrolyte. For any unconsolidated medium b in

Equation 2.37 can be neglected as there will be negligible contact between the solid particles. So, Equation 2.37 can be used by considering, [23]

$$c = \phi - 0.03, b = 0, a = 1 - c \; and \; d = {}^{(1-\phi)}/_{a}$$

de Vries' model:

de Vries's model [56] is a modified Eucken's and Burger's Maxwell's [23] equation for ellipsoidal particles. This model was used to estimate the ETC of unconsolidated soil medium with two-phases consisting of continuous fluid and dispersed solids. The main structure of the model is given below [23]:

$$K_{eff} = \frac{\phi k_f + (1-\phi) T_1 k_s}{\phi + (1-\phi) T_1} \qquad \text{Equation 2.38.}$$

T_1 is a factor that indicates the average temperature gradients in the two phases and is given by:

$$T_1 = \frac{1}{3}\sum_{i=1}^{3}[1 + \left(\frac{k_s}{k_f} - 1\right) s_i]^{-1} \qquad \text{Equation 2.39.}$$

And, $$\sum_{i=1}^{3} s_i = 1; \; s_1 = s_2 = \frac{1}{8}; \; s_3 = \frac{3}{4} \qquad \text{Equation 2.40.}$$

The factor s_i is the shape factor and when s_1=s_2=s_3, i.e., for spherical particles, Equation 2.38 is same as Maxwell's equation. The values of s_1,s_2 and s_3 in de Vries' model, as given in Equation 2.40, are based on ellipsoidal particles with major axis of revolution being six times the minor axis.

Effective Medium Theory (EMT) model:

This model is based on the random distribution of the solid and the fluid phases in the medium and was developed to estimate the electrical conductivity of the system. The main structure of the model can be summarized as below [8]:

$$K_{eff} = \frac{1}{4}[(3\phi - 1)k_f + (3(1-\phi) - 1).k_s + \{\left((3\phi - 1).k_f + (3(1-\phi) - 1).k_s\right)^2 + 8k_s k_f\}^{0.5}]$$

Equation 2.41.

2.5.2. Percolation model:

When the filler (solid) volume fraction increases, then the particles come into contact with each other and form conductive channels. If it is assumed that the solid particles are highly conductive then the effective thermal conductivity rises sharply at higher solid volume fraction. The point where the ETC show a sharp rise with increase in solid volume fraction is known as percolation threshold. Mixing rule models fail to predict the effective thermal conductivity beyond this percolation threshold.

Devpura et al. [57] suggested numerical modelling of percolation and ITR. The model was built on the concept that the medium was an array of cubes of equal sizes and performed calculations using matrix algebra. They also considered spherical particles by adding a sphericity parameter to the existing matrix. The thermal conductivity of the solid particles was assumed to be much higher than the thermal conductivity of the fluid matrix. Interfacial thermal resistance (ITR) along the walls of the particles was also taken into account. The ITR was estimated from Acoustic Mismatch Model (AMM) so it included only Thermal Boundary Resistance (TBR). Though the model was simple, it matched very well with the experimental results [17]. Devpura et al. [57] estimated the ITR of the system by using the Biot number for a spherical particle using the equation:

$$Bi = \frac{R_{int}.k_f}{2a} \qquad \text{Equation 2.42.}$$

Where a is the particle radius and R_{int} is the Interfacial thermal resistance.

At higher Bi, the ETC of the medium is low and the percolation threshold was high. It is evident from Equation 2.42 that Bi can be increased by enhancing the ITR or by lowering the particle radius.

2.5.3. Temperature and Pressure dependant models:

The temperature dependency of ETC can be studied by considering three thermal zones. First zone is the region of low temperature (below 700 ºC) and heat transfer is mainly due to pore conduction and the radiation effect is negligible. The second zone is the high temperature region (above 700 ºC) where

the radiation is quite significant and the third zone is the very high temperature zone where thermal reactions take place thus altering the composition and structure of the minerals and may also change the phase of the imbibed fluid. Eucken [58] proposed a model for temperature dependency of thermal conductivity of amorphous materials, which is given as below [24]:

$$K_{eff} = (AT + B + C/T)^{-1} \quad \text{Equation 2.43.}$$

Where A, B and C are constants that depends on the relative influence of solid particles.

Thermal conductivity of a medium is the combined action of lattice conductivity (k_{lat}) and radiative conductivity (k_{rad}). The lattice conductivity is the heat transferred due to thermal vibrations of the solid particles of the medium and radiative conductivity is the heat transferred due to infrared electromagnetic waves. As mentioned before, at temperatures below 600-700 ºC, radiative conductivity is insignificant. Based on three-phonon approach, k_{lat} is inversely proportional to temperature and k_{rad} is proportional to third power of temperature and based on four-phonon approach, k_{lat} is inversely proportional to $5/4^{th}$ power of temperature [24]. The three-phonon approach is valid only for perfect isotropic crystal structure of particles and shows a considerable variation for disordered medium. The most common equation used to fit experimental data of ETC with varying temperatures for porous rock is:

$$k_{eff}(T) = A + \frac{B}{350+T} \quad \text{Equation 2.44.}$$

A and B are experimental parameters. This equation was used by Kukkonen et al., Zoth and Hanel and Seipold [59]. At higher temperatures, Seipold [59] added one additional parameter CT^3 by including radiative conductivity.

The ETC of a medium depends on pressure based on the fact that porosity gets affected under stress and by temperature. According to Fricke's model [24], when porosity is a function of pressure $\phi(P)$, the thermal conductivity equation is given as below:

$$\frac{k_{eff}}{k_s} = \frac{1-\phi(P)}{(1-\phi(P))+\beta\phi(P)} \quad \text{Equation 2.45.}$$

Where, β is an experimental factor. The experimentally derived porosity relation with pressure is given by [24]:

$$\phi(P) = \phi_{\infty} + \phi_1 e^{\frac{-P}{P_0}} \qquad \text{Equation 2.46.}$$

ϕ_{∞} is the minimum value of porosity at highest pressure P_0 (i.e., as $P \rightarrow \infty$) and $\phi_1 = \phi_0 - \phi_{\infty}$, ϕ_0 is the porosity at zero pressure. Abdulagatova et al. [24, 25] also estimated the thermal conductivity of sandstones up to 400 MPa pressure [25]. They observed that the ETC of a rock, increases sharply between 0.1 and 100 MPa, but at pressure above 100 Ma the effect of pressure was not that significant. They concluded that, at low to medium pressure ranges, with the increase in pressure, the micro-cracks in solid grains of rock tend to get minimized resulting in the decrease of distance of particles and thus the ETC rises sharply. Whereas, at very high pressures, the micro-cracks are closed as the particles come close to each other and ETC becomes almost constant with pressure.

Chapter 3: Previous Experimental Measurements

3.1. Previous works on thermal conductivity measurements with the transient method

Woodside and Messmer [23] used the linear heat source transient method to determine the ETC of unconsolidated sands under various conditions and concluded that the results were fast and accurate to within one to two percent. They performed all the tests with five different unconsolidated sand packs at room temperature using air and water as the saturating fluids. For water saturated quartz sand, with porosities ranging from 0.19 to 0.59, the ETC values were found to be stretching from 12.3 to 5.17 mcal/cm.sec ºC (5.15 to 2.16 W/mK). With air in the pores, the ETC values with same porosities varied between 1.57 to 0.416 mcal/cm.sec ºC (0.657 to 0.174 W/mK). A test was conducted on two sand packs having same porosity but solid grains thermal conductivities varying by a factor of 33. They found that the sand grains having greater thermal conductivity showed larger increase in ETC when saturated with water compared to air. The ETC ratio was 2.0 in case of air and was 6.05 in case of water. They observed that not only the ETC of a sand pack increased as the conductivity of the saturating fluid increased, but the sand pack showed a sharper rise in ETC with increasing conductivity of grains when the saturated fluid conductivity is lower. The ETC of all the sand packs in vacuum were one-hundredth times lower than the thermal conductivities of the solid grains and the ETC showed a sharp rise when the pressure was increased by injecting gas.

Asher et al. [12] used the transient needle-probe method to estimate the thermal conductivity of liquid tertiary butyl alcohol, 1-methylnaphthalene and glycerine and found that the results had an accuracy of better than 5%. They also confirmed that this method is able to predict the thermal conductivity of liquids having viscosity greater than 3 cP at room temperature without considering convective uncertainties.

Hanafi and Karim [26] measured the ETC of oil sands samples using the unsteady state method over a temperature range of -100 ºC to 200 ºC at atmospheric pressure. They measured the transient temperature rise both at the centre and at the surface of the oil sands samples with a convective heated stream of air and also with an above boiling liquid nitrogen at atmospheric pressure. They observed that with the decrease in oil percentage of the samples, the temperature difference between the centre and the surface of the sample also reduces. This led them to draw the conclusion that when the bitumen saturation decrease in the sample, the solid phase dominates the temperature gradient and that results in more uniform temperature distribution in the sample. In their measurements of ETC from -110 ºC to -20 ºC, they found that the ETC was almost constant in this range and it increased slightly near 0 ºC. The figures 10 and 11 show the observations of ETC for natural and artificially prepared oil sands from Hanafi and Karim experiments:

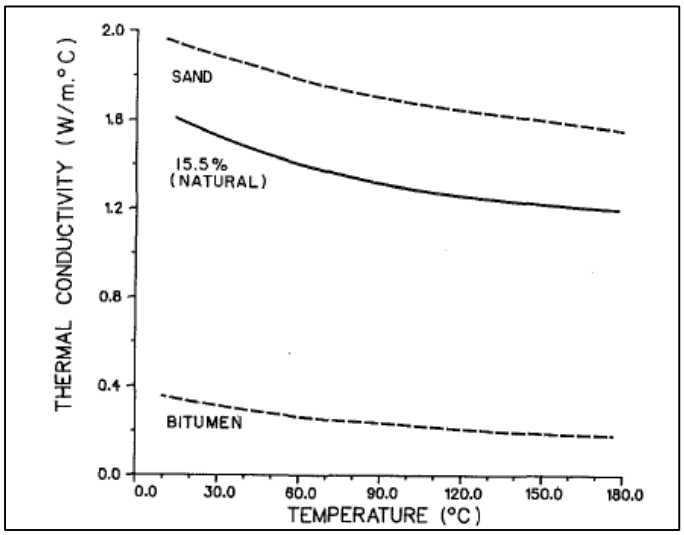

Fig.10: Thermal conductivity variation of natural oil sand samples, pure bitumen and pure sand with temperature. [26].

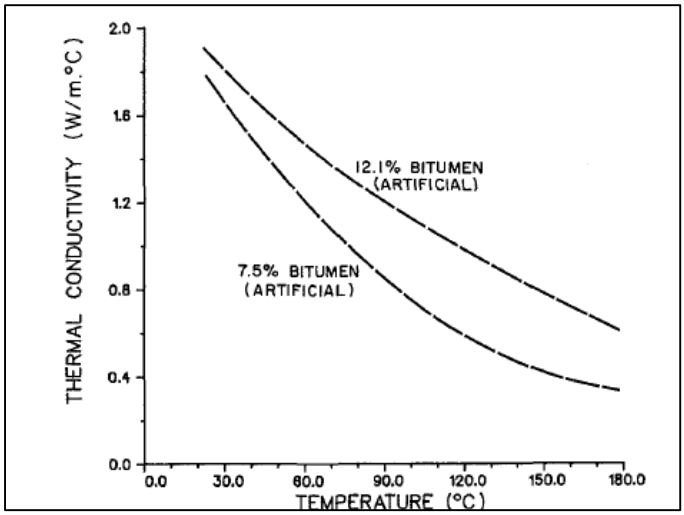

Fig.11: Thermal conductivity variation of artificially prepared oil sand samples with temperature [26].

Using the least square method they provided the following relation of K_{eff} with temperature for the natural oil sands sample with 15.5% oil content [26]:

$$K_{eff} = 1.7528 - 0.0052T(1 - 0.00285T) \qquad \text{Equation 3.1.}$$

They compared their results with naturally occurring oil sands samples. They found that at temperatures above 60 ºC, the differences of ETC between the natural oil sands samples and the artificially prepared samples, increases considerably. They concluded that when bitumen and sand are mixed artificially the resulting thermal conductivity may differ significantly than naturally occurring oil sands samples with well distributed phases. They found that the thermal conductivities rapidly increased when the temperature was increased above 0 ºC. This was mainly because of the phase change of water and the increased contribution of bitumen to the ETC at higher temperatures. They also concluded that with the increase in bitumen content in the samples, the ETC of the medium also increased and the ETC values obtained from transient method was slightly higher than those obtained from steady state methods.

Herzen and Mazwell [27] measured the ETC of deep sea sediments using the needle-probe method and concluded that this method is capable of measuring ETC of a sample with an accuracy of 3-4% compared to steady-state methods. Their experiment running time was 10 minutes or less. The ETC of

bentonite clay was (1.83 $\pm$ 0.02)*10^{-3} cal/sec.cm^{o}C (0.0032 W/mK) obtained from steady-state method and was (1.82 $\pm$ 0.03)*10^{-3} cal/sec.cm^{o}C (0.0031 W/mK) obtained from the needle-probe method. They also mentioned that in case of taking repeated measurements, one should take care that the material in the nearest vicinity of the needle-probe should not dehydrate and increase the overall thermal conductivity.

Lockmuller and Redgrove [28] conducted experiments on graphite, Perspex, AFS testing sand and silica microspheres to validate the transient needle-probe technique for measurement of thermal conductivity of soft solids such as foods, powders, slurries and biological materials. The experimental results for Perspex and graphite were within 2% accuracy for a suggested power range of 0.35 W/m to 4 W/m. They stated that if the thermal contact resistance between the probe and the specimen is high, that can lead to high standard deviations of the experimental results. The effective thermal conductivity obtained for powder specimens showed high reproducibility and thus they concluded that, as these specimens show lower increase of thermal conductivities with density, they are the probable materials to be used as reference materials for determining thermal conductivity using needle-probe method. Their findings showed that the needle-probe method show satisfactory results for specimens having thermal conductivities between 0.2 and 6.0 W/mK.

3.2. Previous works on developing effective thermal conductivity models of multiphase porous/packed structures and oil sands

Cervenan et al. [29] conducted experiments on unconsolidated sands and Athabasca oil sands to study the heat conduction process and developed correlations of ETC with water saturation, thermal conductivity of the solid phase and porosity using Somerton et al. model [33]. Somerton estimated ETC of quartz sands and different Kern River oil sand samples using multiple regression analysis. According to Somerton model, water saturation, thermal conductivity of solid phase and porosity play a dominating role in determining the ETC of sands having porosity of 0 to 0.40, but oil saturation didn't have any

significant effect and the error percent between the measured and calculated data didn't change much with the inclusion of oil saturation [33]. As the grain size and permeability were related to porosity, so the correlation included only porosity of the sample. The Somerton et al model is provided below:

$$K_{eff} = 1.27 - 2.25\phi + 0.39k_s\sqrt{S_w} \qquad \text{Equation 3.2.}$$

Where, k_s and S_w are the thermal conductivity of solid phase and water saturation in pore space.

Considering a typical mixture of Athabasca sand (95% quartz, 3% feldspar, 1% mica and 1% clays), weighted average of the composition was used to calculate the thermal conductivity of sands as 7.4 W/mK. Using a mean value of 0.4 porosity, the ETC was determined as a function of only water saturation. The model was found to differ considerably with the experimental data at lower water saturations. The difference was expected due to variations in sand compositions. The model matched well with the experimental observations when bitumen extracted oil sands samples were used. So it was assumed that bitumen should have a noteworthy effect on the ETC of oil sands, contrary to Somerton et al. model, and the equation should include bitumen saturation. The experimental data by Cervenan et al. [29] showed that the thermal conductivity of Athabasca oil sand increases from 1.3 to 2.0 W/mK as water saturation was increased from 0.9% to 44%.

Tsotsas and Martin [30] reviewed various available thermal conductivities models for multiphase packed beds and compared them with experimental data. They identified that the primary factors affecting the ETC of an identical spherical particle containing packed bed, are the thermal conductivity of the solid (dispersed) phase (k_s), thermal conductivity of the fluid (continuous) phase (k_f), the porosity of the medium and a factor used to define the arrangement of the phases (a). For the spherical solid particles in the medium, porosity can be used as the single parameter to explain the packing structure. So, according to them:

$$K_{eff} = K_{eff}(k_s, k_f, \phi, a) \qquad \text{Equation 3.3.}$$

Along with these primary factors, ETC may also depend on the following secondary parameters:

- Heat transfer through radiation which depends on the temperature level of the system, optical properties of the surface solid particles and liquid phase (when the liquid dispersed phase is not completely transparent), and the distance between two solid particles or the particles diameter.
- Pressure dependence of ETC when the medium contains gases. As per molecular theory of gases, the thermal conductivity of dilute gases is independent of pressure. The pressure dependency of ETC of gases can be related to Knudsen number (Kn) (ratio of mean free path of gas molecules to dimension of the corresponding void spaces). For small Kn, the thermal conductivity does not depend on pressure, but for higher Kn, thermal conductivity of gases is inversely proportional to pressure and the ETC correlations need a correction factor considering non-ideal collisions of gas molecules with the solid particles. So, to summarize, the mean free path of gas molecules is dependent on pressure and thus, the ETC also depends on the pressure.
- If there is any external pressure or load (even due to weight of the bed), the solid particles near the contact points may get flattened, which may alter the heat conduction process and also the physical properties of the solid particles.
- Convection should also be considered in case of large void spaces due to difference in temperatures.

They also mentioned that particle shape and particle size distribution may also alter the ETC of a packed bed and finally gave the following equation:

$$K_{eff} = K_{eff}(k_s, k_f, \phi; P, T, D_p, size\ distribution, particle\ shape, physical\ and\ optical\ properties\ of\ particles, thermodynamic\ and\ optical\ properties\ of\ fluid, particle\ flattenng\ )$$

Equation 3.4.

To give a theoretical prediction of the ETC of the packed bed, they considered the Zehner and Bauer model [34, 35] where ETC was estimated considering a unit cell with parallel heat flux gradients. In the Zehner and Bauer model, a part of the area of the considered unit cell (1-√(1-ϕ)) was allotted to the liquid phase and in the remaining part heat conduction was through inter-particular contact in gas filled pore space. The model also took into account a deformation factor B, which included various shapes of the solid particles. B was mathematically approximated by the following equation:

$$B = 1.25\left(\frac{1-\phi}{\phi}\right)^{10/9} \qquad \text{Equation 3.5.}$$

The final ETC of the unit cell and the system considering the primary factors was given by:

$$\frac{K_{eff}}{k_f} = 1 - \sqrt{1-\phi} + \sqrt{1-\phi}.\frac{k_c}{k_f} \qquad \text{Equation 3.6.}$$

k_c is the thermal conductivity at the core of the unit cell and was estimated from the following relation:

$$\frac{k_c}{k_f} = \frac{2}{N}\left(\frac{B}{N^2}\frac{k_s-k_f}{k_s} ln\frac{k_s}{Bk_f} - \frac{B+1}{2} - \frac{B-1}{N}\right) \qquad \text{Equation 3.7.}$$

Where N was:

$$N = \frac{k_s - Bk_f}{k_s} \qquad \text{Equation 3.8.}$$

The Zehner Bauer model [34,35] was also used by Tsotsas and Martin which included the secondary parameters mentioned above. The model included parameters such as thermal radiation; particle flattening; and shape and size distribution. Tsotsas and Martin observed that most of their experimental points lie within ±30% interval around the Zehner Bauer model [34,35] and they concluded that this model can be used for estimating ETC of multiphase packed beds or porous structures.

As discussed earlier, Woodside and Messmer [23] conducted experiments on unconsolidated sands under various conditions and compared their results with different models of ETC. They observed that the Geometric mean model overestimated the ETC when the ratio of k_s/k_f is more than 20. Maxwell's model underestimated the ETC, while de Vries' model and Kunni Smith model gave satisfactory results for a

wide ranges of porosity, fluid conductivity and solid grains conductivity. The detailed equation structure of Woodside and Messemer model [23] was discussed in the section 2.5.1.

Pietrak and Winiewski [17] conducted experiments on the Al_2O_3 filler in a polyethylene matrix at different porosities for different Biot numbers. The experimental results were compared with the theoretical results from the EMT model, Lewis-Neilson [55] model and the Percolation model [57]. The following inferences can be drawn from their observations:

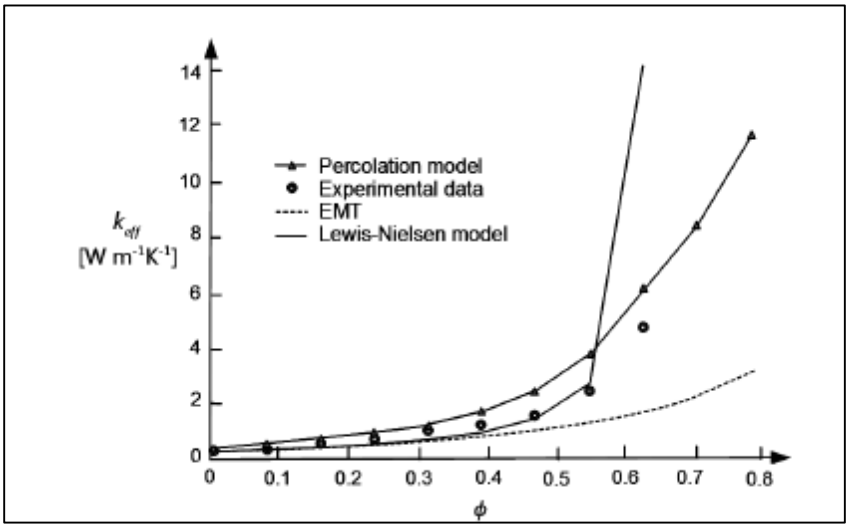

Fig. 12: ETC of bimodal distribution of Al_2O_3 filler in a polyethylene matrix predicted by different models and compared with experiments conducted by Pietrak and Winiewski [17].

- They found that Lewis-Neilson model could not predict the effective thermal conductivity when the solid fraction was more than 40%.
- EMT model gave lower values of effective thermal conductivity when the solid fraction was more than 40%.
- Devpura et al. [57] (Percolation) model gave closer values of effective thermal conductivity for higher solid fraction. This was useful to predict the maximum values of effective thermal conductivity. Further, Devpura et al. model was used for various Biot numbers to study the effect of Interfacial Thermal Resistance (ITR). The observations implied that for higher Biot number, the effective thermal

conductivity was low and also percolation threshold was reached at lower porosity. From the provided simulation results it could be concluded that if filler with Biot number greater than unity is used, it can reduce the effective thermal conductivity of the composite below the thermal conductivity of the pure matrix, even if the filler to matrix conductivity ratio is 1000:1. Knowing the value of ITR, critical radius of particle at Bi=1 can be calculated. Thus, if particles size smaller than the critical radius are used, that will also decrease the effective thermal conductivity. Devpura et al. model proved to be a great tool for predicting the effective thermal conductivity for its accurate results, simplicity and lower numerical simulations cost.

Pietrak and Winiewski [17] concluded that the porous media can be modelled as composite system with solid matrix having gaseous inclusions. The effective thermal conductivity of a porous medium is the combined effect of solid conduction, gas convection and conduction, and radiation. But the gas convection can be neglected for smaller pore sizes. Gas conduction can also be neglected for pore sizes smaller than 80 nm.

Dul'nev and Zarichnyak [32] developed a new model to estimate the ETC of non-reacting binary liquids as a mixture of two non-penetrating continuous media. They analysed both emulsions and solutions. They mentioned that the Filippov and Novoselova model [60] was found to predict the ETC of binary liquid mixtures, by considering non-reacting and interpenetrating continuous media, to within 1-5%. The model is given below:

$$K_{eff} = k_1(1 - n_2) + k_2 n_2 - 0.72(k_2 - k_1)n_1(1 - n_2) \qquad \text{Equation 3.9.}$$

Where k_1, k_2 are the thermal conductivities of individual components and n_1 and n_2 are the weight compositions of those components.

Dul'nev and Zarichnyak [32] considered each liquid component as a continuous medium having a thermal conductivity same as the liquid for a definite temperature. If the liquid mixture formed an

emulsion, its structure would be such like that one component would be enclosed by the second component. The effective thermal conductivity of such mixture was structured using the **Odelevskii's** [61] equation as given below:

$$K_{eff} = k_1\left(1 - \frac{p}{\frac{1}{1-v} - \frac{1-p}{3}}\right) \quad \text{Equation 3.10.}$$

Where $v=k_2/k_1$ and p is volume fraction of the second component.

If the liquid formed a solution, the molecules are supposed to randomly move in the volume of mixture and the molecules at any specific volume, were considered as two spatially continuous interpenetrating matrix. Dul'nev model was used to predict the ETC of such structure and is given by:

$$K_{eff} = k_1 \frac{(x^2+v(1-x)^2+2vx(1-x)}{vx+(1-x)} \quad \text{Equation 3.11.}$$

Where x is a lattice parameter, related to volume fraction of the second component, p and can be obtained from the following equation:

$$p = 2x^3 - 3x^2 + 1 \quad \text{Equation 3.12.}$$

Dul'nev and Zarichnyak compared the experimental results with the above model and found that for methylformate and carbon tetrachloride mixture, the maximum deviation was 14% and the mean deviation for various mixtures was between 2-7%. The experimental data was slightly on the higher side compared to the model for two associated liquids and the maximum deviation was -7% for ethanol and water system and the mean deviation was 0-3%. Dul'nev and Zarichnyak concluded that for any binary liquid system the structure of the liquid mixture should be taken into account while estimating their ETC.

Chapter 4: Experimentation

4.1. Method Overview

The measurements are conducted in a specially designed cell (pressure vessel) equipped with a needle probe, which performs in compliance with ASTM D5334-14, ASTM D5930-97 and IEEE 442-1981 standards [36] . In this method a constant electrical energy is supplied to the needle probe, which is placed in the center of the cell containing the specimen, for a specific amount of time. The rise in temperature of the probe surface with time is then recorded. The details of the mathematical equations are discussed in Section 2.4.

To obtain thermal conductivities under different conditions, experiments were conducted using clean silica sand, bitumen, water and non-condensable gas (NCG), i.e. nitrogen at temperatures ranging from 21 ºC to 150 ºC and pressures ranging from atmospheric pressure to 500 psig (34.5 barg). Starting from dry sands, different values of oil, water and gas saturations were created by displacement techniques. The thermal conductivity data obtained from the experiments were fitted to several effective thermal conductivity (ETC) models and modified correlations were derived from the same. The ETC model developed in this work is a function of gas saturation and temperature.

4. 2. Experimental set-up

As mentioned above, to calculate the thermal conductivity of the specimen, the sensor side of the needle probe is kept immersed in a pressure vessel containing the oil sands specimen and the other end is connected to an electrical source and a Data Acquisition System (DAS), as shown in Figure 13. The electrical source supplies a constant current to the probe and increases the temperature of the probe. The rise in temperature with time is recorded by DAS (which converts analog signal to digital data) on a computer using the software supplied by the manufacturer of the probe. The rise in temperature versus logarithm of time is then plotted. The inverse of the slope of this plot gives the thermal conductivity of

the system, as was discussed in Section 2.4. The main components of the experimental set-up are described below:

4.2.1. Needle-probe (TP02):

The needle-probe is the main component of the set-up which helps in estimating the thermal conductivity of the specimen. As discussed in Section 2.4, the needle-probe is designed based on an infinite length assumption, which was done by keeping a large length of the needle to diameter of the needle ratio. The length of the needle-probe (TP02) is 150 mm and the diameter is 1.5 mm [36]. The internal structure of TP02 probe is shown below in Figure 14.

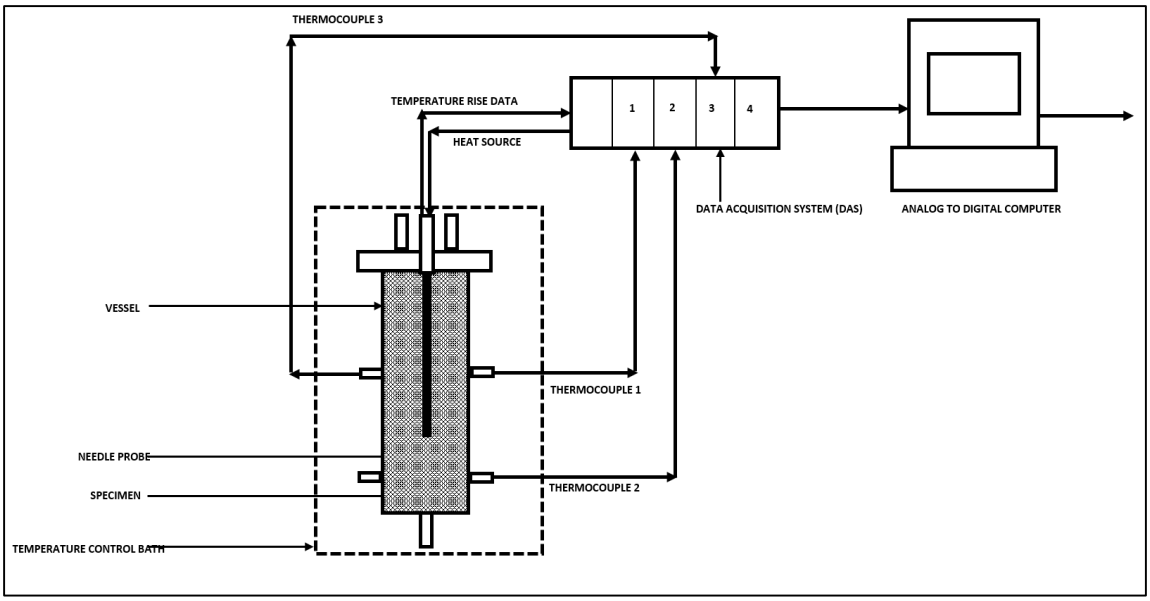

Fig.13: Basic experimental set-up.

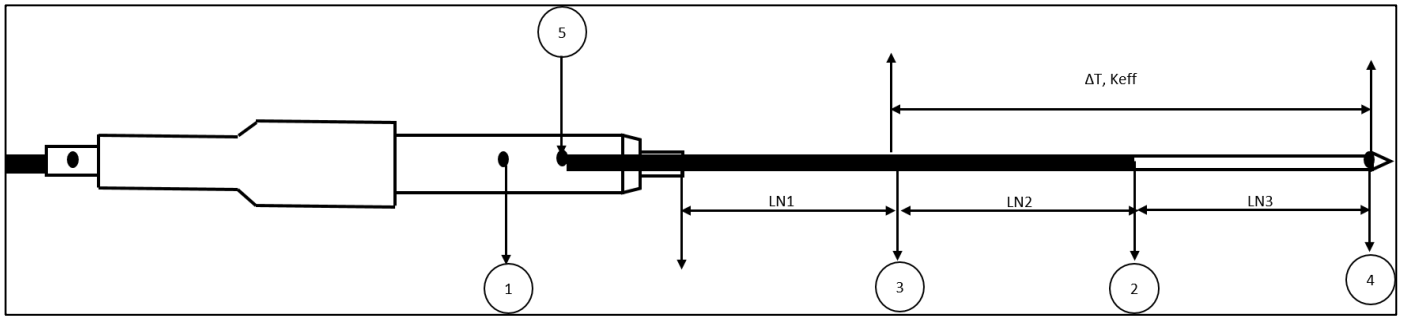

Fig.14: Structure of TP02. [1. Reference temperature sensor (Pt1000) 2. Heating wire, that runs 2/3rd of the needle length (LN2) 3. First thermocouple joint that runs 1/3rd of the needle length (LN1) 4. Second thermocouple joint at the tip of TP02 (LN3) 5.The heater wire starting point.]

The two main functions of TP02 are:

- **Providing the heating source to the medium:** There is a heater wire inside the probe which supplies electrical energy to TP02 and it runs only to 2/3rd of the length of the needle (till length LN2). To calculate the constant energy supplied to the medium, the heater power per unit length (Q in W/m) is measured by measuring the current at the heater wires using a sensor resistance ($R_{current}$) of 10 Ω and the wire resistance per unit length (R_{wire}: 85 Ω/m) [36]. The equation for Q is given by:

$$Q = I^2 R_e = \left(\frac{V_{current}}{R_{current}}\right)^2 R_{wire} \qquad \text{Equation 4.1}$$

- **Measuring rise in temperature of the medium:** There are two K-type thermocouple junctions along the length of the needle, which are in reverse-series. The first thermocouple junction is at the 1/3 length of the needle (LN1) and the second thermocouple junction is at the end of LN3 (at the tip of the needle), as shown in Figure 14. When the temperature increases at the first junction, a voltage is generated, which is proportional to differential temperature ΔT, as given in Equation 2.16.

$$\Delta T = (T_2 - T_1) = -\frac{Q}{4\pi K_{eff}} \ln(t_2) \qquad \text{Equation 2.16.}$$

The thermocouple at the end of LN1 is called the hot junction and at the end of LN3 is called the cold junction of the needle probe TP02. As the heating wire runs only until length LN2, the cold junction (at LN3) remains at the initial temperature of the specimen throughout the measurement. Both the hot and the cold junction inside TP02 remain submerged in the specimen, which minimises the error due to change in medium temperature. Before the start of a measurement, the junctions are at same temperatures, so the voltage is very small and is independent of the medium temperature. This also ensures high accuracy in the estimation of the rise in temperature after the start of the experiment.

There is also a reference RTD temperature sensor (Pt1000) at the base of TP02 that can serve as the cold junction in the programming of the probe. Pt1000 is a requirement of ASTM standard and it

serves to confirm the absolute medium temperature which eliminates the error in estimating thermocouple sensitivity at the starting point of a measurement [36].

The temperature difference is calculated by dividing the voltage generated at the junction by the sensitivity of the thermocouple joints (E_{sen} in μV/K). The equation of k-type thermocouples with temperature used to estimate E_{sen} is given by:

$$E_{sen} = 10^{-6}(39.4 + 0.050T - 0.0003T^2) \qquad \text{Equation 4.2.}$$

Up to temperature 20 ºC, E_{sen} is estimated to be around 40.35 μV/K. It follows the above equation at higher temperatures.

Thus, $$\Delta T = \frac{V_{sen}}{E_{sen}} = \frac{V_{sen}}{10^{-6}(39.4+0.05T-0.0003T^2)} \qquad \text{Equation 4.3.}$$

Where, V_{sen} is the voltage difference between the hot and cold joints.

To understand the calculation procedure of the temperatures at hot and cold joints (T_{hot} and T_{cold}), we need to take a look at the wiring schedule of TP002. The wiring schedule of TP002 is shown in Figure 15 [36, page 28]:

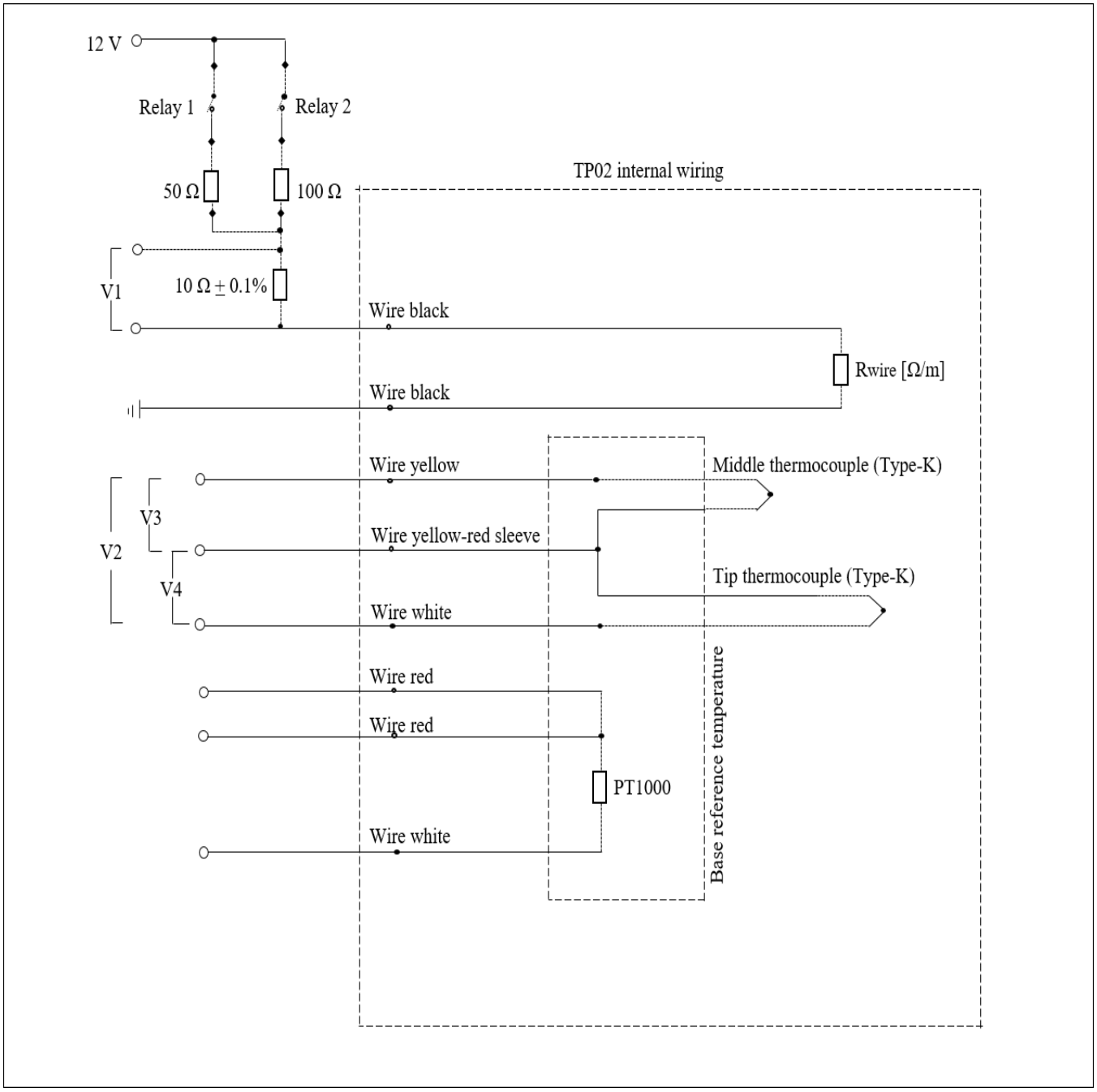

Fig.15: A typical wiring diagram of TP02 [36, page 28].

The V_{sen} in Equation 4.3 is V2, and can be used to calculate the ΔT. The measurement procedure of the temperatures at different points follow the underneath sequence:

Step 1: The temperature at Pt1000 (T_{Pt1000}) is measured directly from the RTD sensor which has a 3-wire connection.

Step 2. The temperature at cold junction T_{cold} is estimated using T_{Pt1000} as the reference junction and measuring the voltage V4 (Refer fig.15), using the following equation:

$$T_{cold} = T_{Pt1000} + (\frac{V4}{E_{sen}}) \quad \text{Equation 4.4.}$$

Step 3: The temperature at hot junction T_{hot} is estimated using T_{cold} as the reference junction and measuring the voltage V2 (Refer fig.15), using the following equation:

$$T_{hot} = T_{cold} + (\frac{V2}{E_{sen}}) \quad \text{Equation 4.5.}$$

The other two resistors 50 Ω and 100 Ω are given to supply variable power to the heater and reduce the voltage of the heater wire from 12 VDC to 3 VDC.

This needle-probe can be used to measure the thermal conductivities of samples ranging from 0.1 to 6 W/mK with an expected accuracy at 20 ºC of (3%+0.02) W/mK [36]. Further detailed information on the needle-probe is present in the TP02 manual [36].

4.2.2. Vessel containing the specimen

The needle-probe TP02 was designed to work as an infinite long heat source and one of the design assumptions for accurate measurements, was to consider the medium (where TP02 is inserted) to be extended infinitely. It was already discussed in Section 2.4 that, to make the above assumption valid, the radius of the sample should be greater than 30 times of the needle probe radius. The vessel was specially designed for this experiment, and has an inner diameter of 7.6 cm and the height of 16.2 cm (without the vessel cap). Figure 16 shows the in-house designed vessel which was pressure tested to work safely up to 600 psig (41.4 barg) and could be used for even high pressures. The needle-probe was inserted from the top of the vessel. In addition to having two inlet-outlet points at the top and one inlet-outlet point at the bottom, the vessel has three thermocouples ports on its cylindrical surface at different heights. These three thermocouples were used to ensure that the temperatures at all the positions in the medium was same. The

vessel cap was designed to apply compression to the sand pack after filling the vessel with the sand specimen.

Fig.16: The vessel used to contain the specimen.

4.2.3. Data Acquisition System (DAS)

To convert the temperature data from the needle-probe TP02 into digital form and to tabulate the data, a Campbell datalogger system (CR1000) and the LoggerNet software were used [43]. One part of the datalogger was connected to the needle probe to receive the data and another part was connected to a computer to record the final data. The CRBasic program, which was used to calculate the thermal conductivity of the system in LoggerNet software, is described in the CR1000 operating manual [44]. The wiring schedule with “no second power” switch was used to estimate the thermal conductivity of the medium. The parameters that were set in the LoggerNet software at the start of the measurement were:

a. **Voltage mode:** The voltage mode (low: 0.7 VDC, medium: 1 VDC or high: 2 VDC) at which the measurement are to be taken, is specified before starting the measurements.

b. **Measurement time:** To avoid errors due to convection or boundary conditions, the transient time should be very small. It is recommended to keep the measuring time below 100 secs [36]. The user sets the measurement time for the experimental runs. The switching on and off of the heater that supplies heat to the system is based on this set time. It is recommended to set it in such a way that the heater till turn on at half time of the doubled set time. As for example, if the user sets the measurement time as 50 secs, the total time of the measurement will be doubled up to 100 secs and the heater will turn on at 50 secs, which ensures that the system is completely stabilized before switching on the heater.

c. **Resistance per unit length of the internal wires:** This data is given in the manual of TP02 [36] as 85 Ω/m but can be changed if needed.

The procedure of analysing the data to get the final thermal conductivities of the medium, was described in Section 2.4.

4.3. Equipment/Apparatus and Materials used in the experiments

Equipment and apparatus

- Needle-probe (Huskeflux TP02) [36] [43]
- Pressure vessel (in-house design) (Height with cap: 19.4 cm, Inner diameter: 7.6 cm, Height without cap: 16.2 cm, Volume: 735 ml)
- Transfer vessel for injecting bitumen (Height: 21.6 cm, Inner diameter: 5.08 cm, Volume: 438 ml)
- Transfer vessel for injecting surfactant (Height above piston: 7.62 cm, Inner diameter: 3.8 cm, Volume above piston: 87 ml)
- t-type Thermocouples to measure the temperatures at different position in the pressure vessel

- Data Acquisition System (Campbell CR1000) and LoggerNet software (Appendix)
- Computer
- Thermal Bath (in-house design) (Height: 40.3 cm, Length: 30.5 cm, Width: 34 cm, Volume: 42 litres)
- Syringe pump (Teledyne ISCO D-series)
- Vacuum pump
- Coil Heater to heat the thermal bath
- Heating tapes to heat the transfer vessel and flex pipes carrying bitumen
- Swagelok fitting to attach the needle-probe to the vessel
- Nitrogen Cylinder
- Regulator for nitrogen cylinder
- Flow control valves
- Burette for water flooding
- Flex pipes (1/4 inch and 1/8 inch), Stainless steel Nipple Fittings (1/4 inch and 1/8 inch), Stainless steel Tee Fittings, Compression nuts, and Fitting caps
- Pressure gauges (2)
- Beakers (to collect product)
- Thermometer
- Weighing Balance
- Variac transformer for providing power to the heating tapes across the bitumen transfer vessel
- Vise
- Tools for setup (Wrenches, Adjustable Wrench, Torque range, Hammer, O-rings, Screwdriver)

Materials and chemicals

- Glycerol (CAS# 56-81-5) [46] for calibration of the needle-probe
- Silica sand (CAS# 14808-60-7) [47]
- DM water
- Athabasca Bitumen
- Nitrogen gas
- Surfactant [45]
- Silicone oil (PSF-50 cSt Silicone fluid) [48]
- Toluene for vessel and line cleaning
- Vacuum grease (for friction between the vessel and vessel cap threads) and Kopr-Kote (anti-seize lubricant)

4.4. Experimental set-ups used for measurements

To get the thermal conductivities of dry sand, water saturated sand, water-bitumen saturated sand, water-bitumen-NCG saturated sand and water-bitumen-NCG-surfactant saturated sand, displacement methods were used. To measure the thermal conductivities at higher temperatures, the pressure vessel containing the specimen was kept inside the thermal bath. The thermal bath was completely filled with silicone oil which was heated using a coil heater. The required temperature, at which the thermal conductivity was to be measured, was set at the coil heater. Once all the three thermocouples inside the pressure vessel and the thermocouples inside the needle-probe showed the specified temperature, indicating that the whole specimen was at that specific temperature, the heater inside the needle-probe was turned on for a very small amount of time (around 20-50 secs). The system reached steady state in that duration of time. The rise in temperature in that small amount of time, before attainting steady state, was recorded from where the thermal conductivity of the system was calculated. To obtain measurements at

higher pressures, the system was pressurized using the same fluid which was injected to displace the existing fluid. These experiments involve five set-ups which are described below.

4.4.1. Setup 1: Measuring thermal conductivity of dry sand:

The pressure vessel was initially completely packed with silica sands with compression. A vacuum pump was then connected from the top of the vessel to evacuate the sands. The maximum achieved vacuum pressure was 25.5 inch Hg (The atmospheric pressure of Calgary was 26.5 inch Hg). After evacuating the sands, the thermal conductivity of the system is measured at room temperature. The pressure vessel with the probe is then immersed in a thermal bath filled with silicone oil and the thermal conductivities are measured at temperatures ranging from 21 ºC to 150 ºC. The silicone oil is heated using a coiled heater. The process flow diagram of the setup is given below in Figure 17.

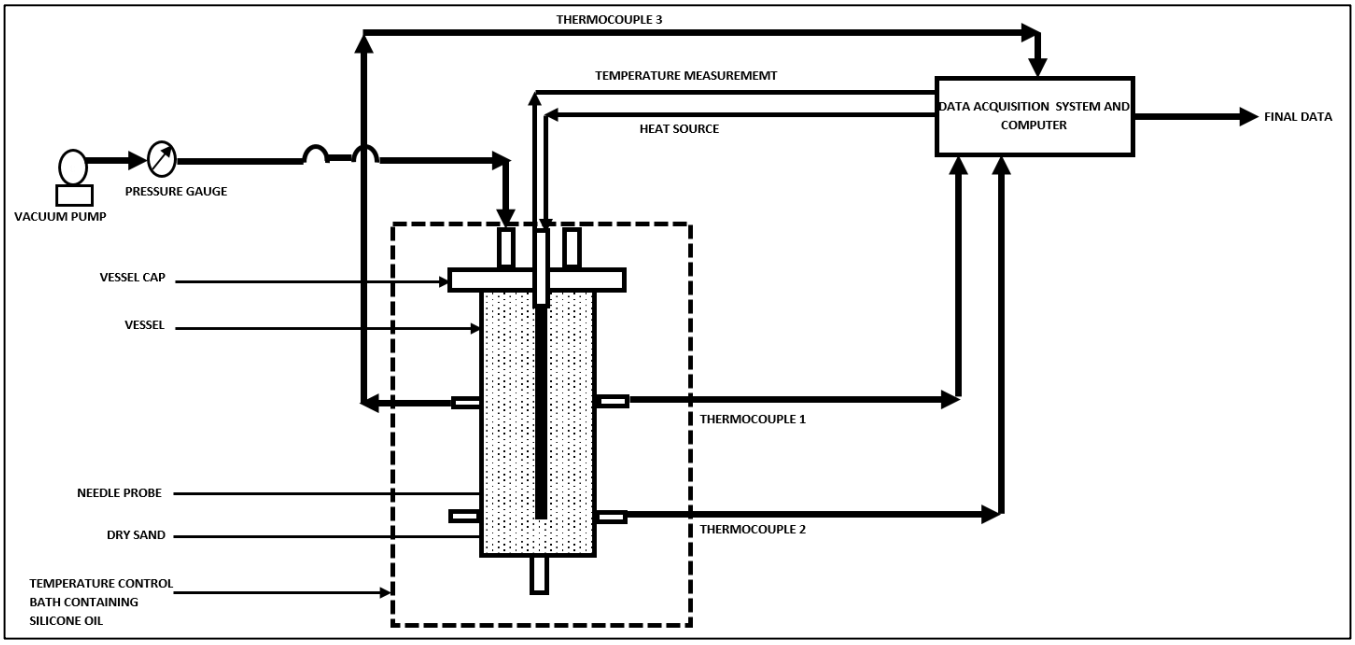

Fig. 17: Process flow diagram for Setup 1.

4.4.2. Setup 2: Measuring thermal conductivity of water saturated sand:

The evacuated sand pack was then saturated with demineralized (DM) water through a burette connected to the top of the vessel. The corresponding thermal conductivity was measured at room

temperature (21 ºC) and atmospheric pressure. The amount of water required to saturate the sand pack was recorded through the burette readings and was used to calculate the porosity of the sand pack [Appendix 5]. The porosity of the sand pack was 0.35.

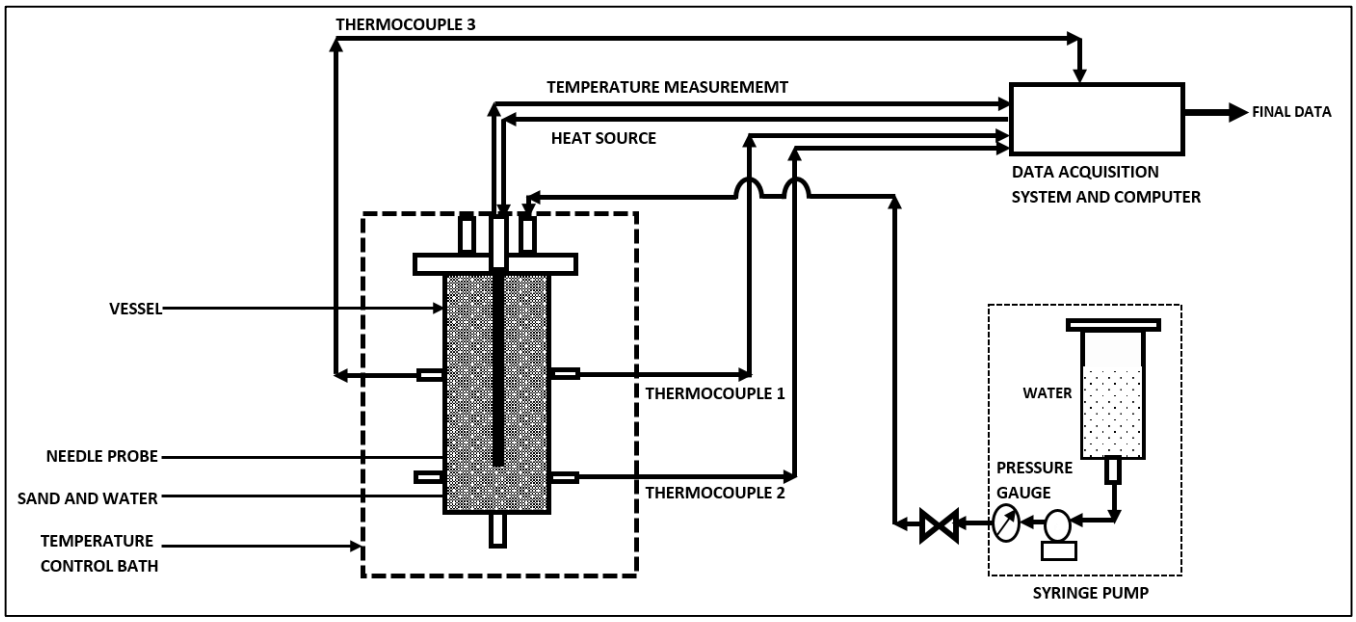

Fig. 18: Process flow diagram for Setup 2.

The burette was then disconnected and a vessel was connected to a syringe pump which was used to pressurize the system using water. A pressure gauge was connected at the pump outlet to monitor the system pressure. The pressure vessel along with its connections were then transferred to the thermal bath where the thermal conductivities of water saturated sands were measured at different temperatures ranging from 21 ºC to 150 ºC and pressures ranging from atmospheric pressure to 500 psig (34.5 barg). At temperatures 100 ºC or above, the measurements of thermal conductivities were avoided at lower pressures (below 150 psig (10.3 barg)) to prevent steam generation in the sand-pack. The process flow diagram of this experimental set-up is shown below in Figure 18.

4.4.3. Setup 3: Measuring thermal conductivity of sands saturated with water and bitumen:

Heated bitumen (at 70-80 ºC) was then introduced into the system at a constant flow rate of 1 ml/min and keeping a check on the pressure to not exceed beyond 25 psig (1.7 barg), through a transfer vessel to displace maximum water from the sand pack. Knowing the volume of water pumped to one side of the piston of the transfer vessel (from pump initial and final volume readings), bitumen volume that was pumped into the system and the water volume that was produced out of the sand-pack were monitored. After getting the maximum volume of displaced water, the irreducible water saturation in the pores was calculated. The total water imbibed initially into the sand pack gave the total volume of pores of the sand pack (V_{total}). The difference between the initial water volume and the volume of water displaced by bitumen injection was the volume of irreducible water remaining in the sand pack. This volume divided by the total pore volume was the irreducible water saturation, which came around 9.9%. So, at that point the sand pack was saturated with 90.1% bitumen and 9.9% water. Thermal conductivities of this arrangement were measured at different temperatures and pressures. The sand pack was pressurized using bitumen in the transfer vessel with other side of the piston filled with water and connected to the syringe pump.

The transfer vessel was then filled with water on both sides of the piston and water was injected into the system again to displace bitumen. The sand pack was kept at constant temperature (75 - 100 ºC) to displace the bitumen from the pores. The displaced bitumen samples were analysed using Dean Stark method [described in Section 4.8.] to get the percentage of bitumen and water in the collected sample. The saturations of bitumen and water was calculated by performing mass balance of the system. The calculations of bitumen saturations at different levels is presented in Appendix 7. It was found that after achieving 70% saturation of bitumen in the system, the temperature of the sand pack had to be increased higher than 100 ºC to displace further bitumen from the pores. The final bitumen saturation obtained in

this setup was around 48% bitumen and 52% water. The thermal conductivities of the sand pack were measured at each level of bitumen saturations and at temperatures ranging from 21 ºC to 150 ºC and pressures ranging from atmospheric pressure to 500 psig (34.5 barg). At temperatures 100 ºC or above, the measurements of thermal conductivities were avoided at lower pressures (below 150 psig (10.3 barg)) to prevent water vapor formation. The system was pressurized using water from the transfer vessel using the syringe pump. The process flow diagram for this setup is shown below in Figure 19.

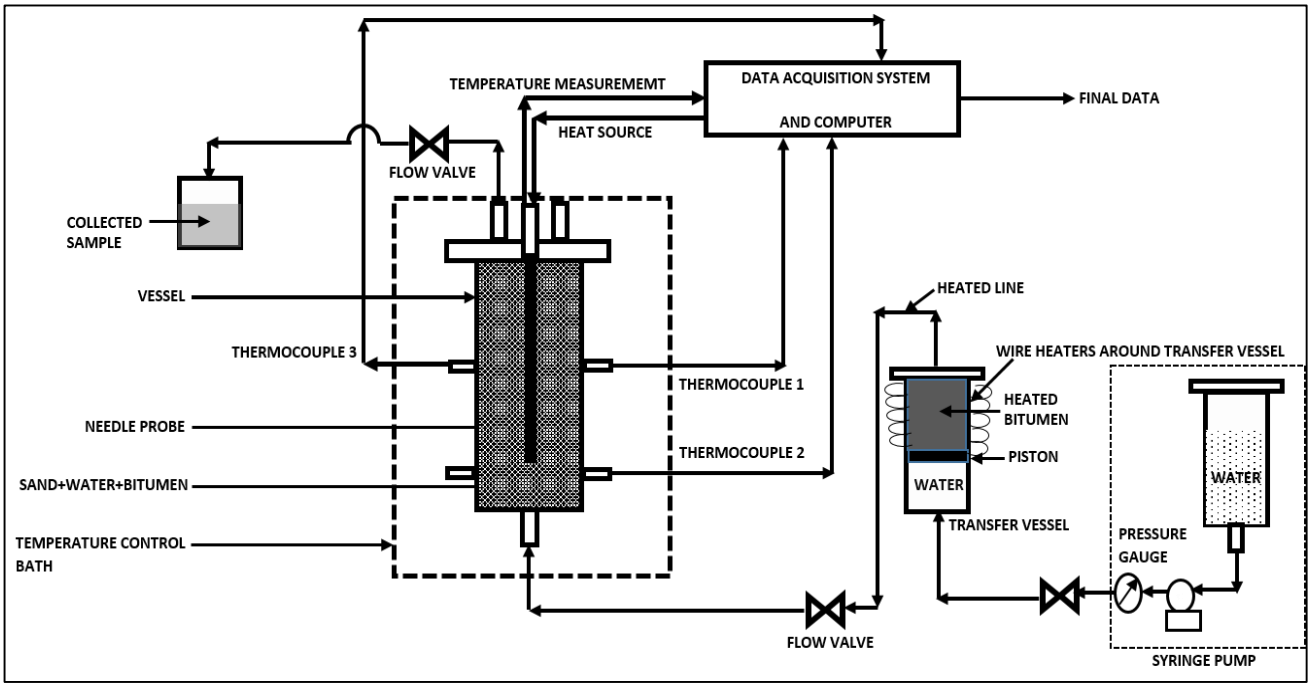

Fig. 19: Process flow diagram for Setup 3.

4.4.4. Setup 4: Measuring thermal conductivity of sands saturated with water, bitumen and NCG:

To ensure that the system contained the maximum bitumen saturation in the sand pack before injection of NCG (nitrogen), heated bitumen was again injected into the same sand-pack to displace the mobile water. The bitumen saturation after this step was 90.6% bitumen and 9.4% water. Nitrogen gas was then injected into the system to displace bitumen from the pores. The sand pack was heated to around 100 ºC so that the bitumen could be displaced from the pores. The sand pack was pressurized using nitrogen and depressurized (when needed) by opening the outlet valve. The nitrogen was introduced from

the top of the sand pack and the sample was collected from the bottom of the sand pack to make sure that maximum bitumen could be displaced from the sand pack. As the initial saturation of the pores in this setup contained only irreducible water, the displaced sample from the sand pack contained only bitumen. The gas saturations at each level were calculated by performing mass balance on the system using the weight of the displaced sample. The sand-pack was allowed to equilibrate overnight at elevated temperature after each change in bitumen saturation to give the capillary forces time to re-distribute the fluids within the pores. The calculation of the pore saturations at each level of gas saturation are attached with Appendix 8. The final saturation of pores in this setup was 32.8% bitumen, 57.8% nitrogen and 9.4% water. The thermal conductivities of the sand pack were measured at each levels of gas saturations and at temperatures ranging from 21 ºC to 150 ºC and pressures ranging from atmospheric pressure to 500 psig (34.5 barg). At temperatures 100 ºC or above, the measurements of thermal conductivities were avoided at lower pressures (below 150 psig (10.3 bar)) to prevent water evaporation in the system. The process flow diagram for this setup is given below in Figure 20:

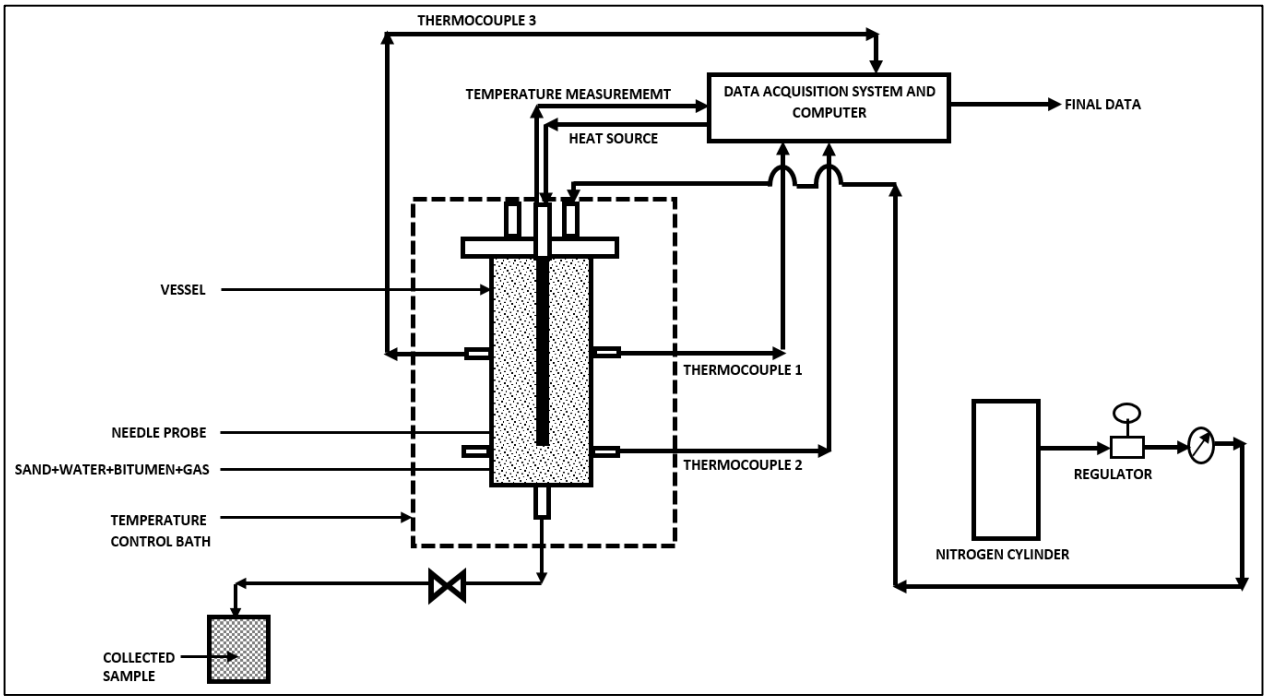

Fig. 20 : Process flow diagram for Setup 4.

4.4.5. Setup 5: Measuring thermal conductivity of sand saturated with bitumen, NCG and a surfactant solution:

In the final stage, a surfactant solution (Sodium Decylglucosides Hydroxypropylsulfonate) was injected into the system using a transfer vessel, to displace the bitumen and nitrogen. The thermal conductivities were measured at different saturations of the surfactant solution. The saturations of surfactant were measured by performing mass balance on the system using the weight of the displaced product. The saturation of fluids at this stage was 32.8% bitumen, 17.2% nitrogen and 50.0% surfactant solution, assuming that the injected surfactant solution displaced out the connate water. Nitrogen was then injected into the system to displace surfactant from the pores and create a foam in the pores of the sand-pack. Thermal conductivities were measured at different saturations of surfactant solution and nitrogen. The final saturation was 31.6% bitumen, 54.6% nitrogen and 13.8% surfactant solution. In this way, the thermal conductivities of the system were obtained at different qualities of foam. The calculations of different saturations of surfactants and nitrogen are attached with Appendix 9. The process flow diagram of this set up is shown in Figure 21:

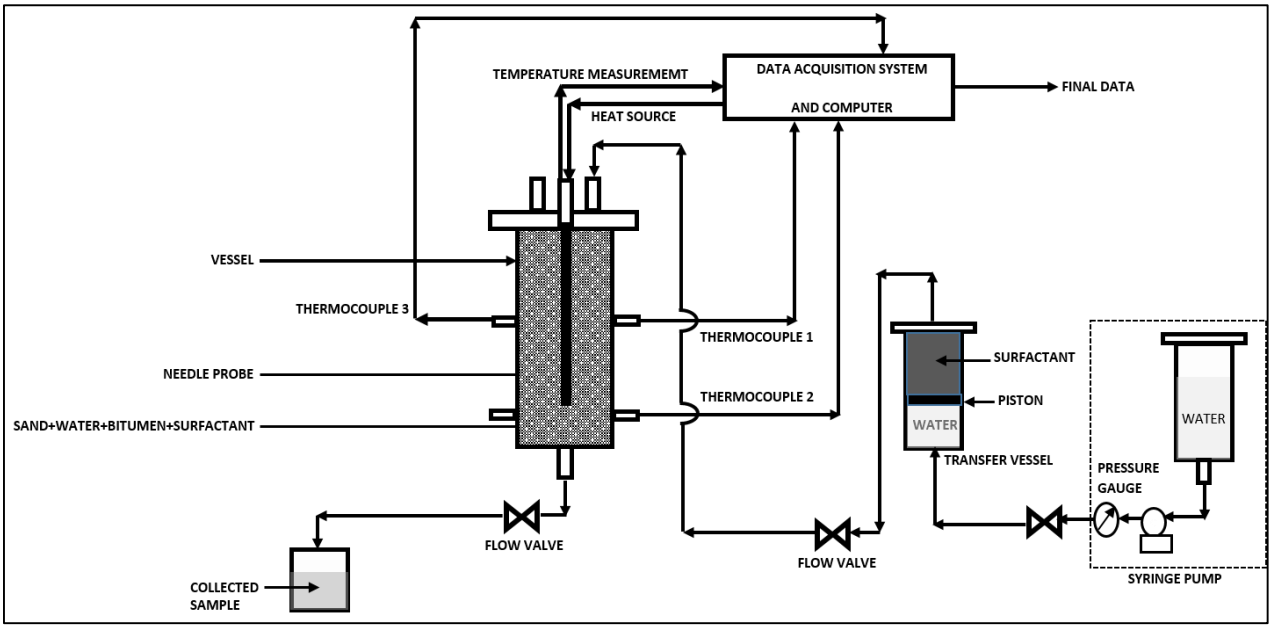

Fig. 21: Process flow diagram for Setup 5.

4.5. Calibration of the needle-probe TP02

The needle-probe was calibrated following the ASTM D5334-14, ASTM D5930-97 and IEEE 442-1981 standards using Glycerol. The calibration procedure is explained in details in the TP02 user manual [36, page 52]. The expected thermal conductivity of Glycerol is 0.29 W/mK (36, page 52) and the obtained thermal conductivity from the calibration experiment was 0.27 W/mk. The calibration sample calculation is attached with Appendix 6.

4.6. Data analysis

The LoggerNet software generated an excel file in which the temperature at the hot and cold joints, temperature of Pt1000, current and voltage supplied were tabulated at each interval of time (0.5 secs). These data were used to calculate the power input to the needle-probe and subsequently the temperature difference, using equations 4.1, 4.4, 4.5 and 2.16. The rise in temperature was plotted with logarithm of time. The inverse of the slope of linear portion of the graph gave the thermal conductivity of the medium as shown in Figure 10. A sample data sheet obtained from the LoggerNet software along with the calculation sheet are attached as Appendix 4 and Appendix 10.

4.7. Experiment set points and parameters

Parameters	Set point / Range
Temperature	21-150 ºC with 25 ºC increment
Pressure	0 psig to 500 psig with 100 psig increment
Pump pressure for bitumen injection	25 psig (1.72 barg)
Pump flow rate for bitumen injection	1 ml/min
Temperature of bitumen injection	70-100 ºC

Needle-probe heater power level	Medium / 1 VDC
Transition time for measurement	40 secs

4.8. Dean-Stark extraction method

Dean-Stark method was used to measure the concentrations of bitumen and water in the collected product sample. Dean-Stark analysis is a method for the measurement of fluid concentrations in a sample (bitumen-water) by distillation extraction using another solvent. The Dean-stark traps can be of two types- one with using a solvent of density lower than water or with a density higher than water. To analyse the product sample in this study, a solvent of lower density than water (toluene, density 867 kg/m^3) was used. The figure 22 shows a typically used Dean-Stark apparatus:

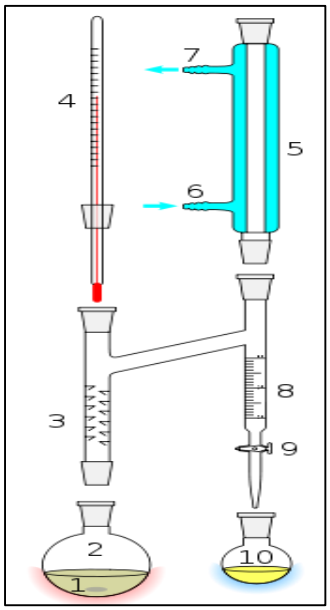

1. Stirrer bar/ anti-bumping granules
2. Still pot
3. Fractionating column
4. Thermometer/Boiling point temperature
5. Condenser
6. Cooling water in
7. Cooling water out
8. Burette
9. Tap
10. Collection vessel

Fig.22: Dean–Stark apparatus setup for an azeotrope with a solvent whose density is less than that of water [31].

The sample was first dissolved in toluene and then the resulting mixture (bitumen-water-toluene) was boiled in the still pot. Boiling chips in the still pot helped in the formation of bubbles of solvent vapor. The solvent vapor was then passed onto the condenser where cooling water was circulated to condense the solvent vapor. The condensed solvent was then collected in a distillation trap. In the distillation trap the two immiscible liquids (water and toluene) were separated in two layers (toluene on top of water). When the total volume of the two layers reached the level of the side-arm, toluene being less dense, glided back to the still pot and the water remained in the trap. When the level of water reached the level of the side arm, it indicated that the trap was completely full and the water was drained into the collection vessel. This cycle of evaporation, condensation and collection was continued till the water production came to a halt. Thus the total weight of water in the sample could be measured. As the initial weight of the sample was also known, the weight of bitumen could also be estimated.

4.9. Possible errors in the measurements.

The probe is designed by assuming only radial heat conduction process occurs during the measurement, and there is no other temperature variation from other sources (axial conduction, convection, radiation). For this the probe should be very stable while taking the measurements, otherwise it can lead to errors in the results. Another source of error can be from evaporation, melting or phase change of liquids surrounding the needle probe due to excess heating. To prevent this it is advisable to keep low levels of heating. If any phase change occurs, it can also alter the contact resistance between the probe and the surrounding medium, which can also lead to possible errors. This also increases the transition time of the measurement as discussed earlier. To get the most accurate graphs it’s better to keep the lowest heating power and least measurement time. If there is thermal convection at high temperature in the fluids of the medium, it can also generate errors in the data.

Another source of error could be the visual selection of the linear portion of the thermal conductivity graph. To get accurate measurements, each experimental steps were repeated at least 3-4 times. The standard deviation for each measurements are calculated with 95% confidence interval using Student's t-test method. This is explained in details in Section 5.1.

Chapter 5: Results and Discussions

The experimental results for the sand pack at evacuated condition and also at different saturations of water, bitumen, nitrogen and surfactant are presented in this chapter. The effect of temperature and pore fluid saturations on thermal conductivities of the sand pack are analyzed and discussed. The thermal conductivities of the sand pack at different pressures for every saturations and temperatures were also measured but very minimal effects were observed, so average values of thermal conductivities for the pressure range (14.6 psia to 514 psia) are considered in presenting the effect of temperature.

An attempt is made to develop a correlation of effective thermal conductivity of bitumen, water and nitrogen saturated sand pack system as a function of temperature and fluid concentrations by comparing the measured results with literature models. The correlation results are discussed in the later part of this chapter.

5.1. Experimental Results

The errors in the experimentally derived data are estimated by measuring the standard deviation for each “data point” and the “Student’s t-test” method is used to estimate the standard deviation of each “data set” with 95% confidence of probability on the measured data. Here, an individual “data point” indicates the measured thermal conductivity of the sand pack at a particular “pore fluid saturation” and at a particular temperature and pressure. The standard deviation of each “data point” is calculated based on the number of times the measurements were repeated to confirm the reproducibility of the data. In this analysis, “data set” indicates a sample of thermal conductivities measured at a particular “pore fluid saturation”, at a particular temperature and at different pressures (14.6 psia (1 bar) to 514 psia (35.5 bar)). It is confirmed from this analysis that the standard deviations of the averaged measurements at all pressures are similar to the standard deviation of repeated measurements at a fixed pressure, thus justifying

the elimination of pressure factor from the correlation of effective thermal conductivity of the sand pack. This analysis also gives an idea about the extent of errors in the experimental measurements.

The "Student's t-test" or "t-test" is a statistical hypothesis tool in which the test sample follows the "Student's t-distribution under "null hypothesis" [38]. "Student's t-distribution" or "t-distribution" is a probability distribution that is developed while estimating the mean of a normally distributed sample when the sample size is small and the standard deviation of the population is not known [38]. The t-distribution is a bell-shaped curve that looks similar to normal distribution curve with the exception of having a heavier tail that helps in generating values lying further away from mean. If a sample is picked from a normal distribution, then the t-distribution with degrees of freedom (sample size (n) -1) can be defined as the distribution of the position of the sample relative mean to the true mean, divided by the standard deviation of the sample, times the standardizing factor. Thus, t-distribution can be used to develop the confidence interval of the true mean [38]. "Null hypothesis" is a statistical statement used when it is considered that the different measured data in a sample has no correlations. The equation for the "Student T-score" used to estimate the 95% confidence interval of the measured data is given below [39]:

$$Confidence\ interval = X_m \pm t\frac{\sigma}{\sqrt{n}} \qquad \text{Equation 5.1.}$$

Where, X_m is the mean of the sample, t is the t-score, σ is the standard deviation, n is the sample size. The t-score for a particular confidence interval and degrees of freedom (n-1) is calculated using the excel function or can be calculated using online available calculators. The 95% confidence interval calculated for each data point, gives the error range for each measured data, with 95% probability that the true value will lie in the calculated range.

5.1.1. Effective thermal conductivity of evacuated sand pack:

The measurements for the thermal conductivity of evacuated sand pack at different temperatures are provided in Table 2. The sand pack was evacuated till 25.5 inch Hg of vacuum when the atmospheric pressure of Calgary was 26.5 inch Hg.

Table 2: The effective thermal conductivity data for evacuated sands system:

K_{eff} (W/mK)	Temp. (deg C)	Vaccum Pressure (inch Hg)	Pore saturation			Standard Deviation	Number of Runs n	t-value (two tailed) for probability level 0.05	95% confidence interval	Confidence interval (%)
			Bitumen saturation (%)	Water saturation (%)	Nitrogen saturation (%)					
0.162	25	25.5	0	0	0	0.012	3	3.182	0.021	13.1
0.152	50	25.5	0	0	0	0.007	3	3.182	0.013	8.2
0.143	100	25.5	0	0	0	0.005	3	3.182	0.010	6.8
0.133	150	25.5	0	0	0	0.010	3	3.182	0.017	13.1

The 95% confidence interval or standard deviation for the above set of data is in the range of $\pm$6.8% to $\pm$13.1%. The relationship of the effective thermal conductivity (ETC) of the evacuated sands observed at different temperatures is shown in Figure 23. The ETC of the evacuated sand pack was found to be slightly decreasing with increase in temperature, which was also stated earlier in the literature [24].

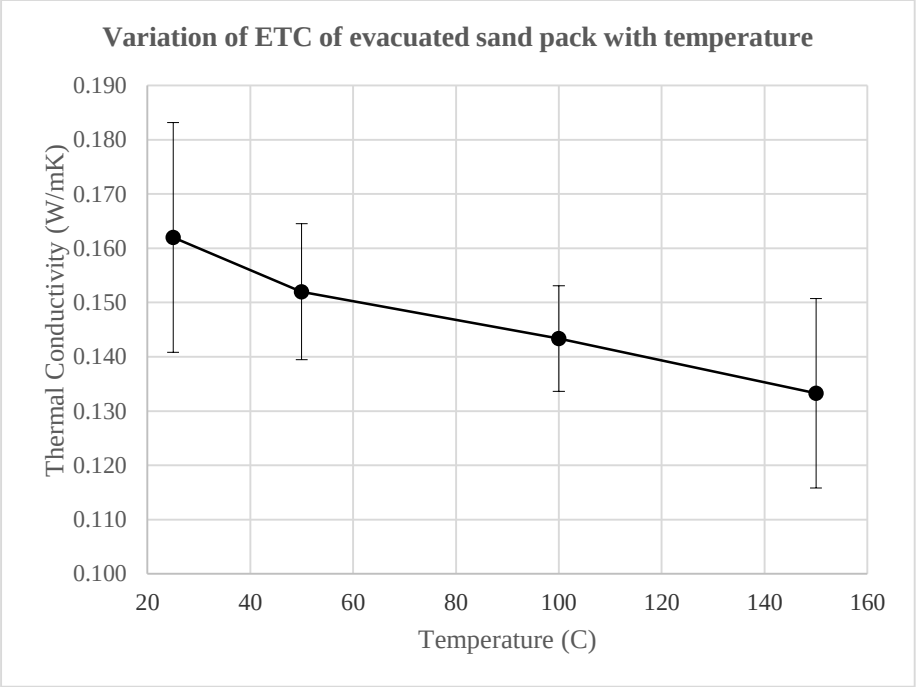

Fig. 23: Effective thermal conductivity of evacuated sand pack.

With increase in temperature, the lattice vibrations in the solids increase which enhance the interspatial distance between the molecules, and as a result ETC of the medium decreases which can be seen in Figure 23.

5.1.2. ETC of Sand pack saturated with water:

For the water saturated sand pack, the effective thermal conductivity of the system, didn't show much variation with pressure as water is an incompressible fluid. Thus, the average thermal conductivity values taken at different pressures are considered. The standard deviations of measurements at different pressures are shown in details in Appendix 1. The measured data for the ETC of the water saturated sand pack at different temperature is provided in Table 3.

Table 3: Effective thermal conductivity data for water saturated sands:

K_{eff} (W/mK)	Temp. (C)	Pore saturation			Standard Deviation	Number of Runs n	t-value (two tailed) for probability level 0.05	95% confidence interval	Confidence interval (%)
		Bitumen saturation (%)	Water saturation (%)	Nitrogen saturation (%)					
1.110	50	0	100	0	0.231	12	2.179	0.145	13.1
1.106	75	0	100	0	0.210	12	2.179	0.132	11.9
1.087	100	0	100	0	0.252	12	2.179	0.159	14.6
0.900	125	0	100	0	0.216	15	2.131	0.119	13.2
0.808	150	0	100	0	0.078	10	2.228	0.055	6.8

The 95% confidence interval range for the effective thermal conductivities is found to be in the range of $\pm$6.8% to $\pm$14.6%.

The ETC of the water saturated sand pack is found to be decreasing with temperature as is shown in Figure 24.

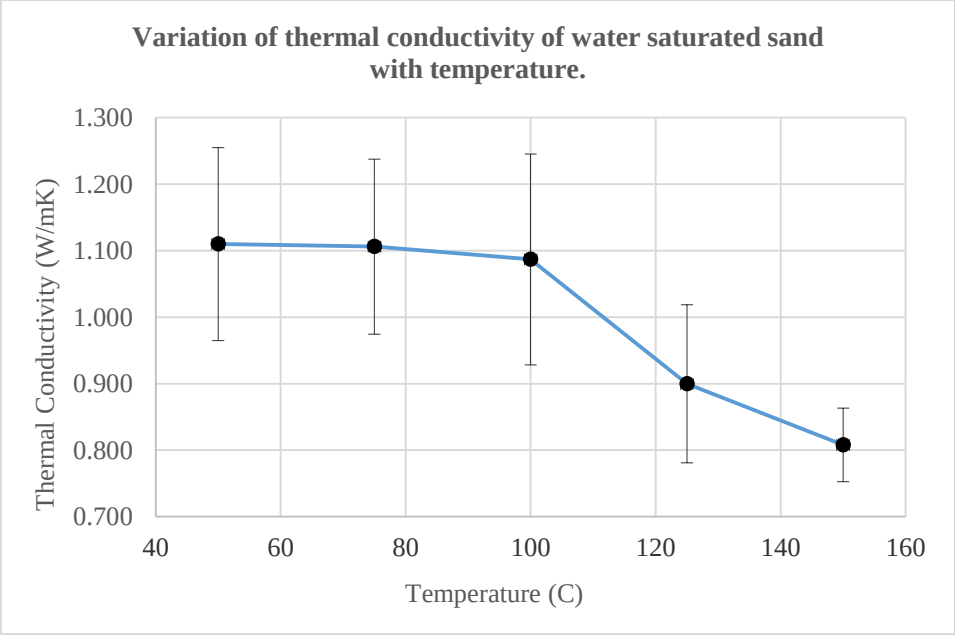

Fig. 24: Effective thermal conductivity of water saturated sand pack.

This trend is quite similar to the observations recorded by Hanafi and Karim [26] in the literature. The ETC of the medium slightly decreases with temperature till around 100 ºC and sharply drops after that. The thermal conductivity of pure water decreases after 130 ºC [39], which can reduce the overall thermal conductivity of the system. If the thermal conductivity data of the evacuated sand pack (shown in Fig.23) is compared to the thermal conductivity of water saturated sand pack (shown in the Fig. 24), where in the latter case the thermal conductivity is much higher (around 7 times higher), it can be concluded that the water saturation plays a significant role in enhancing the ETC of the sand pack.

5.1.3. Sand pack saturated with bitumen and water:

The sand pack saturated with bitumen and water also didn't show significant variation with pressure and thus the mean thermal conductivity was calculated for each set of pressure range (14.6 psia to 514.6 psia). The thermal conductivity values for this system at different temperatures and fluid (bitumen and water) saturations are shown in Table 4. The standard deviation figures at each pressure range are shown in details in Appendix 1. In Table 4, the pressure averaged values are shown with their respective standard deviations.

Table 4: Effective thermal conductivity data for bitumen and water saturated sands:

K_{eff} (W/mK)	Temp (C)	Pore saturation			Standard Deviation	Number of Runs n	t-value (two tailed) for probability level 0.05	95% confidence interval	Confidence interval (%)
		Bitumen saturation (%)	Water saturation (%)	Nitrogen saturation (%)					
0.626	41	90.1	9.9	0	0.051	12	2.179	0.032	5.2
0.621	75				0.065	12	2.179	0.041	6.6
0.611	100				0.063	12	2.179	0.039	6.5
0.612	125				0.059	15	2.131	0.033	5.3
0.653	150				0.027	10	2.228	0.019	2.9
0.988	41	73.5	26.5	0	0.145	14	2.145	0.083	8.4
0.982	75				0.140	11	2.201	0.093	9.5
0.953	100				0.069	14	2.145	0.040	4.2

K_{eff} (W/mK)	Temp (C)	Pore saturation			Standard Deviation	Number of Runs n	t-value (two tailed) for probability level 0.05	95% confidence interval	Confidence interval (%)
		Bitumen saturation (%)	Water saturation (%)	Nitrogen saturation (%)					
0.935	125				0.077	15	2.131	0.043	4.6
0.927	150				0.160	13	2.160	0.096	10.4
0.905	41	70.4	29.6	0	0.036	10	2.228	0.025	2.8
0.904	75				0.105	17	2.110	0.054	6.0
0.836	125				0.128	15	2.131	0.071	8.4
0.821	150				0.121	15	2.131	0.066	8.1
0.894	41	67.8	32.2	0	0.127	15	2.131	0.070	7.8
0.836	75				0.099	18	2.101	0.049	5.9
0.812	100				0.089	10	2.228	0.063	7.7
0.797	125				0.136	13	2.160	0.082	10.2
0.789	150				0.105	11	2.201	0.069	8.8
0.684	41	48.1	51.9	0	0.087	18	2.101	0.043	6.3
0.662	75				0.085	12	2.179	0.053	8.1
0.642	100				0.091	10	2.228	0.064	10.0
0.647	125				0.080	10	2.228	0.056	8.7
0.640	150				0.076	11	2.201	0.050	7.9

The 95% confidence interval range or the standard deviation for the effective thermal conductivities is found to be in the range of $\pm$2.8% to $\pm$10.4%. The variation of thermal conductivity of the system with temperature at different bitumen saturations can be observed from Figure 25.

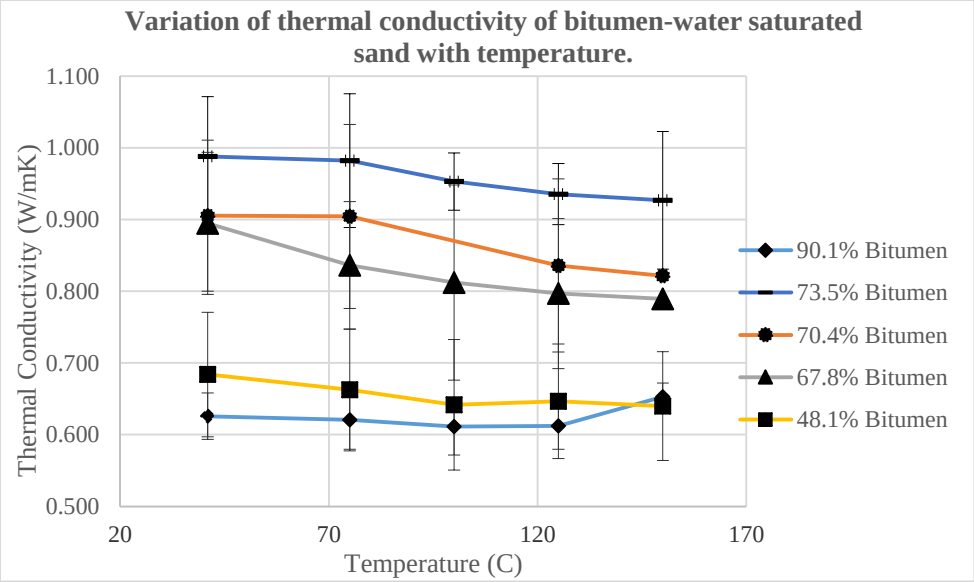

Fig. 25: Effect of temperature on effective thermal conductivity of bitumen and water saturated sand pack.

Another representation of Table 4 is to plot the effect of bitumen saturation on the thermal conductivity of the sand pack at different temperatures as is shown in Figure 26. As the data points in the Figure 26 is quite close to each other, the error bars are not shown here to avoid confusions but error bar for each data point can be read from Figure 25.

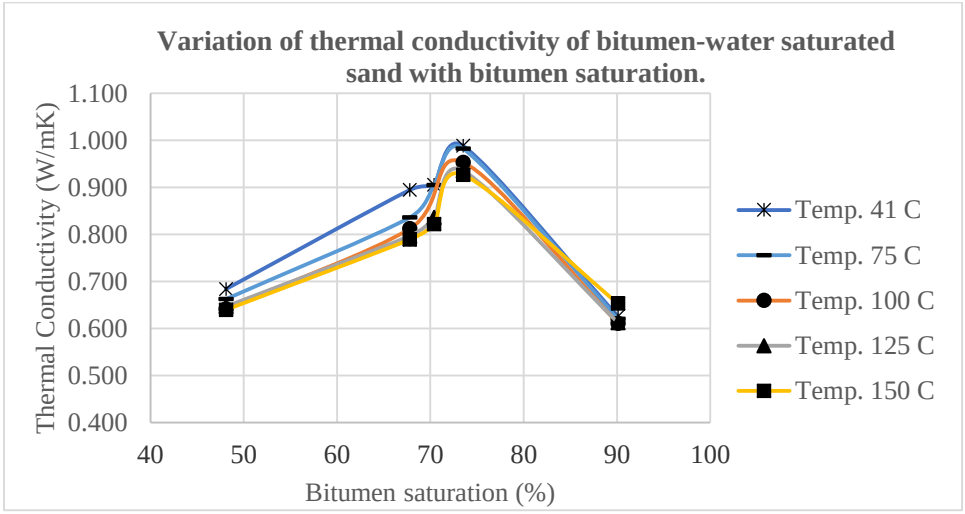

Fig. 26: Effect of bitumen saturation on effective thermal conductivity of bitumen and water saturated sand pack.

Overall, the thermal conductivity of the system is found to be decreasing with temperature which is similar to trends observed by Hanafi and Karim [26, 69]. The thermal conductivity of bitumen was found to be decreasing with temperature in literature [26], a similar trend is observed in the bitumen-water saturated sands as well. The thermal conductivity values at the intermediate saturations of bitumen in pores (73.5% to 67.8%) were expected to increase with decrease in bitumen saturation as thermal conductivity of bitumen is lower than that of water. But a different trend is observed here where the thermal conductivity of the sand pack decreases with decrease in bitumen saturation. One possible reason behind this observation, is that, the water used to displace bitumen fingered through the pack giving rise to non-uniform saturations along the sand pack. Although, these trends are similar to the trends observed by Hanafi and Karim [69], the thermal conductivity data at the intermediate saturations of bitumen are not reliable. The irreducible water saturation (90.1% bitumen) and the residual oil saturation (48.1% bitumen) were established after reaching steady-state saturation conditions and are relatively free from fingering errors. Between them, the thermal conductivity decreased with increase in bitumen concentration in pores and these two values are taken for developing correlations.

5.1.4. Sand pack saturated with bitumen-water-nitrogen:

The thermal conductivity data of the sand pack saturated with bitumen, water and nitrogen also showed minimal variation with pressure in most of the sets of measurements. Although, the thermal conductivity of gas increases with pressure, the value of gas thermal conductivity is much smaller compared to that of the liquids. It makes the contribution of gas phase to the ETC of the pack, relatively very small, thereby masking the effect of pressure. The pressure independency of gas filled pores on effective thermal conductivity of a porous system was also confirmed by Tsotsas and Martin [30] and is discussed in details in Section 3.2. The standard deviation figures at each pressure range are shown in

details in Appendix 2.The measurements indicating the thermal conductivities of the sand pack at different temperatures and pore fluids saturations are shown in Table 5.

Table 5: Effective thermal conductivity data for bitumen, water and nitrogen saturated sands:

K_{eff} (W/mK)	Temp (C)	Pore saturation			Standard Deviation	Number of Runs n	t-value (two tailed) for probability level 0.05	95% confidence interval	Confidence interval (%)
		Bitumen saturation (%)	Water saturation (%)	Nitrogen saturation (%)					
0.836	85	67.8	32.2	0	0.127	15	2.131	0.070	8.3
0.812	100				0.099	18	2.101	0.049	6.0
0.797	125				0.089	10	2.228	0.063	7.9
0.789	150				0.136	13	2.160	0.082	10.3
0.783	85	62.3	9.4	28.3	0.121	18	2.101	0.060	7.6
0.736	100				0.118	11	2.201	0.078	10.7
0.722	125				0.071	13	2.160	0.043	5.9
0.693	150				0.208	10	2.228	0.147	21.1
0.715	85	46	9.4	44.6	0.111	13	2.160	0.066	9.3
0.706	100				0.170	14	2.145	0.097	13.8
0.639	125				0.067	12	2.179	0.042	6.6
0.594	150				0.101	13	2.160	0.061	10.2
0.607	85	32.8	9.4	57.8	0.063	12	2.179	0.040	6.6
0.581	100				0.102	11	2.201	0.068	11.7
0.574	125				0.084	11	2.201	0.056	9.7
0.518	150				0.107	15	2.131	0.059	11.4

The 95% confidence interval range or the standard deviation for the effective thermal conductivities is found to be in the range of $\pm$5.9% to $\pm$21.1%. The first set of data in Table 5 indicates the thermal conductivity of the system when nitrogen was not present in the system. This data set is taken from Table 4 to compare the effect of addition of nitrogen gas to the system. It is clear from Table 5 that, at almost same bitumen concentration, addition of nitrogen slightly decreased the effective thermal conductivity of the system. This reduction was expected, because nitrogen has a lower thermal conductivity than water and bitumen. Overall, the thermal conductivity of the system didn't show a significant change after the addition of nitrogen, except that the bitumen displacement from the sand pack

was much faster and could be done at lower temperatures (below 100 ºC) when nitrogen was added to the system. The graphs showing the effects of temperature and nitrogen saturation on the effective thermal conductivity of the system are shown in Figures 27 and 28.

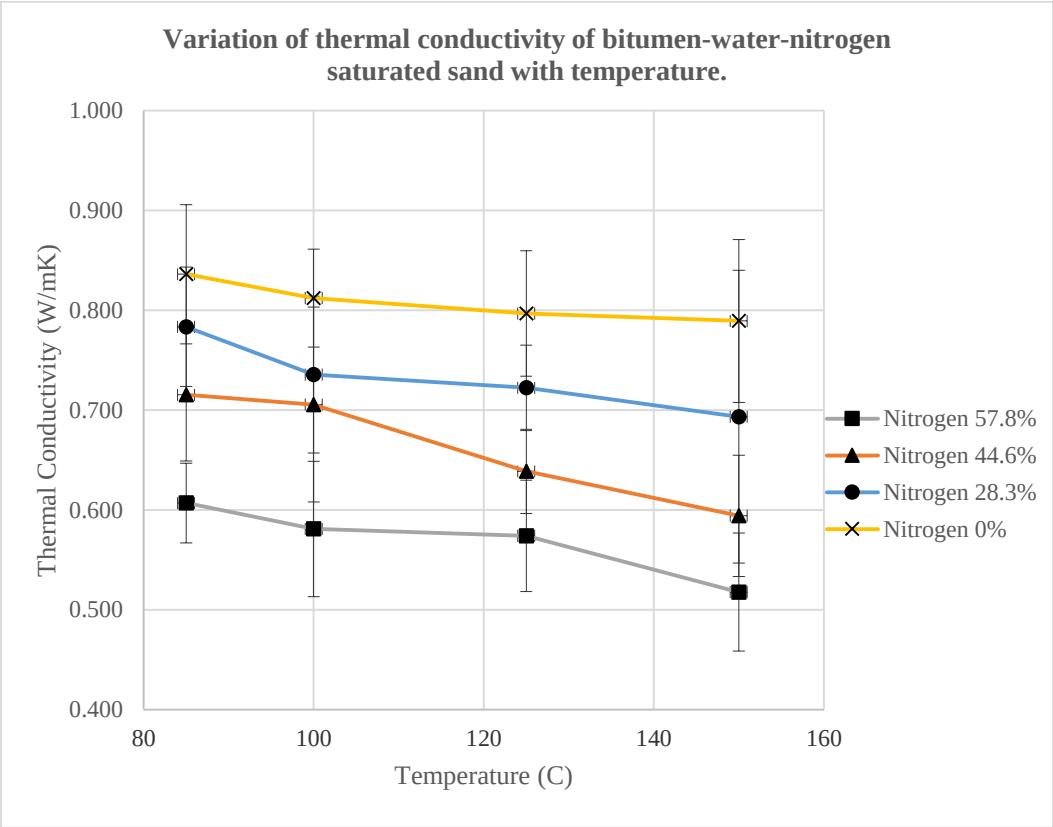

Fig.27: Effect of temperature on effective thermal conductivity of bitumen, water and nitrogen saturated sand pack.

It can be inferred from Figure 27 that thermal conductivity of the system decreased significantly with temperature. The slopes of the trends of Figure 27, are found to be steeper compared to the slope of the bitumen-water system (Figure 25). In this case, when nitrogen gas gets dissolved in bitumen, it increases its volume and successively the density of the mixture gets reduced. Also, with the increase in temperature, the density of liquid mixture decreases. As discussed in Section 2.3.2, the thermal conductivity of liquids decrease when the density of the medium decreases, which can be observed here.

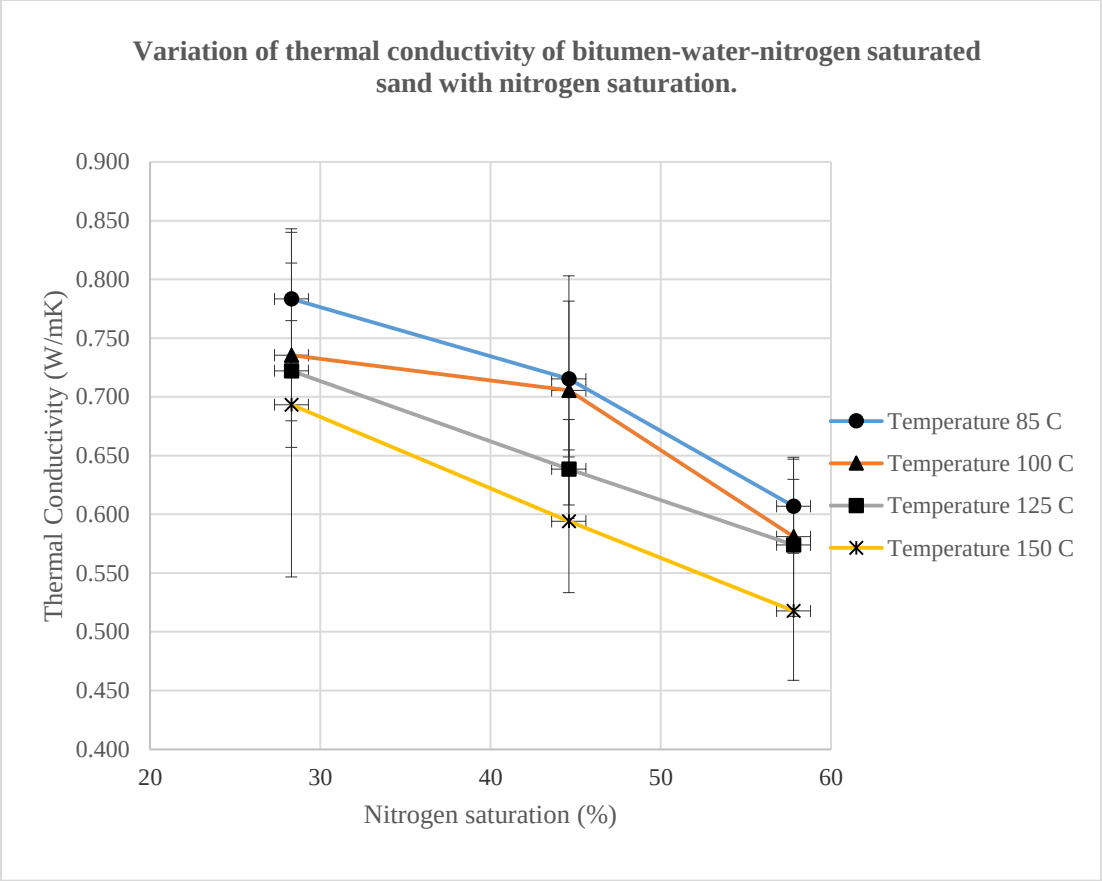

Fig. 28: Effect of nitrogen saturation on effective thermal conductivity of bitumen, water and nitrogen saturated sand pack.

From Fig. 28, it can be deduced that with the addition of nitrogen gas, the thermal conductivity dropped consistently. This is because the thermal conductivity of nitrogen gas is much lower compared to the thermal conductivities of bitumen and water, which led to the reduction of the overall thermal conductivity of the system. Also, as discussed above, nitrogen reduces the density of bitumen-nitrogen mixture which also leads to a decline in the effective thermal conductivity of the medium.

5.1.5. Sand pack saturated with bitumen-water-nitrogen-surfactant:

The effective thermal conductivity (ETC) of the sand pack saturated with bitumen, nitrogen and surfactant solution are plotted at different surfactant saturations keeping the bitumen saturation constant

as shown in Figure 29. The measurements for this set of data are shown in Table 6. There was irreducible water in the system which was a part of the surfactant solution.

Table 6: Effective thermal conductivity data for bitumen, nitrogen and surfactant solution saturated sands:

K_{eff} (W/mK)	Temp (C)	Pore saturation			Standard Deviation	Number of Runs n	t-value (two tailed) for probability level 0.05	95% confidence interval	Confidence interval (%)
		Bitumen saturation (%)	Nitrogen saturation (%)	Surfactant solution saturation (%)					
0.615	75	32.8	48.5	18.7	0.001	3	3.18	0.001	0.2
0.810	75	32.8	39.3	28.0	0.014	5	2.57	0.016	2.0
0.964	75	32.8	30.0	37.2	0.001	4	2.78	0.001	0.1
0.903	75	32.8	20.7	46.5	0.004	4	2.78	0.005	0.6
0.798	75	32.8	17.2	50.0	0.001	4	2.78	0.001	0.2
0.661	75	32.1	40.0	27.8	0.006	4	2.78	0.008	1.2
0.672	75	31.7	46.3	22.0	0.001	3	3.18	0.001	0.2
0.662	75	31.6	54.5	13.9	0.001	4	2.78	0.001	0.2

The 95% confidence interval range or the standard deviation for the effective thermal conductivities is found to be in the range of $\pm$0.1% to $\pm$2%. The ETC of the medium is found to be increasing till 37.5% of surfactant saturation and then it started to decline when further surfactant was added to the system. Initially the injection of surfactant solution simply displaced the gas out, which increased the ETC due to increasing water phase saturation. When the surfactant concentration was increased beyond 37.5%, the foam formation began and it started to decrease the ETC of the medium. It is likely that the distribution of fluid phase changed when the saturation of surfactant solution became high enough. Interestingly, when the surfactant solution concentration was decreased by injecting gas to displace the surfactant solution, foam formation continued and the ETC remained low. For example, the

ETC at 28% surfactant saturation was 0.810 W/mK during the initial surfactant solution injection but it was only 0.661 at 27.8% surfactant saturation during the displacement of surfactant solution by gas injection. It shows that the foam formation can have significant effect on the effective thermal conductivity of the system.

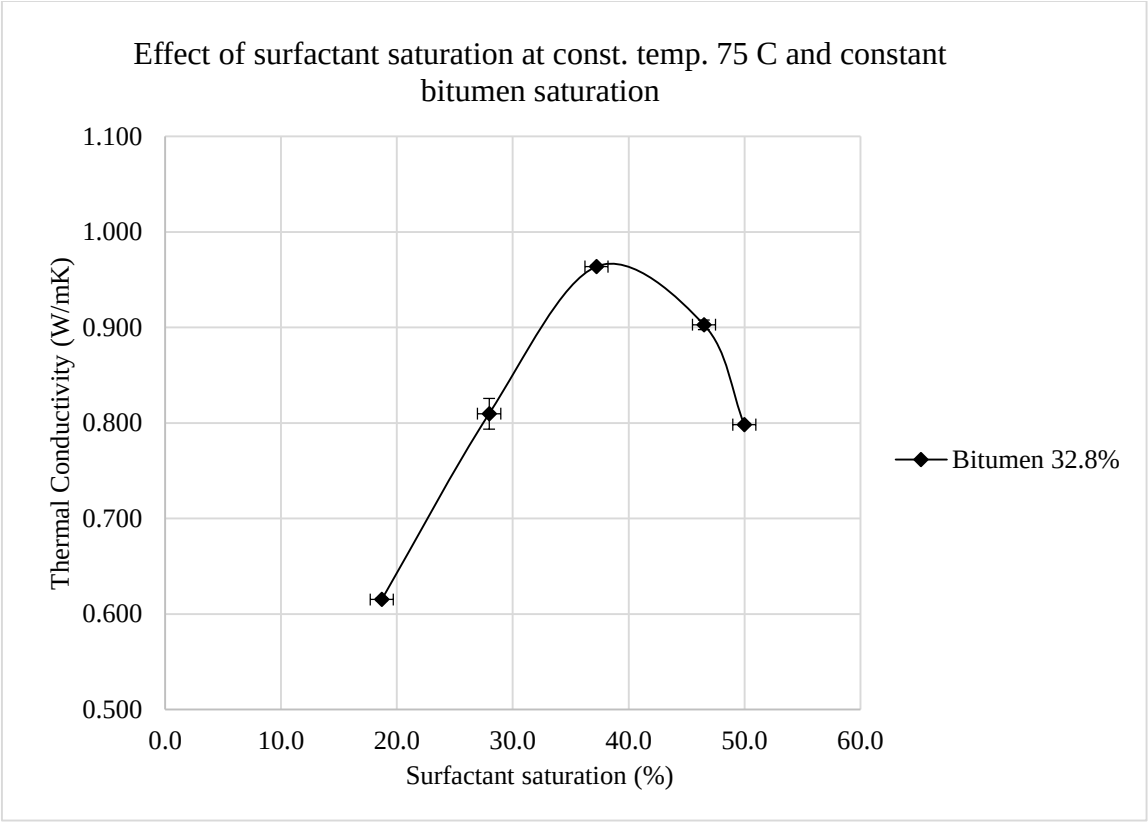

Fig.29: Effect of surfactant on ETC of the sand-pack saturated with bitumen-nitrogen-surfactant solution.

All the experimental data are listed in Appendix 1 and 2.

5.2. Correlations on effective thermal conductivity of the sand pack

An approach is made to develop correlations of effective thermal conductivity of the sand pack having three phase saturations (bitumen, water and nitrogen gas) with temperature. The experimental results for each set of sand pack, i.e. evacuated sand, water saturated sand, bitumen-water saturated sand

and bitumen-water-nitrogen saturated sand, are compared with common thermal conductivity models to get the thermal conductivity equations for sand, water, bitumen and nitrogen respectively, at different temperatures. The thermal conductivity equations of these components are tallied with thermal conductivity data available in the literature, which confirmed the usability of the models. The experimental data are correlated with existing models using "Coefficient of Determination" or "R squared or R^2" regression analysis. For a data set of "n" number of variable, if y_1, y_2, y_3……y_n are the observed data (experimental data) and f_1, f_2, f_3……..f_n are the predicted data from the model, then R^2 value can be determined from the following equation [40] :

$$R^2 = 1 - \frac{\Sigma(y_i - f_i)^2}{\Sigma(y_i - y_m)^2} \qquad \text{Equation 5.2.}$$

y_m is the mean of the observed data and $\Sigma(y_i - f_i)^2$ is known as the residual sum of squares and $\Sigma(y_i - y_m)^2$ is known as the total sum of squares. As, R^2 value approaches unity or 1, it indicates a better fit of predicted data with the experimental data [40].

5.2.1. Estimating thermal conductivity of pure sand:

The thermal conductivity of sand was estimated from the experimental data of evacuated sand using the "**Parallel model**" (Eq. 2.17). The thermal conductivity equation of sands obtained from Parallel model, was compared with literature [41]. The thermal conductivity calculated from the equation closely resembled the thermal conductivity of sand grain given in the literature [41]. Figure 30 shows a plot of the predicted thermal conductivity vs the observed thermal conductivity.

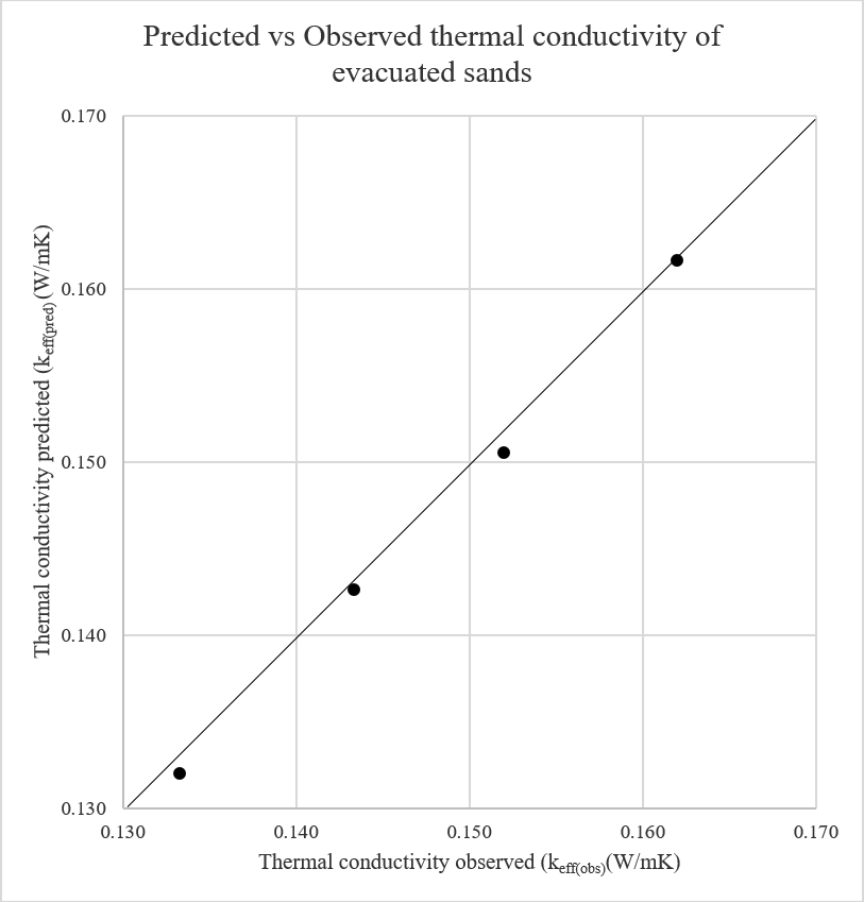

Fig. 30: Predicted vs Observed effective thermal conductivity of evacuated sands using "Parallel model".

The R^2 value for the parallel model was 0.99 with a maximum error of 0.97% and mean error 0.67%. The detailed calculation of this set of data is shown in Appendix 3. The thermal conductivity of sand grains obtained from this model is given below:

$$k_s = -0.0003T + 0.2534 \qquad \text{Equation 5.3.}$$

Where T is the temperature of the system in ºC. According to the literature [41], the thermal conductivity of sand grains should lie between 0.25 to 0.27 W/mK at 25 ºC and as per the equation 5.3, it came around 0.249 W/mK.

5.2.2. Estimating thermal conductivity of sands saturated with bitumen and water:

The thermal conductivity equation of sands (Equation 5.3) is used to estimate the ETC of sands saturated with bitumen and water. Several models were used to fit into the experimental data, but the **Maxwell-Eucken's** model [17] was found to be most closely predicting the ETC of the system. The thermal conductivity equation of water that is used from the literature is given below [39]:

$$k_{H2O} = -0.00000744T^2 + 0.00188T + 0.5636 \qquad \text{Equation 5.4.}$$

Where T is the temperature of the system in ºC.

The Maxwell-Eucken's model equation is used to predict the effective thermal conductivity of the system with a correction factor of 1.23 and is given below:

$$K_{eff} = 1.23.\left(\frac{2k_s + k_f - (k_s - k_f)\phi}{2k_s + k_f + (k_s - k_f)\phi}\right).k_f \qquad \text{Equation 5.5.}$$

Where k_s is the thermal conductivity of sand in W/mK, k_f is the used as the thermal conductivity of the pore fluid in W/mK and ϕ is the porosity of the sand pack which was 0.35. Equation 5.5 is used to predict the thermal conductivity of the system when the bitumen saturation in the pores is the range of 73.5% to 48.1%. The thermal conductivity of the fluid in pores (k_f) is predicted by Filippov and Novoselova model [60] which is given by the following equation:

$$K_{eff} = k_1(1 - x_2) + k_2x_2 - 0.72(k_2 - k_1)x_1(1 - x_2) \qquad \text{Equation 5.6.a.}$$

When $x_{Bit} > x_{H2O}$, $x_1 = x_{H2O}$, $k_1 = k_{H2O}$, $x_2 = x_{Bit}$ and $k_2 = k_{Bit}$.and when $x_{Bit} < x_{H2O}$, $x_1 = x_{Bit}$, $k_1 = k_{Bit}$, $x_2 = x_{H2O}$ and $k_2 = k_{H2O}$. The thermal conductivity of bitumen is calculated by parameter fitting method using temperature as the parameter, while tallying the experimental and Maxwell-Eucken model values of effective thermal conductivities. The calculated value of bitumen thermal conductivity from this method matched well with the values provided by Hanafi and Karim [26] in the literature. The derived equation for bitumen thermal conductivity (k_{bit} in W/mK) with temperature is given as below:

$$k_{Bit} = 0.00000379T^2 - 0.0012T + 0.4731 \qquad \text{Equation 5.6.b.}$$

Where T is the temperature of the system in ºC.

The relation of the predicted vs the observed thermal conductivity of the system is shown in Figure 31. The "Maxwell-Eucken" model is found to predict the thermal conductivity of the system with an accuracy of R^2 value as 0.64 for the bitumen saturation of 0.901 and 0.48 in the pores. The maximum error of 4% and mean error 1.9%. The predicted value of ETC with this model tends to be somewhat higher than the observed value.

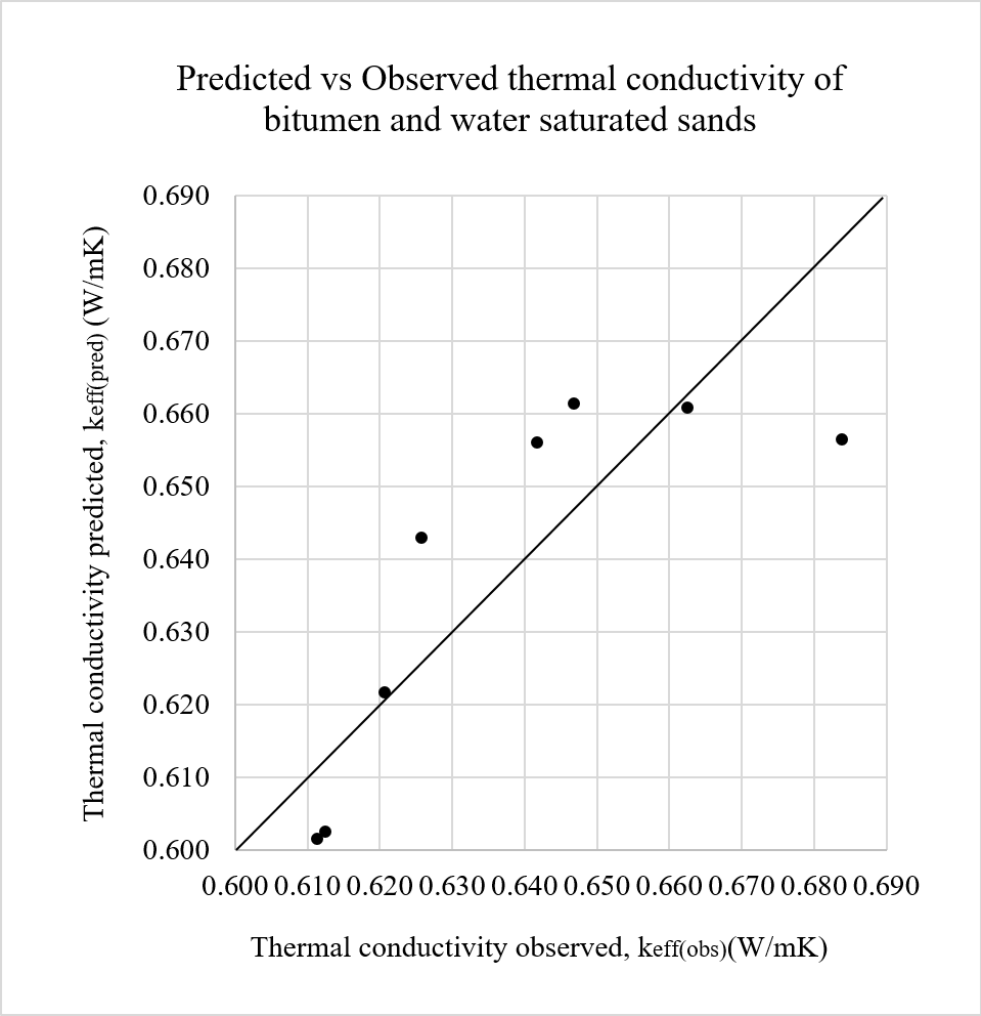

Fig. 31: Predicted vs Observed effective thermal conductivity of bitumen and water sands using "Maxwell Eucken" model.

5.2.3. Estimating thermal conductivity of sands saturated with bitumen, water and nitrogen:

To predict the effective thermal conductivity of the sand pack saturated with bitumen, water and nitrogen, the thermal conductivity equations of sand, water and bitumen (Equations 5.3, 5.4 and 5.6.b) are used in the Maxwell-Eucken equation [17] (Equation 5.5). The nitrogen thermal conductivity equation is obtained by parameter fitting keeping temperature as the only parameter. The derived thermal conductivity equation of nitrogen gas, matches with the literature data [42].

The thermal conductivity equation of nitrogen obtained from this method is given below:

$$k_{Nitro} = 0.0000007T + 0.023 \qquad \text{Equation 5.7.}$$

Where T is the temperature of the system in (ºC). The thermal conductivity of fluid mixture in the pores (k_f) at different temperatures, is estimated by adding a temperature parameter to the "Parallel model" (Equation 2.17) and is shown in Equation 5.8. The relation of predicted thermal conductivity with the observed thermal conductivity is shown in Figure 32. The R^2 value for the above model is 0.935 with a maximum error of 6.1% and mean error of 2.4%. The detailed correlation calculations are attached with Appendix 3.

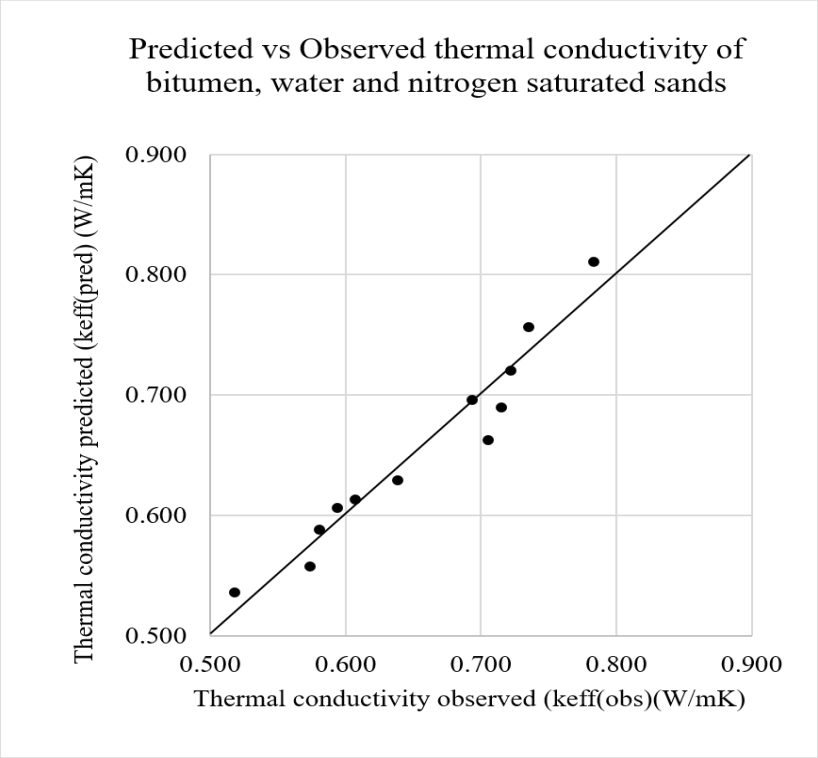

Fig. 32: Predicted vs Observed effective thermal conductivity of bitumen, water and nitrogen saturated sands using "Maxwell Eucken" model.

The equations and correlations used to predict the thermal conductivity of sand pack saturated with bitumen, water and gas, are summarized as below. All temperatures are reported in ºC:

The effective thermal conductivity equation according to "Maxwell-Eucken's model":

$$K_{eff} = \left(\frac{2k_s + k_f - (k_s - k_f)\phi}{2k_s + k_f + (k_s - k_f)\phi}\right).k_f \qquad \text{Equation 5.5.}$$

Thermal conductivity equation for sand (k_s):

$$k_s = -0.0003T + 0.2534 \qquad \text{Equation 5.3.}$$

Thermal conductivity equation for fluid mixture in pores (k_f):

$$k_f = x_{Bit}.k_{Bit} + x_{H2O}.k_{H2O} + x_{N2}.k_{Nitro} + 1.55/T^{0.376} \qquad \text{Equation 5.8.}$$

Where x_{H2O}, x_{Bit}, x_{Nitro} are the volume fractions of water, bitumen and nitrogen in the pores respectively.

Thermal conductivity equation for water (k_{H2O}):

$$k_{H2O} = -0.00000744T^2 + 0.00188T + 0.5636 \quad \text{Equation 5.4.}$$

Thermal conductivity equation for bitumen (k_{Bit}):

$$k_{Bit} = 0.00000379T^2 - 0.0012T + 0.4731 \quad \text{Equation 5.6.}$$

Thermal conductivity equation for nitrogen gas (k_{Nitro}):

$$k_{Nitro} = 0.0000007T + 0.023 \quad \text{Equation 5.7.}$$

The following conclusions could be drawn from the experimental work:

1. The transient unsteady method proved to be an efficient method to measure the effective thermal conductivity of a porous media with multiphase saturations (sand saturated with oil, water and gas). However, the possible errors in the experiment need to be controlled by setting an optimum heating power (1 VDC or lower), keeping the measurement time below 100 secs and avoiding taking measurements at low pressures when the temperature is 100°C or above to eliminate evaporation of the water in the system. Also, it is to be noted that the effective thermal conductivity was measured based on assumption that there was uniform distribution of phases along the axis of the needle-probe, which may not be true in all cases, so this assumption can lead to some error while fitting the experimental data into theoretical models. To avoid this error, it is recommended to keep the temperature of the system around 150 ºC when bitumen is injected or displaced from the system and sufficient time (24 hours) is given to equalize the bitumen saturation in the sand pack.
2. The thermal conductivity of the evacuated sand is found to be in the range of 0.133 to 0.162 W/mK and the 95% confidence interval or standard deviation for the above set of data is in the between $\pm$6.8% and $\pm$13.1%. The thermal conductivity is observed to be slightly decreasing with temperature, possibly due to increase in lattice vibrations leading to reduction of molecular distance between the particles.
3. The thermal conductivity of the sand pack didn't show much variation with pressure, for which the thermal conductivity values at different pressures, ranging from 14.6 psia (1 bar) to 515 psia (35.5 bar), were averaged and the standard deviations are calculated to get an estimate of the errors.

4. For the water saturated sand system, the thermal conductivity of the system lies in the range of 0.808 to 1.110 W/mK and the 95% confidence interval is in the range of $\pm$6.8% to $\pm$13.1%. The following observations can be drawn from the experimental data:
    - A considerable rise in thermal conductivity of the medium is observed from the evacuated sand pack when the sand pack is saturated with water. This confirmed the phenomena explained by Carson et al. [9] that for external porosity structure, the optimum heat transfer pathway will be through the continuous phase, which is the fluid phase in this sand pack.
    - The thermal conductivity of the system is found to be decreasing with temperature as was also observed by Hanafi and Karim [26]. A sharper decline in thermal conductivity is observed at temperature above 100°C. The thermal conductivity of water decreases with temperature above 130°C [39], which would decrease the thermal conductivity of the sand pack.
5. For the bitumen-water saturated system, the thermal conductivity of the medium lies between 0.611 to 0.988 W/mK and the 95% confidence interval range or the standard deviation for the effective thermal conductivities is found to be in the range of $\pm$2.8% to $\pm$10.4%. The following conclusions can be drawn from the experimental data:
    - The thermal conductivity of the medium is observed to be decreasing with increase in temperature as was also observed by Hanafi and Karim [26,69]. The thermal conductivity of bitumen decreases with temperature according to literature [26], and the thermal conductivity of water also decreases with temperature after 130°C, which leads to the overall drop in thermal conductivity of the medium with temperature.
    - When the pore saturation contained maximum bitumen concentration (90.1%) and only irreducible water, the thermal conductivity of the sand pack is found to be lower than at the residual oil saturation (48.1%). A possible reason behind this increase in thermal conductivity is because of

the fact that the thermal conductivity of water (0.55 to 0.68 W/mK or 50 to 150 °C) [39] is higher than bitumen (below 0.4 W/mK) [26].

- The values of thermal conductivity of the sand pack at the intermediate bitumen saturations (73.5% to 67.8%) are found to be decreasing with decrease in bitumen saturation, whereas a reverse trend was expected as the thermal conductivity of bitumen is lower than that of water. This may be because, the water used to displace bitumen fingered through the pack giving rise to non-uniform saturations along the sand pack. Although, these trends are similar to the trends observed by Hanafi and Karim [69], the thermal conductivity data at the intermediate saturations of bitumen are not considered reliable. Thus only the thermal conductivity data at the irreducible water and residual oil saturation were considered for developing correlations.

6. The thermal conductivity of the bitumen-water-nitrogen saturated sand is measured to lie in the range of 0.518 to 0.836 W/mK and 95% confidence interval range or the standard deviation for the effective thermal conductivities is found to be in the range of $\pm$5.9% to $\pm$21.1%. The following points can be concluded from the experimental data:
   - At around same bitumen concentration, addition of nitrogen slightly decreased the effective thermal conductivity of the system. This decrease is conceivably because nitrogen has a lower thermal conductivity than water and bitumen.
   - Though the addition of nitrogen didn't make a significant effect on the effective thermal conductivity of the sand pack, the bitumen displacement from the sand pack was much faster in this case compared to the previous case.
   - It is also observed that thermal conductivity of this system decreases more sharply with temperature. The slopes of the trends of Figure 27, are found to be steeper compared to the slope

of the bitumen-water system (Figure 25). This is probably because gas solubility decreases with temperature and some dissolved gas comes out of solution as the temperature is increased.

- As the nitrogen saturation is increased in the system, the thermal conductivity of the medium is found to be falling. This is because the thermal conductivity of nitrogen gas is much lower compared to the thermal conductivities of bitumen and water, which led to the reduction of the overall thermal conductivity of the system. Also, as discussed above, nitrogen reduces the density of bitumen which also leads to a decline in the effective thermal conductivity of the medium.

7. The effective thermal conductivity of the sand pack saturated with bitumen, nitrogen and surfactant solution is found to be lying in between 0.615 to 0.964 W/mK and the 95% confidence interval range or the standard deviation for the effective thermal conductivities is found to be in the range of $\pm$0.1% to $\pm$2%. The thermal conductivity of the medium is found to be increasing till 37.5% of surfactant saturation and then it started to decline. When surfactant injection is started, it displaced some of the nitrogen gas from the pores. This increased the overall thermal conductivity of the system as the thermal conductivity of the surfactant solution is higher than that of the gas. But when the surfactant concentration was increased beyond 37.5%, the surfactant created foam, in which the gas becomes a dispersed phase. This rearrangement of fluid distribution reduces the effective thermal conductivity of the medium.
8. For the evacuated sand system, the experimental results are tallied with "Parallel Model" of effective thermal conductivity. The parallel model used for estimating the effective thermal conductivity is given below:

$$K_{eff} = \phi k_f + (1-\phi) k_s$$

The R^2 value for the above model was 0.99 with a maximum error of 0.97% and mean error 0.67%. The thermal conductivity of sands obtained from this model is given by:

$$k_s = -0.0003T + 0.2534$$

Where T is the temperature of the system in ºC and k_s is the thermal conductivity of sand in W/mK. According to the literature [41] the thermal conductivity of coarse to sand grains, should lie between 0.25 to 0.27 W/mK at 25 ºC and as per the equation 5.3, it came around 0.249 W/mK.

9. Maxwell-Eucken's [17] model (Equation 5.5) is found to be the best match for the water-bitumen saturated sand when the bitumen saturation is 48.1% and 90.1%. The thermal conductivity equation of water is taken from literature [39] and the thermal conductivity of the pore is predicted by Filippov and Novoselova model [60] (Equation 5.6.a). The model predicted that the thermal conductivity of bitumen will be between 0.404 and 0.378 W/mK for temperature ranging from 75 ºC to 150 ºC, and according to the literature [26] it was measured to be below 0.4 W/mK. The R^2 value for the above model [17] is 0.64 with a maximum error of 4% and mean error of 1.9%. The bitumen thermal conductivity equation obtained from this model is given as:

$$k_{Bit} = 0.00000379T^2 - 0.0012T + 0.4731$$

Where T is the temperature of the system in ºC and k_{Bit} is the thermal conductivity of bitumen in W/mK.

10. The experimental data of the thermal conductivity of the bitumen-water-nitrogen saturated sand is best predicted using the Maxwell-Eucken's [17] model. The sand and bitumen's thermal conductivity derived from previous equations, along with the thermal conductivity equation of water from literature [39], are used to predict the thermal conductivity of fluid mixture in the pores. The thermal conductivity of nitrogen is first assumed and then finally derived while matching the experimental data with the model predicted data. The thermal conductivity equation of nitrogen matched with the literature data [42]. The Maxwell-Eucken's equation [17] used to predict the effective thermal conductivity of the sand pack is given below:

$$K_{eff} = \left(\frac{2k_s + k_f - (k_s - k_f)\phi}{2k_s + k_f + (k_s - k_f)\phi} \right) . k_f$$

Where k_f if the pore fluid thermal conductivity (W/mK), ϕ is the porosity of the medium. The R^2 value for the above model is 0.935 with a maximum error of 6.1% and mean error of 2.4%.

Chapter 6: Conclusions and Recommendations

6.1. Conclusions

The main findings of this research could be concluded with the following points:

1. The transient unsteady method proved to be an efficient method to measure the effective thermal conductivity of a porous media with multiphase saturations (sand saturated with oil, water and gas).
2. The thermal conductivity of the evacuated sand is found to be in the range of 0.133 to 0.162 W/mK and is observed to be slightly decreasing with temperature.
3. The thermal conductivity of the sand pack didn't show much variation with pressure.
4. For the water saturated sand system, the thermal conductivity of the system lies in the range of 0.808 to 1.110 W/mK. The following observations can be drawn from the experimental data:
    - A considerable rise in thermal conductivity of the medium is observed from the evacuated sand pack when the sand pack is saturated with water.
    - The thermal conductivity of the system is found to be decreasing with temperature as was also observed by Hanafi and Karim [26].
5. For the bitumen-water saturated system, the thermal conductivity of the medium lies between 0.611 to 0.988 W/mK. The following conclusions can be drawn from the experimental data:
    - The thermal conductivity of the medium is observed to be decreasing with increase in temperature as was also observed by Hanafi and Karim [26, 69].
    - When the pore saturation contained maximum bitumen concentration (90.1%) and only irreducible water, the thermal conductivity of the sand pack is found to be lower than at the residual oil saturation (48.1%).

- The values of thermal conductivity of the sand pack at the intermediate bitumen saturations (73.5% to 67.8%) are found to be decreasing with decrease in bitumen saturation, as was also observed by Hanafi and Karim [69], whereas a reverse trend was expected.

6. The thermal conductivity of the bitumen-water-nitrogen saturated sand is measured to lie in the range of 0.518 to 0.836 W/mK. The following points can be concluded from the experimental data:
   - At around same bitumen concentration, addition of nitrogen slightly decreased the effective thermal conductivity of the system.
   - Though the addition of nitrogen didn't make a significant effect on the effective thermal conductivity of the sand pack, the bitumen displacement from the sand pack was much faster in this case compared to the previous case.
   - It is also observed that thermal conductivity of this system decreases more sharply with temperature.
   - As the nitrogen saturation is increased in the system, the thermal conductivity of the medium is found to be falling.
7. The effective thermal conductivity of the sand pack saturated with bitumen, nitrogen and surfactant solution is found to be lying in between 0.615 to 0.964 W/mK. The thermal conductivity of the medium is found to be increasing till 37.5% of surfactant saturation in the pores and then it started to decline.
8. For the evacuated sand system, the experimental results best matched with the "Parallel Model" of effective thermal conductivity.
9. For the water-bitumen saturated sand pack, Maxwell-Eucken's [17] model (Equation 5.5) is found to be most closely predicting the thermal conductivity when the bitumen saturation in the pores are 48.1% and 90.1%.

10. The experimental data of the thermal conductivity of the bitumen-water-nitrogen saturated sand is best predicted using the Maxwell-Eucken's [17] model.

6.2 Recommendations for Future Work

1. The same experiments can be conducted for sand pack with various porosities to estimate the thermal conductivity variation with porosity.
2. The experiments can be conducted with sands of various particle sizes and quality to estimate the thermal conductivities of oil sands from varying geographical locations.
3. The experiments can also be conducted with real oil sands samples and the results of the artificially prepared sand pack and the real oil sands samples can be compared.
4. Future work can be conducted to estimate the convection and heat loss effects in the system.

References

1. Canadian Association of Petroleum Producers (CAPP), Canada's Oil and Natural Gas Producers, "What are the Oil Sands?", Natural Resources Canada report promotes Canadian energy, https://www.capp.ca/oil/, 9th Nov, 2019.
2. Oil Sands Magazine 2020, https://www.oilsandsmagazine.com/technical/properties (Accessed Feb, 2020).
3. Steam Assisted Gravity Drainage, Facts and Stats, https://open.alberta.ca/dataset/f7c779ea-9776-4d59-a1b3-178d533f0ebc/resource/aac73d46-3ae0-478e-9b19-e64afa41b1f2/download/FSSAGD.pdf, Alberta Government, (Accessed Feb, 2020).
4. K. R. Alnoaimi, "Addition of Condensable or Non-Condensable Gas to Steamflood Processes for Improved Heavy Oil Recovery by Gravity Drainage," A Report Submitted to the Department of Energy Resources Engineering, Stanford University, August, 2010.
5. Cottrell, J.H., "Development of an Anhydrous Process for Oil-Sand Extraction." *In the K.A. Clark Volume; a collection of papers on the Athabasca oil sands presented to K.A. Clark on the 75th anniversary of his birthday*, edited by M.A. Carrigy, 193-206. Edmonton: Research Council of Alberta, 1963 [E-book].
6. Speight, G.James, "Thermal Methods of Recovery." Enhanced Recovery Methods for Heavy Oil and Tar Sands, Chapter 7, 2009 [E-book].
7. Butler, R.M.,Thermal Recovery of Oil and Bitumen, Prentice Hall, Englewood Cliffs, New Jersey. (pg. 122-123), 1991. [E-book].
8. Skripkin,E. "Effective Thermal Conductivity of Porous Media: An Integrated Approach", A Master of Science thesis submitted to the Department of Chemical and Petroleum Engineering, University of Calgary, 2015.

9. Carson, J. K., S. J. Lovatt, D. J. Tanner, and A. C. Cleland. "Thermal conductivity bounds for isotropic, porous materials." International Journal of Heat and Mass Transfer 48: 2150-2158, 2005.
10. Bird, R. B., W. E. Stewart, and E. N. Lightfoot, Transport phenomena. John Willey and Sons, 2007. [E-book].
11. Midttomme, K, Roaldset, “The effect of grain size on thermal conductivity of quartz sands and slits”, Article at Petroleum Geoscience, Department of Geology and Mineral Resources Engineering, Norwegian University of Science and Technology, Paper 5, 1998.
12. Asher, G. B., Sloan, E. D., and Graboski, M. S., “A computer-controlled transient needle-probe thermal conductivity instrument for liquids,” International Journal of Thermophysics., vol. 7, no. 2, pp. 285–294, 1986.
13. N. Lockmuller, J. Redgrove, and L. Kubičár, “Measurement of thermal conductivity with the needle probe,” Presented at the 16th European Conference on Thermophysical Properties, Imperial College, London, England, 14 September 2002, High Temp. - High Press., vol. 35–36, no. 2, pp. 127–138, 2003.
14. Robert, Hans.M, “A Transient Hot Wire Thermal Conductivity Apparatus for Fluids,” National Bureau of Standards, Boulder, CO 80303 May 26, 1981.
15. Cengel, Yunus A, “Heat and Mass Transfer”, McGraw-Hill, 2nd Edition, 2007. [E-book].
16. ASTM D5334-08, Standard Test Method for Determination of Thermal Conductivity of Soil and Soft Rock by Thermal Needle Probe Procedure, ASTM Int’l, 2011.
17. K. Pietrak and T. S. Winiewski, “A review of models for effective thermal conductivity of composite materials,” Open Access J. J. Power Technol., vol. 95, no. 1, pp. 14–24, 2015.

18. Maxwell, J. C., A treatise on electricity and magnetism, vol. I, 3rd Ed, Oxford University Press, 1904.
19. Kunii, Daizo, and J M Smith. "Heat Transfer Characteristics of Porous Rocks." AIChE Journal 6 (1): 71-78. 1960.
20. Krupiczka, R. "Analysis of thermal conductivity in granular materials." International Chemical Engineering 7 (1): 122-144. 1967.
21. D. P. H. Hasselman, L. F. Johnson, Effective thermal conductivity of composites with interfacial thermal barrier resistance, J. Compos. Mater. 21 (6) 508, 1987.
22. A. G. Every, Y. Tzou, D. P. H. Hasselman, R. Raj, The effect of particle size on the thermal conductivity of ZnS/diamond composites, Acta Metall. Mater. 40 (1), 123, 1992.
23. Woodside, W, and J H Messmer. "Thermal Conductivity of Porous Media. I. Unconsolidated Sands." Journal of Applied Physics 32 (9): 1688-1699. 1961.
24. Z. Abdulagatova, I. M. Abdulagatov, and V. N. Emirov, "Effect of temperature and pressure on the thermal conductivity of sandstone," Int. J. Rock Mech. Min. Sci., vol. 46, no. 6, pp. 1055–1071, 2009.
25. Do, Duc P. and Dashnor H., "Temperature and Pressure Dependence of the Effective Thermal Conductivity of Geomaterials: Numerical Investigation by the Immersed Interface Method", Journal of Applied Mathematics, Research Article, vol. 2013, Article ID 456931, July, 2013.
26. Hanafi,A., Karim, G.A., "The Thermal Conductivity of Oil Sands Using a Transient Method", Journal of Energy Resources Technology, vo. 108(4), 315-320, 1986.
27. Herzen, R.Von and Maxwell, A.E., "The Measurement of Thermal Conductivity of Deep-Sea Sediments by a Needle-Probe Method", J. Geophysical Res. 64(10): 1557-1563, 1959.

28. Lockmuller.n., Redgrove.J., and Kubičár.L., “Measurement of thermal conductivity with the needle probe,” High Temp- High Press., vol. 35–36, no. 2, pp. 127–138, 2003.
29. Cervenan,M.R.,Vermeulen.F.E., Chute, F.S., “Thermal conductivity and specific heat of oil sand samples”, Canadian Journal of Earth Sciences, 18(5): 926-931, 1981.
30. Tsotsas, E. and Martin, H., “Thermal Conductivity of Packed Beds: A Review”, Chemical Engineering and Processing: Process Intensification, Volume 22, Issue 1, Pages 19-37, July 1987.
31. Dean-Stark apparatus, “https://en.wikipedia.org/wiki/Dean%E2%80%93Stark_apparatus”, Wikipedia, (Accessed Feb, 2020).
32. Dul’nev, G.N. and Zarichnyak,Yu.P. , “Thermal Conductivity of Liquid Mixtures”, Journal of engineering physics, volume 11, 400–402, 1966.
33. Somerton, W. H., Keesej, A, and Chu,S . L., “Thermal behavior of unconsolidated oil sands”, Society of Petroleum Engineers Journal, 14, pp. 513-52 1. 1974.
34. Zehner, P.,”Experimentelle und theoretische Bestimmung der effektiven WarmeleXihigkeit durchstriimter Kugelschiittungen bei massigen und hohen Temperaturen, Dissertation”, Karlsruhe, 1972.
35. Bauer, R., “Effektive radiale Wrmeleitfhigkeit gasdurchstromter Schtlttungen mit Partikeln unterschiedlicher Formund GrGBenvcrteilung, Dissertation, Karlsruhe, 1976.
36. TP02 manual v1209, “TP02 Non-Steady-State Probe for Thermal Conductivity Measurement”, Edited & Copyright by: Hukseflux Thermal Sensors, http://www.hukseflux.com, (Accessed Feb, 2020).
37. Student's t-distribution, “https://en.wikipedia.org/wiki/Student%27s_t-distribution”, Wikipedia, (Accessed June, 2020).

38. Student's t-test, "https://en.wikipedia.org/wiki/Student%27s_t-test", Wikipedia, (Accessed June, 2020).
39. Water structure and science,"http://www1.lsbu.ac.uk/water/thermodynamic_anomalies.html,", (Accessed June, 2020).
40. Coefficient of Determination, "https://en.wikipedia.org/wiki/Coefficient_of_determination", Wikipedia, (Accessed June, 2020).
41. Hamdhan, I.N. and Clarke, B.G., "Determination of Thermal Conductivity of Coarse and Fine Sand Soils", Bandung National of Institute of Technology, Leeds University, Proceedings World Geothermal Congress, Bali, Indonesia, April, 2010.
42. Thermal conductivity of gases chart, "https://www.engineersedge.com/heat_transfer/thermal-conductivity-gases.htm", Engineers Edge, (Accessed June, 2020).
43. TPSYS02 Thermal Conductivity Measurement System, "TPSYS02 manual v1709", Edited & Copyright by: Hukseflux Thermal Sensors, http://www.hukseflux.com, (Accessed Feb, 2020).
44. Operating manual, "CR1000 Measurement and Control System", Campbell Scientific Inc., Revision 5/05, 2000-2005.
45. SugaNate 100 NC, "Naturally-derived high-foaming surfactant, CAS# 742087-48-5", Colonial Chemical, Inc., Innovative Specialty Surfactants, LISTINGS: USA (TSCA); Canada (NDSL); EU (REACH); Taiwan (NECI).
46. Material Safety Data sheet, "Glycerine, CAS# 56-81-5", Central Drug House (P) Ltd., cdhfinechemical.com.
47. Material Safety Data sheet, "Silica Sand 100 Mesh", U. S. SILICA COMPANY.
48. Safety Data sheet, "PSF-50cSt Pure Silicone Fluid", Clearco Products Co Inc., Data Prepared: January 17, 2019.

49. Blackwell, J.H., “The Axial-Flow Error in the Thermal-Conductivity Probe” ,Can. J. Phys. 34, 412, 1956.
50. Hashin,Z., and Shtrikman,S., “A Variational Approach to the Theory of the Effective Magnetic Permeability of Multiphase Materials”, Journal of Applied Physics 33, 3125 (1962), 02 April 1962.
51. Strutt,J. (Lord Rayleigh), “On the influence of obstacles arranged in rectangular order upon the properties of a medium”, Phil. Mag., vol. 34, pp. 481, 1892.
52. Krupiczka, R., "Analysis of thermal conductivity in granular materials." International Chemical Engineering 7 (1): 122-144, 1967.
53. Bruggeman, D.A.G., “Berechnung verschiedener physikalischer kkonstanten von heterogenen ssubstanzen”, Ann. Phys. 24 (1935) 636, 1935.
54. Zehner, P, and E U Schlunder, "Wärmeleitfähigkeit von Schüttungen bei mäßigen Temperatu." Chemie. Ingr.-Tech. 42 (14): 933-941, 1970.
55. Nielsen, L.E., “The thermal and electrical conductivity of two-phase systems”, Ind. Eng. Chem. Fundam. 13 (1) (1974) 17, 1974.
56. de Vries, D. A., “Thermal properties of soils: Mededelingen van de Landbouwhogeschool te Wageningen”, vol 52, no. 1, p 1-73, Translated by Building Research Station, Library Communication no. 759, England, 1952.
57. Devpura, A., Phelan, P. E., Prasher, R. S., “Percolation theory applied to the analysis of thermal interface materials in flip-chip technology, in: Thermomechanical Phenomena in Electronic Systems”,- Proceedings of the Intersociety Conference, Vol. 1, Las Vegas, Nevada, 200, p. 21.
58. Eucken A., “Die Wrmeleitfhigkeit keramischer feuerfester Stoffe,” Forsch Geb. Ing. B3, Forsch., 353(16), 1932.

59. Kukkonen IT, Jokinen J, Seipold U. Temperature and pressure dependencies of thermal transport properties of rocks: implications for uncertainties in thermal lithosphere models and new laboratory measurements of high- grade rocs in the central Fennoscandian shield", Surv Geophys;20: 33–59, 1999.
60. Dul'nev, G.N. and Zarichnyak,Yu.P. , "Thermal Conductivity of Liquid Mixtures", Journal of engineering physics, volume 11, 400–402, 1966.
61. Odelevskii, V.I., "Calculation of the Generalized Conductivity of Heterogeneous Systems", Journal of Technical Physics (USSR), 21, 678-685, 1951.
62. Souraki ,Y., Ashrafi, M., Karimaie,H. & Torsaeter, O., "Experimental Analyses of Athabasca Bitumen Properties and Field Scale Numerical Simulation Study of Effective Parameters on SAGD Performance", Energy and Environment Research; Vol. 2, No. 1; Department of Petroleum Engineering and Applied Geophysics, Norwegian University of Science and Technology – NTNU, Trondheim, Norway, Published by Canadian Center of Science and Education, May 2012.
63. Heat Transfer (Energy Engineering), "http://what-when-how.com/energy-engineering/heat-transfer-energy-engineering/#:~:text=Conduction%20can%20take%20place%20in,energy%20transport%20by%20free%20electrons.",What-When-How,Indepth Tutorials and information.
64. Askari, R., S.H. Hejazi and M. Sahimi, "Effect of deformation on the thermal conductivity of granular porous media with rough grain surface": Geophysical Research Letters. 44(16), 8285–8293., 2017.
65. Askari,R.,Taheri,S. and S.H.Hejazi, "Thermal conductivity of granular porous media: A pore scale modelling approach:AIP Advances, Vol.5(9), 097106, 2015.

66. Askari,R.,S.H.Hejazi and M.Sahimi, “Thermal conduction in deforming isotropic and anisotropic granular porous media with rough grain surface”, Transport in Porous Media. 124(1):221-. J236, 2018.
67. Askari, R.,M.F.Ikram, and S.H.Hejazi, “Pore scale evaluation of thermal conduction anisotropy in granular porous media using lattice Boltzmann method: Int. J. Numerical Methods in Heat and Fluid Flows. 27 (4), 867-868.
68. Ikram, M.F.,R.Askari, S.H.Hejazi and M.Sahimi, “Effect of elastic deformation and rough grain surface on heat conduction in partially-saturated granular porous media: Water Resources Research. 54(11), 2018.
69. Hanafi,A., Karim, G.A., “The Thermal Conductivity of Oil Sands”, The Canadian Journal of Chemical Engineering, Vol. 59, August, 1981.

Appendix 1: Experimental data for water saturated and bitumen-water saturated sand pack:

Keff (W/mK)	Keff (W/mK) (Average)	Temp (C)	Press (psia)	Bit Sat (%)	H_20 Sat (%)	N_2 Sat (%)	Range	Standard Deviation	Standard Deviation	Sample number
0.811	1.110	50	14.6	0	100	0	0.182	0.086	0.231	12
1.093		50	114.6	0	100	0	0.299	0.150		
1.031		50	214.6	0	100	0	0.327	0.182		
1.092		50	314.6	0	100	0	0.406	0.209		
1.223		50	414.6	0	100	0	0.800	0.406		
1.746		50	514.6	0	100	0	0.113	0.080		
0.916	1.106	75	14.6	0	100	0	0.128	0.060	0.210	12
1.125		75	114.6	0	100	0	0.122	0.054		
1.185		75	214.6	0	100	0	0.463	0.250		
1.198		75	314.6	0	100	0	0.385	0.212		
1.350		75	414.6	0	100	0	0.504	0.290		
0.803		75	514.6	0	100	0	1.032	0.519		
1.089	1.087	100	164.6	0	100	0	0.031	0.018	0.252	12
1.046		100	214.6	0	100	0	0.420	0.236		
1.084		100	314.6	0	100	0	0.554	0.259		
1.128		100	414.6	0	100	0	0.668	0.374		
0.791	0.900	125	164.6	0	100	0	0.042	0.023	0.216	15
0.817		125	214.6	0	100	0	0.144	0.075		
0.855		125	314.6	0	100	0	0.026	0.013		
1.136		125	414.6	0	100	0	0.339	0.190		
1.228		125	514.6	0	100	0	0.356	0.198		
0.808	0.808	150	164.6	0	100	0	0.000	0.000	0.078	10
0.989		150	214.6	0	100	0	0.000	0.000		
0.989		150	314.6	0	100	0	0.000	0.000		
0.989		150	414.6	0	100	0	0.000	0.000		
0.954		150	514.6	0	100	0	0.000	0.000		
0.626	0.626	41	14.6	90.1	9.9	0	0.074	0.039	0.051	12
0.581		41	114.6	90.1	9.9	0	0.126	0.070		
0.564		41	214.6	90.1	9.9	0	0.083	0.046		
0.530		41	314.6	90.1	9.9	0	0.036	0.021		
0.512		41	414.6	90.1	9.9	0	0.085	0.043		
0.539		41	514.6	90.1	9.9	0	0.009	0.005		
0.520	0.621	75	14.6	90.1	9.9	0	0.014	0.010	0.065	10
0.656		75	114.6	90.1	9.9	0	0.011	0.104		

Keff (W/mK)	Keff (W/mK) (Average)	Temp (C)	Press (psia)	Bit Sat (%)	H_20 Sat (%)	N_2 Sat (%)	Range	Standard Deviation	Standard Deviation	Sample number
0.554		75	214.6	90.1	9.9	0	0.000	0.000		
0.602		75	314.6	90.1	9.9	0	0.115	0.058		
0.604		75	414.6	90.1	9.9	0	0.108	0.054		
0.556		75	514.6	90.1	9.9	0	0.015	0.009		
0.608		100	164.6	90.1	9.9	0	0.180	0.102		
0.625		100	214.6	90.1	9.9	0	0.040	0.023		
0.552	0.611	100	314.6	90.1	9.9	0	0.149	0.086	0.063	15
0.629		100	414.6	90.1	9.9	0	0.068	0.039		
0.641		100	514.6	90.1	9.9	0	0.031	0.018		
0.603		125	164.6	90.1	9.9	0	0.111	0.078		
0.622		125	214.6	90.1	9.9	0	0.123	0.063		
0.643	0.612	125	314.6	90.1	9.9	0	0.087	0.050	0.059	10
0.633		125	414.6	90.1	9.9	0	0.050	0.027		
0.679		125	514.6	90.1	9.9	0	0.172	0.086		
0.653		150	164.6	90.1	9.9	0	0.047	0.027		
0.747		150	214.6	90.1	9.9	0	0.084	0.042		
0.710	0.653	150	314.6	90.1	9.9	0	0.098	0.057	0.027	10
0.701		150	414.6	90.1	9.9	0	0.025	0.015		
0.808		150	514.6	90.1	9.9	0	0.121	0.064		
0.857		41	14.6	73.5	26.5	0	0.282	0.199		
0.888		41	114.6	73.5	26.5	0	0.220	0.155		
0.907	0.988	41	214.6	73.5	26.5	0	0.182	0.129	0.145	14
0.998		41	314.6	73.5	26.5	0	0.000	0.000		
0.893		41	414.6	73.5	26.5	0	0.182	0.094		
1.155		41	514.6	73.5	26.5	0	0.110	0.063		
1.150		75	40.6	73.5	26.5	0	0.249	0.176		
0.810		75	114.6	73.5	26.5	0	0.021	0.015		
1.025	0.982	75	214.6	73.5	26.5	0	0.000	0.000	0.140	11
0.900		75	314.6	73.5	26.5	0	0.188	0.108		
0.768		75	414.6	73.5	26.5	0	0.000	0.000		
1.025		75	514.6	73.5	26.5	0	0.000	0.000		
0.924		100	164.6	73.5	26.5	0	0.185	0.093		
0.916		100	214.6	73.5	26.5	0	0.177	0.101		
1.014	0.953	100	314.6	73.5	26.5	0	0.000	0.000	0.069	14
0.986		100	414.6	73.5	26.5	0	0.084	0.049		
0.925		100	514.6	73.5	26.5	0	0.044	0.024		
1.028	0.935	125	164.6	73.5	26.5	0	0.044	0.025	0.077	15

Keff (W/mK)	Keff (W/mK) (Average)	Temp (C)	Press (psia)	Bit Sat (%)	H_20 Sat (%)	N_2 Sat (%)	Range	Standard Deviation	Standard Deviation	Sample number
0.893		125	214.6	73.5	26.5	0	0.135	0.078		
0.910		125	314.6	73.5	26.5	0	0.183	0.091		
0.922		125	414.6	73.5	26.5	0	0.195	0.099		
0.924		125	514.6	73.5	26.5	0	0.023	0.013		
0.947		150	164.6	73.5	26.5	0	0.082	0.058		
0.788		150	214.6	73.5	26.5	0	0.087	0.062		
0.868	0.927	150	314.6	73.5	26.5	0	0.181	0.104	0.160	13
1.094		150	414.6	73.5	26.5	0	0.488	0.255		
0.936		150	514.6	73.5	26.5	0	0.156	0.090		
0.746		41	14.6	70.4	29.6	0	0.063	0.036		
0.792		41	114.6	70.4	29.6	0	0.138	0.069		
0.905		41	214.6	70.4	29.6	0	0.480	0.261		
0.728	0.905	41	314.6	70.4	29.6	0	0.089	0.051	0.036	10
0.787		41	414.6	70.4	29.6	0	0.003	0.001		
0.757		41	514.6	70.4	29.6	0	0.088	0.051		
0.799		75	14.6	70.4	29.6	0	0.001	0.000		
0.962		75	114.6	70.4	29.6	0	0.130	0.065		
0.969		75	214.6	70.4	29.6	0	0.105	0.054		
0.828	0.904	75	314.6	70.4	29.6	0	0.183	0.129	0.105	17
1.014		75	414.6	70.4	29.6	0	0.186	0.093		
0.854		75	514.6	70.4	29.6	0	0.164	0.095		
1.223		100	164.6	70.4	29.6	0	0.315	0.182		
0.769		100	214.6	70.4	29.6	0	0.063	0.036		
0.719	0.844	100	314.6	70.4	29.6	0	0.026	0.015	0.223	15
0.721		100	414.6	70.4	29.6	0	0.012	0.009		
0.790		100	514.6	70.4	29.6	0	0.000	0.000		
0.926		125	164.6	70.4	29.6	0	0.221	0.127		
0.782		125	214.6	70.4	29.6	0	0.358	0.179		
0.811	0.836	125	314.6	70.4	29.6	0	0.282	0.163	0.128	15
0.869		125	414.6	70.4	29.6	0	0.079	0.046		
0.791		125	514.6	70.4	29.6	0	0.222	0.128		
0.907		150	164.6	70.4	29.6	0	0.181	0.092		
0.868		150	214.6	70.4	29.6	0	0.388	0.212		
0.750	0.821	150	314.6	70.4	29.6	0	0.061	0.035	0.121	15
0.750		150	414.6	70.4	29.6	0	0.082	0.058		
0.833		150	514.6	70.4	29.6	0	0.125	0.088		
1.026	0.894	41	14.6	67.8	32.2	0	0.278	0.152	0.127	15

Keff (W/mK)	Keff (W/mK) (Average)	Temp (C)	Press (psia)	Bit Sat (%)	H_20 Sat (%)	N_2 Sat (%)	Range	Standard Deviation	Standard Deviation	Sample number
0.902		41	114.6	67.8	32.2	0	0.163	0.094		
0.527		41	214.6	67.8	32.2	0	0.000	0.000		
0.901		41	314.6	67.8	32.2	0	0.163	0.094		
0.826		41	414.6	67.8	32.2	0	0.226	0.116		
0.817		41	514.6	67.8	32.2	0	0.252	0.128		
0.917		75	14.6	67.8	32.2	0	0.188	0.102		
0.942		75	114.6	67.8	32.2	0	0.187	0.096		
0.833	0.836	75	214.6	67.8	32.2	0	0.227	0.117	0.099	18
0.778		75	314.6	67.8	32.2	0	0.064	0.037		
0.778		75	414.6	67.8	32.2	0	0.063	0.037		
0.767		75	514.6	67.8	32.2	0	0.063	0.044		
0.844		100	164.6	67.8	32.2	0	0.163	0.094		
0.727		100	214.6	67.8	32.2	0	0.000	0.000		
0.790	0.812	100	314.6	67.8	32.2	0	0.001	0.000	0.089	10
0.802		100	414.6	67.8	32.2	0	0.225	0.130		
0.700		100	514.6	67.8	32.2	0	0.270	0.155		
0.777		125	164.6	67.8	32.2	0	0.000	0.000		
0.784		125	214.6	67.8	32.2	0	0.135	0.096		
0.888	0.797	125	314.6	67.8	32.2	0	0.193	0.137	0.136	13
0.757		125	414.6	67.8	32.2	0	0.061	0.035		
0.777		125	514.6	67.8	32.2	0	0.000	0.000		
0.938		150	164.6	67.8	32.2	0	0.284	0.149		
0.709		150	214.6	67.8	32.2	0	0.122	0.061		
0.740	0.789	150	314.6	67.8	32.2	0	0.061	0.043	0.105	11
0.823		150	414.6	67.8	32.2	0	0.159	0.092		
0.885		150	514.6	67.8	32.2	0	0.230	0.163		
0.653		41	14.6	48.1	51.9	0	0.037	0.022		
0.672		41	114.6	48.1	51.9	0	0.197	0.114		
0.753	0.684	41	214.6	48.1	51.9	0	0.153	0.088	0.087	18
0.621		41	314.6	48.1	51.9	0	0.010	0.007		
0.728		41	414.6	48.1	51.9	0	0.113	0.062		
0.676		41	514.6	48.1	51.9	0	0.254	0.180		
0.662		75	14.6	48.1	51.9	0	0.090	0.045		
0.699		75	114.6	48.1	51.9	0	0.200	0.105		
0.599	0.662	75	214.6	48.1	51.9	0	0.119	0.068	0.085	12
0.622		75	314.6	48.1	51.9	0	0.116	0.058		
0.635		75	414.6	48.1	51.9	0	0.067	0.034		

Keff (W/mK)	Keff (W/mK) (Average)	Temp (C)	Press (psia)	Bit Sat (%)	H_20 Sat (%)	N_2 Sat (%)	Range	Standard Deviation	Standard Deviation	Sample number
0.654		75	514.6	48.1	51.9	0	0.292	0.149		
0.565	0.642	100	164.6	48.1	51.9	0	0.045	0.032	0.091	10
0.631		100	214.6	48.1	51.9	0	0.002	0.002		
0.896		100	314.6	48.1	51.9	0	0.197	0.105		
0.730		100	414.6	48.1	51.9	0	0.198	0.105		
0.757		100	514.6	48.1	51.9	0	0.243	0.129		
0.996	0.647	125	164.6	48.1	51.9	0	0.315	0.174	0.080	10
0.932		125	214.6	48.1	51.9	0	0.155	0.110		
0.703		125	314.6	48.1	51.9	0	0.048	0.034		
0.666		125	414.6	48.1	51.9	0	0.130	0.092		
0.571		125	514.6	48.1	51.9	0	0.089	0.051		
0.612	0.640	150	164.6	48.1	51.9	0	0.053	0.031	0.076	11
0.730		150	214.6	48.1	51.9	0	0.172	0.099		
0.831		150	314.6	48.1	51.9	0	0.087	0.062		
0.619		150	414.6	48.1	51.9	0	0.044	0.024		
0.598		150	514.6	48.1	51.9	0	0.080	0.057		

Appendix 2: Experimental data for bitumen, nitrogen and saturated sands:

Keff (W/mK)	Keff (W/mK) (Average)	Temp (C)	Press (psia)	Bit Sat (%)	H_20 Sat (%)	N_2 Sat (%)	Range	Standard Deviation	Standard Deviation	Sample number
0.887	0.783	85	64.6	62.3	9.4	28.3	0.219	0.126	0.121	18
0.884		85	114.6	62.3	9.4	28.3	0.153	0.079		
0.791		85	214.6	62.3	9.4	28.3	0.039	0.021		
0.795		85	314.6	62.3	9.4	28.3	0.039	0.027		
0.726		85	414.6	62.3	9.4	28.3	0.200	0.115		
0.616		85	514.6	62.3	9.4	28.3	0.085	0.043		
0.754	0.736	100	164.6	62.3	9.4	28.3	0.144	0.078	0.118	11
0.583		100	214.6	62.3	9.4	28.3	0.054	0.038		
0.623		100	314.6	62.3	9.4	28.3	0.050	0.027		
0.779		100	414.6	62.3	9.4	28.3	0.086	0.050		
0.786		100	514.6	62.3	9.4	28.3	0.280	0.198		
0.742	0.722	125	164.6	62.3	9.4	28.3	0.079	0.046	0.071	13
0.698		125	214.6	62.3	9.4	28.3	0.025	0.013		
0.616		125	314.6	62.3	9.4	28.3	0.092	0.048		
0.760		125	414.6	62.3	9.4	28.3	0.103	0.060		
0.795		125	514.6	62.3	9.4	28.3	0.000	0.000		
0.758	0.693	150	164.6	62.3	9.4	28.3	0.102	0.072	0.208	10
0.899		150	214.6	62.3	9.4	28.3	0.064	0.045		
0.820		150	314.6	62.3	9.4	28.3	0.103	0.059		
0.684		150	414.6	62.3	9.4	28.3	0.179	0.098		
0.638		150	514.6	62.3	9.4	28.3	0.673	0.350		
0.729	0.715	85	64.6	46	9.4	44.6	0.020	0.011	0.111	13
0.690		85	114.6	46	9.4	44.6	0.038	0.027		
0.597		85	214.6	46	9.4	44.6	0.036	0.025		
0.695		85	314.6	46	9.4	44.6	0.071	0.050		
0.734		85	414.6	46	9.4	44.6	0.341	0.195		
0.847		85	514.6	46	9.4	44.6	0.157	0.111		
0.764	0.706	100	164.6	46	9.4	44.6	0.240	0.132	0.170	14
0.875		100	214.6	46	9.4	44.6	0.297	0.210		
0.773		100	314.6	46	9.4	44.6	0.187	0.102		
0.631		100	414.6	46	9.4	44.6	0.044	0.031		
0.484		100	514.6	46	9.4	44.6	0.111	0.062		
0.708	0.639	125	164.6	46	9.4	44.6	0.112	0.060	0.067	12
0.679		125	214.6	46	9.4	44.6	0.086	0.045		
0.573		125	314.6	46	9.4	44.6	0.036	0.018		

Keff (W/mK)	Keff (W/mK) (Average)	Temp (C)	Press (psia)	Bit Sat (%)	H_20 Sat (%)	N_2 Sat (%)	Range	Standard Deviation	Standard Deviation	Sample number
0.626		125	414.6	46	9.4	44.6	0.053	0.038		
0.607		125	514.6	46	9.4	44.6	0.000	0.000		
0.629		150	164.6	46	9.4	44.6	0.182	0.129		
0.523		150	214.6	46	9.4	44.6	0.133	0.094		
0.570	0.594	150	314.6	46	9.4	44.6	0.204	0.118	0.101	13
0.616		150	414.6	46	9.4	44.6	0.043	0.031		
0.633		150	514.6	46	9.4	44.6	0.247	0.175		
0.784		85	64.6	32.8	9.4	57.8	0.173	0.094		
0.537		85	114.6	32.8	9.4	57.8	0.062	0.031		
0.600		85	214.6	32.8	9.4	57.8	0.136	0.069		
0.464	0.607	85	314.6	32.8	9.4	57.8	0.318	0.171	0.063	12
0.507		85	414.6	32.8	9.4	57.8	0.054	0.027		
0.496		85	514.6	32.8	9.4	57.8	0.056	0.028		
0.601		100	164.6	32.8	9.4	57.8	0.298	0.164		
0.579		100	214.6	32.8	9.4	57.8	0.252	0.129		
0.537	0.581	100	314.6	32.8	9.4	57.8	0.072	0.036	0.102	11
0.570		100	414.6	32.8	9.4	57.8	0.162	0.087		
0.574		100	514.6	32.8	9.4	57.8	0.021	0.015		
0.521		125	114.6	32.8	9.4	57.8	0.151	0.077		
0.653		125	214.6	32.8	9.4	57.8	0.141	0.078		
0.554	0.574	125	314.6	32.8	9.4	57.8	0.251	0.125	0.084	11
0.599		125	414.6	32.8	9.4	57.8	0.124	0.069		
0.622		125	514.6	32.8	9.4	57.8	0.066	0.046		
0.402		150	114.6	32.8	9.4	57.8	0.053	0.031		
0.521		150	214.6	32.8	9.4	57.8	0.147	0.078		
0.525	0.518	150	314.6	32.8	9.4	57.8	0.317	0.158	0.107	15
0.449		150	414.6	32.8	9.4	57.8	0.209	0.105		
0.577		150	514.6	32.8	9.4	57.8	0.178	0.095		

Appendix 3: Correlations

Evacuated sand pack correlation calculation table using Eq. 2.17:

Sl. No.	Temp. (deg C)	Vaccum Pressure (inch Hg)	NCG saturation (%)	Water saturation (%)	Bitumen saturation (%)	Observed ETC k_{obs} (W/mK)	Predicted ETC k_{pred} (W/mK)	Thermal conductivity of sand k_{sand} (W/mK)	Rec^2	$Total^2$	$\Sigma Rec^2/\Sigma Total^2$	R^2	Error%	Mean error %
1	25	25.5	0	0	0	0.162	0.162	0.249	0.0000001	0.00021			0.22	
2	50	25.5	0	0	0	0.152	0.151	0.232	0.0000022	0.00002	0.010	0.990	0.97	**0.67**
3	100	25.5	0	0	0	0.143	0.143	0.219	0.0000005	0.00002			0.50	
4	150	25.5	0	0	0	0.133	0.132	0.203	0.0000017	0.00021			0.97	

Bitumen-water saturated sand pack correlation calculation table:

		Pore saturation			Pore saturation														
Keff (W/mK)	Temp (C)	Bit. Sat. (%)	H_20 Sat. (%)	N_2 Sat. (%)	Bitumen Sat.	H_20 Sat.	N_2 Sat.	k_{sand} (W/mK)	k_{H2O} (W/mK)	k_{bit} (W/mK)	k_{pore} (W/mK)	keff_pred (W/mK)	keff_obs (W/mK)	Rec^2	$Total^2$	$\Sigma Rec^2/\Sigma Total^2$	R^2	Error %	Mean error %
0.626	41	90.1	9.9	0	0.901	0.099	0	0.241	0.628	0.430	0.447	0.643	0.626	0.000	0.000	0.36	0.64	2.8	1.9
0.621	75	90.1	9.9	0	0.901	0.099	0	0.231	0.663	0.408	0.432	0.622	0.621	0.000	0.000			0.2	
0.611	100	90.1	9.9	0	0.901	0.099	0	0.223	0.677	0.391	0.418	0.602	0.611	0.000	0.001			1.6	
0.612	125	90.1	9.9	0	0.901	0.099	0	0.216	0.682	0.387	0.415	0.603	0.612	0.000	0.001			1.6	
0.684	41	48.1	51.9	0	0.481	0.519	0	0.241	0.628	0.430	0.455	0.656	0.684	0.001	0.002			4.0	
0.662	75	48.1	51.9	0	0.481	0.519	0	0.231	0.663	0.408	0.453	0.661	0.662	0.000	0.001			0.3	
0.642	100	48.1	51.9	0	0.481	0.519	0	0.223	0.677	0.391	0.447	0.656	0.642	0.000	0.000			2.2	
0.647	125	48.1	51.9	0	0.481	0.519	0	0.216	0.682	0.387	0.447	0.661	0.647	0.000	0.000			2.3	

Bitumen-water-nitrogen saturated sand pack correlation calculation table:

Keff (W/mK)	Temp. (C)	Bit. Sat. (%)	H_20 Sat. (%)	N_2 Sat. (%)	Bitumen Sat.	H_20 Sat.	N_2 Sat.	k_{sand} (W/mK)	k_{H2O} (W/mK)	k_{bit} (W/mK)	k_{N2} (W/mK)	kp_2 (W/mK) bit-wat+N_2	keff_pred (W/mK)	keff_obs (W/mK)	Rec^2	$Total^2$	$\Sigma Rec^2/\Sigma Total^2$)	R^2	Error %	Mean error%
0.783	75	62.3	9.4	28.3	0.62	0.09	0.28	0.231	0.663	0.404	0.028	0.628	0.811	0.783	0.001	0.016	0.065	0.935	3.5	2.4
0.736	100	62.3	9.4	28.3	0.62	0.09	0.28	0.223	0.677	0.391	0.030	0.590	0.756	0.736	0.000	0.006			2.8	
0.722	125	62.3	9.4	28.3	0.62	0.09	0.28	0.216	0.682	0.382	0.032	0.563	0.720	0.722	0.000	0.004			0.3	
0.693	150	62.3	9.4	28.3	0.62	0.09	0.28	0.208	0.678	0.378	0.034	0.544	0.696	0.693	0.000	0.001			0.4	
0.715	85	46	9.4	44.6	0.46	0.09	0.45	0.228	0.670	0.398	0.029	0.551	0.690	0.715	0.001	0.004			3.6	
0.706	100	46	9.4	44.6	0.46	0.09	0.45	0.223	0.677	0.391	0.030	0.531	0.662	0.706	0.002	0.002			6.1	
0.639	125	46	9.4	44.6	0.46	0.09	0.45	0.216	0.682	0.382	0.032	0.506	0.629	0.639	0.000	0.000			1.5	
0.594	150	46	9.4	44.6	0.46	0.09	0.45	0.208	0.678	0.378	0.034	0.488	0.607	0.594	0.000	0.004			2.1	
0.607	85	32.8	9.4	57.8	0.33	0.09	0.58	0.228	0.670	0.398	0.029	0.502	0.613	0.607	0.000	0.002			1.1	
0.581	100	32.8	9.4	57.8	0.33	0.09	0.58	0.223	0.677	0.391	0.030	0.483	0.588	0.581	0.000	0.006			1.2	
0.574	125	32.8	9.4	57.8	0.33	0.09	0.58	0.216	0.682	0.382	0.032	0.460	0.557	0.574	0.000	0.007			2.9	
0.518	150	32.8	9.4	57.8	0.33	0.09	0.58	0.208	0.678	0.378	0.034	0.443	0.536	0.518	0.000	0.019			3.5	

Appendix 4: Calculation sheet from the LoggerNet software data

Calculated measurement parameters		
Average base temperature	124.007	°C
Average sensitivity	40.274	uV/K
heating power Q	0.795	W/m
max base temperature change	0.114	°C
sample temperature rise	0.000	°C
total time	100.0	s
heat time	50.0	s
raw data time step	0.5	s
heater resistance	84.28	Ω/m
total temperature drift before heating	#N/A	°C
temperature drift velocity near heating start	#N/A	°C/min

Results for thermal conductivity		
total length of interval	18.48	s
lambda	0.7159	W/mK
standard deviation Lambda	0.1164	W/mK
total temperature rise in interval	0.2321	°C

Calculation of thermal conductivity
Step size in logarithmic time (CR1000 software uses 0.05)

ln(t_step)	0.05		

Fill in time interval in which graph is linear. The CR1000 program uses LN(heat time / 2) till LN(heat time).

ln(t_begin)	1.8	6.0	s

ln(t_end)	3.20	24.5	s

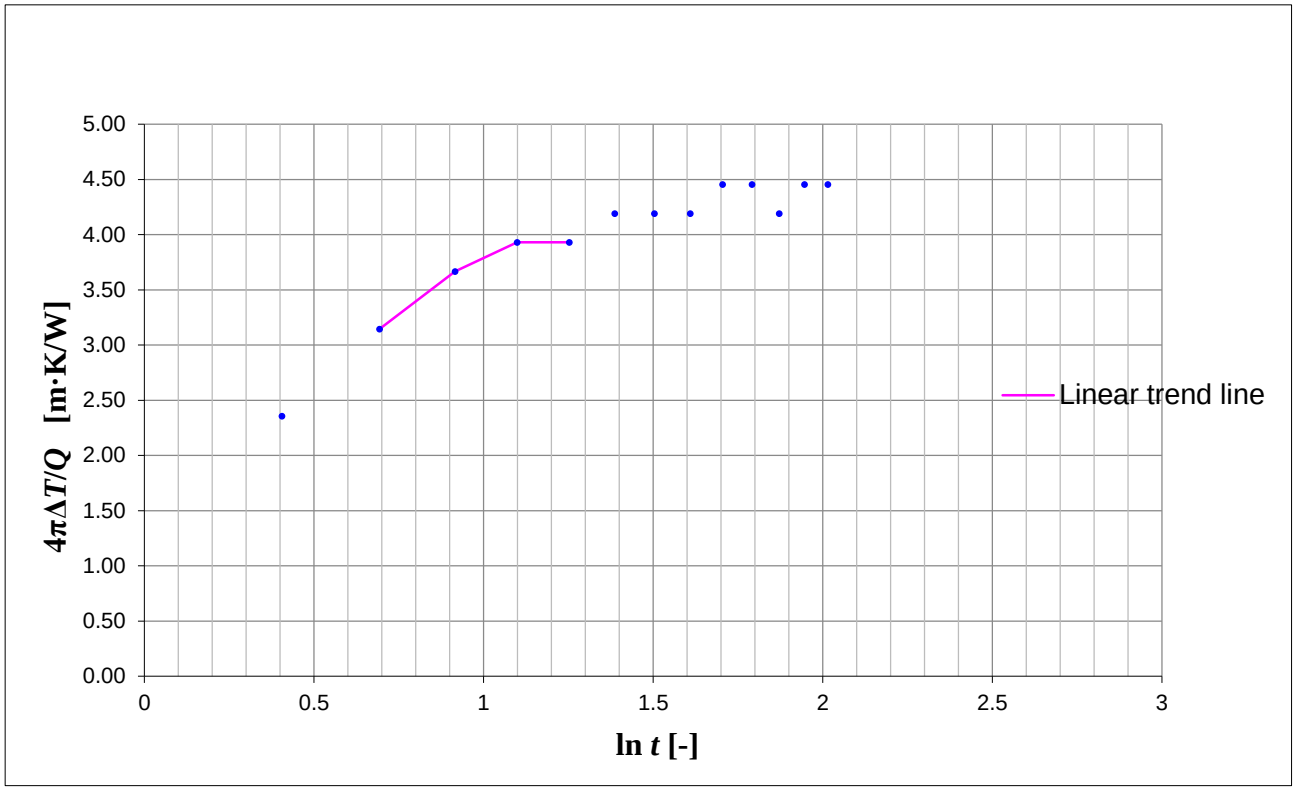

s	ln s	A	mV	mV	Deg C	Deg C	4 Pi (Tdiff/Q)	Calculated	Sensitivity	Change in	Temperature rise
time	ln time	current	U_sen	U_cold	Pt1000	Hot joint Temp	temp rise	Hot joint Temp	Hot joint	temp. rise	Tdiff_sum
0.0		0.00E+00	0.1335404	1.123743	123.9915	154.8535	0.00	154.85	40.279	0.000	0.000
0.5	-0.6931	-9.71E-02	0.1335404	1.123743	123.9915	154.9034	0.00	154.85	40.279	0.000	0.000
1.0	0.0000	-9.71E-02	0.1368789	1.123743	123.9915	154.9865	1.31	154.94	40.277	0.083	0.083
1.5	0.4055	-9.71E-02	0.1395497	1.123743	123.9915	155.053	2.36	155.00	40.276	0.066	0.149
2.0	0.6931	-9.71E-02	0.1415528	1.123743	123.9915	155.0863	3.14	155.05	40.275	0.050	0.199
2.5	0.9163	-9.71E-02	0.1428882	1.12441	123.9915	155.1195	3.67	155.09	40.274	0.033	0.232
3.0	1.0986	-9.71E-02	0.1435559	1.123743	124.1052	155.2409	3.93	155.10	40.274	0.017	0.249
3.5	1.2528	-9.71E-02	0.1435559	1.123743	123.9915	155.1362	3.93	155.10	40.274	0.000	0.249
4.0	1.3863	-9.71E-02	0.1442236	1.123743	123.9915	155.1528	4.19	155.12	40.274	0.017	0.265
4.5	1.5041	-9.71E-02	0.1442236	1.12441	123.9915	155.1528	4.19	155.12	40.274	0.000	0.265
5.0	1.6094	-9.71E-02	0.1442236	1.127081	124.0399	155.2009	4.19	155.12	40.274	0.000	0.265
5.5	1.7047	-9.71E-02	0.1448914	1.123743	123.9915	155.1611	4.45	155.14	40.273	0.017	0.282
6.0	1.7918	-9.71E-02	0.1448914	1.12441	123.9915	155.1528	4.45	155.14	40.273	0.000	0.282
6.5	1.8718	-9.71E-02	0.1442236	1.12441	123.9915	155.1611	4.19	155.12	40.274	-0.017	0.265
7.0	1.9459	-9.71E-02	0.1448914	1.125078	124.1052	155.2825	4.45	155.14	40.273	0.017	0.282
7.5	2.0149	-9.71E-02	0.1448914	1.12441	123.9915	155.1694	4.45	155.14	40.273	0.000	0.282
8.0	2.0794	-9.71E-02	0.1448914	1.12441	123.9915	155.1694	4.45	155.14	40.273	0.000	0.282
8.5	2.1401	-9.71E-02	0.1448914	1.12441	124.1052	155.2825	4.45	155.14	40.273	0.000	0.282
9.0	2.1972	-9.71E-02	0.1448914	1.12441	123.9915	155.1694	4.45	155.14	40.273	0.000	0.282
9.5	2.2513	-9.71E-02	0.1448914	1.12441	123.9915	155.1694	4.45	155.14	40.273	0.000	0.282
10.0	2.3026	-9.71E-02	0.1448914	1.12441	123.9915	155.1694	4.45	155.14	40.273	0.000	0.282
10.5	2.3514	-9.71E-02	0.1448914	1.125078	123.9915	155.1777	4.45	155.14	40.273	0.000	0.282
11.0	2.3979	-9.71E-02	0.1448914	1.12441	123.9915	155.1694	4.45	155.14	40.273	0.000	0.282
11.5	2.4423	-9.71E-02	0.1448914	1.12441	123.9915	155.186	4.45	155.14	40.273	0.000	0.282
12.0	2.4849	-9.71E-02	0.1448914	1.125078	123.9915	155.1777	4.45	155.14	40.273	0.000	0.282
12.5	2.5257	-9.71E-02	0.1448914	1.125078	123.9915	155.1777	4.45	155.14	40.273	0.000	0.282
13.0	2.5649	-9.71E-02	0.1448914	1.125078	123.9915	155.1777	4.45	155.14	40.273	0.000	0.282
13.5	2.6027	-9.71E-02	0.1448914	1.125078	124.1052	155.2908	4.45	155.14	40.273	0.000	0.282
14.0	2.6391	-9.71E-02	0.1448914	1.125078	123.9915	155.1777	4.45	155.14	40.273	0.000	0.282
14.5	2.6741	-9.71E-02	0.1448914	1.125078	123.9915	155.186	4.45	155.14	40.273	0.000	0.282
15.0	2.7081	-9.71E-02	0.1448914	1.125078	123.9915	155.1777	4.45	155.14	40.273	0.000	0.282
15.5	2.7408	-9.71E-02	0.1448914	1.125078	123.9915	155.186	4.45	155.14	40.273	0.000	0.282
16.0	2.7726	-9.71E-02	0.1448914	1.125078	123.9915	155.1777	4.45	155.14	40.273	0.000	0.282
16.5	2.8034	-9.71E-02	0.1448914	1.125078	123.9915	155.1777	4.45	155.14	40.273	0.000	0.282
17.0	2.8332	-9.71E-02	0.1448914	1.125078	123.9915	155.186	4.45	155.14	40.273	0.000	0.282
17.5	2.8622	-9.71E-02	0.1448914	1.125746	123.9915	155.186	4.45	155.14	40.273	0.000	0.282
18.0	2.8904	-9.71E-02	0.1448914	1.126413	123.9915	155.186	4.45	155.14	40.273	0.000	0.282
18.5	2.9178	-9.71E-02	0.1442236	1.126413	123.9915	155.1943	4.19	155.12	40.274	-0.017	0.265
19.0	2.9444	-9.71E-02	0.1448914	1.126413	124.1052	155.2991	4.45	155.14	40.273	0.017	0.282
19.5	2.9704	-9.71E-02	0.1448914	1.126413	123.9915	155.1943	4.45	155.14	40.273	0.000	0.282
20.0	2.9957	-9.71E-02	0.1442236	1.126413	123.9915	155.1943	4.19	155.12	40.274	-0.017	0.265

Appendix 5: Porosity calculation

$$\Phi = \frac{Pore\ volume}{Bulk\ volume} = \frac{V_{bulk} - V_{matrix}}{V_{bulk}} = \frac{V_{bulk} - (W_{dry} / \rho_{matrix})}{V_{bulk}}$$

V_{bulk} = bulk volume of the sand pack

V_{matrix} = volume of dry sands

W_{dry} = total dry weight of the sands

ρ_{matrix} = mean density of the sands

Data available:

Weight of the cylinder with the needle probe (excluding stand and top holder)	8.14	kgs		
Weight of the stand	3.405	kgs		
Weight of the top holder of the cylinder	0.455	kgs		
Weight of the vessel with sands (excluding stand and top holder)	9.185	kgs		
Weight of the cylinder after sand evacuation	13.027	kgs		
Volume of water to saturate the pore	216	ml	0.0002	m^3
Weight of the cylinder after water saturation	13.245	kgs		
Specific gravity of Sand (SiO2 , CAS: 14808-60-7)	2.6			

Porosity calculation from pore volume method		
Inner dia	7.6	cm
Height of the vessel without caps	16.2	cm
Height left for compression	2.6	cm
Sand packed volume in the cylinder, V_{bulk}	617.0	cm^3
Bulk volume of the sand pack, V_{bulk}	0.000616959	m^3
Porosity (Φ)	**0.350**	

Appendix 6: Glycerol calibration calculation

Date Time"	Run Time (ms)	V+ wrt G	V- wrt G	Current	Probe TC	Cell1	Cell2	Cell3	Probe RTD	R1 100 ohm	R2 50 ohm	Calculations					
												ln(time)	delT	$Re_{current}$ =(U1-U2)/I (ohm)	Q $=I^2.Re_{current}$ (W/m)	4PI(T1-T2)	4PI(T1-T2)/Q
2:34:48 PM	0	0	0	0	23.963	1770	1770	23.167	23.939			0	0.024	10	1.1233	1.2566	1.1187
2:34:49 PM	1	1.203	2.351	-0.115	24.039	1770	1770	23.167	23.939			0.69	0.1	10	1.1233	9.3242	8.3005
2:34:50 PM	2	1.203	2.349	-0.115	24.681	1770	1770	23.167	23.939			1.1	0.742	10	1.1233	13.6094	12.1152
2:34:51 PM	3	1.202	2.349	-0.115	25.022	1770	1770	23.167	23.939			1.39	1.083	10	1.1233	15.5069	13.8044
2:34:52 PM	4	1.202	2.349	-0.115	25.173	1770	1770	23.198	23.939			1.61	1.234	10	1.1233	16.9269	15.0685
2:34:53 PM	5	1.201	2.347	-0.115	25.286	1770	1770	23.167	23.939			1.79	1.347	10	1.1233	16.9269	15.0685
2:34:54 PM	6	1.202	2.347	-0.115	25.286	1770	1770	23.167	23.939			1.95	1.347	10	1.1233	17.8819	15.9187
2:34:55 PM	7	1.201	2.346	-0.115	25.362	1770	1770	23.198	23.939			2.08	1.423	10	1.1233	18.3469	16.3326
2:34:56 PM	8	1.201	2.346	-0.115	25.399	1770	1770	23.198	23.939			2.2	1.46	10	1.1233	19.3019	17.1828
2:34:57 PM	9	1.201	2.347	-0.115	25.475	1770	1770	23.198	23.939			2.3	1.536	10	1.1233	19.7795	17.6079
2:34:58 PM	10	1.201	2.345	-0.115	25.513	1770	1770	23.167	23.939			2.4	1.574	10	1.1233	19.7795	17.6079
2:34:59 PM	11	1.201	2.346	-0.115	25.513	1770	1770	23.198	23.939			2.48	1.574	10	1.1233	20.2444	18.0218
2:35:00 PM	12	1.2	2.345	-0.115	25.55	1770	1770	23.198	23.939			2.56	1.611	10	1.1233	20.7219	18.4469
2:35:01 PM	13	1.199	2.344	-0.115	25.588	1770	1770	23.198	23.939			2.64	1.649	10	1.1233	20.7219	18.4469
2:35:02 PM	14	1.199	2.344	-0.115	25.588	1770	1770	23.198	23.939			2.71	1.649	10	1.1233	20.7219	18.4469
2:35:03 PM	15	1.2	2.345	-0.115	25.604	1770	1770	23.198	23.955			2.77	1.649	10	1.1233	21.1995	18.8720
2:35:04 PM	16	1.2	2.345	-0.115	25.642	1770	1770	23.167	23.955			2.83	1.687	10	1.1233	21.6770	19.2971
2:35:05 PM	17	1.199	2.344	-0.115	25.664	1770	1770	23.198	23.939			2.89	1.725	10	1.1039	21.6770	19.6371
2:35:06 PM	18	1.199	2.343	-0.114	25.664	1770	1770	23.198	23.939			2.94	1.725	10	1.1233	22.1545	19.7221
2:35:07 PM	19	1.198	2.343	-0.115	25.702	1770	1770	23.198	23.939			3	1.763	10	1.1039	22.1545	20.0697
2:35:08 PM	20	1.198	2.342	-0.114	25.702	1770	1770	23.198	23.939			3.04	1.763	10	1.1039	22.6195	20.4909
2:35:09 PM	21	1.199	2.342	-0.114	25.755	1770	1770	23.198	23.955			3.09	1.8	10	1.1039	22.6195	20.4909
2:35:10 PM	22	1.198	2.341	-0.114	25.739	1770	1770	23.198	23.939			3.14	1.8	10	1.1039	22.6195	20.4909
2:35:11 PM	23	1.198	2.34	-0.114	25.755	1770	1770	23.198	23.955			3.18	1.8	10	1.1039	23.0970	20.9235
2:35:12 PM	24	1.197	2.338	-0.114	25.777	1770	1770	23.198	23.939			3.22	1.838	10	1.1039	23.0970	20.9235
2:35:13 PM	25	1.197	2.338	-0.114	25.793	1770	1770	23.198	23.955			3.26	1.838	10	1.1039	23.0970	20.9235
2:35:14 PM	26	1.197	2.34	-0.114	25.793	1770	1770	23.198	23.955			3.3	1.838	10	1.1039	23.0970	20.9235
2:35:15 PM	27	1.197	2.341	-0.114	25.793	1770	1770	23.198	23.955								

2:35:16 PM	28	1.198	2.341	-0.114	25.793	1770	1770	23.198	23.955
2:35:17 PM	29	1.197	2.34	-0.114	25.831	1770	1770	23.198	23.955
2:35:18 PM	30	1.197	2.34	-0.114	25.831	1770	1770	23.198	23.955
2:35:19 PM	31	1.197	2.34	-0.114	25.831	1770	1770	23.198	23.955
2:35:20 PM	32	1.197	2.338	-0.114	25.869	1770	1770	23.198	23.955
2:35:21 PM	33	1.197	2.338	-0.114	25.869	1770	1770	23.198	23.955
2:35:22 PM	34	1.197	2.338	-0.114	25.869	1770	1770	23.198	23.955
2:35:23 PM	35	1.195	2.338	-0.114	25.906	1770	1770	23.198	23.955
2:35:24 PM	36	1.195	2.336	-0.114	25.906	1770	1770	23.198	23.955
2:35:25 PM	37	1.196	2.337	-0.114	25.906	1770	1770	23.198	23.955
2:35:26 PM	38	1.196	2.338	-0.114	25.906	1770	1770	23.198	23.955
2:35:27 PM	39	1.196	2.337	-0.114	25.906	1770	1770	23.198	23.955
2:35:28 PM	40	1.196	2.337	-0.114	25.944	1770	1770	23.198	23.955
2:35:29 PM	41	1.196	2.337	-0.114	25.944	1770	1770	23.198	23.955
2:35:30 PM	42	1.195	2.335	-0.114	25.944	1770	1770	23.198	23.955

3.33	1.838	10	1.1039	23.0970	20.9235
3.37	1.838	10	1.1039	23.5745	21.3560
3.4	1.876	10	1.1039	23.5745	21.3560
3.43	1.876	10	1.1039	23.5745	21.3560
3.47	1.876	10	1.1039	24.0520	21.7886
3.5	1.914	10	1.1039	24.0520	21.7886
3.53	1.914	10	1.1039	24.0520	21.7886
3.56	1.914	10	1.1039	24.5170	22.2098
3.58	1.951	10	1.1039	24.5170	22.2098
3.61	1.951	10	1.1039	24.5170	22.2098
3.64	1.951	10	1.1039	24.5170	22.2098
3.66	1.951	10	1.1039	24.5170	22.2098
3.69	1.951	10	1.1039	24.9945	22.6424
3.71	1.989	10	1.1039	24.9945	22.6424
3.74	1.989	10	1.1039	24.9945	22.6424

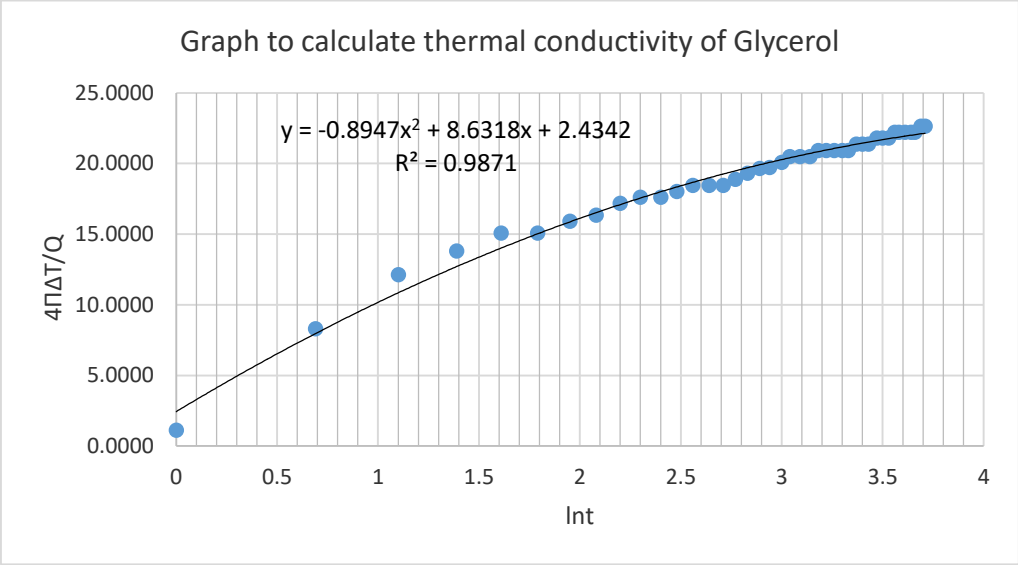

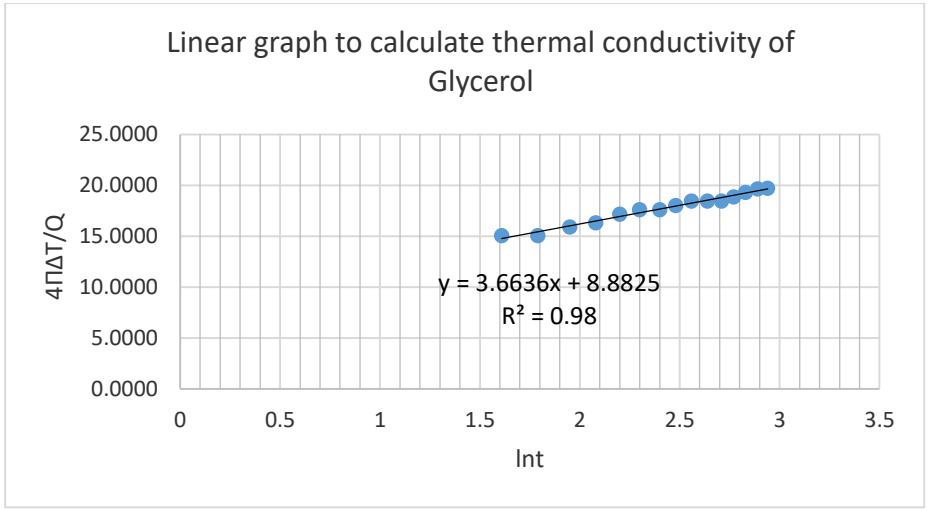

Slope of the graph 3.6636

k **0.27** **W/mK**

Appendix 7: Saturation calculation for bitumen-water saturated sand pack.

*Bitumen density is taken from the literature [62].

Total volume of the pores (water saturated pore volume)	216	ml
First day displaced water weight		
Initial weight of the beaker	299.2	gms
Weight of the pipeline	36.8	gms
Final Weight of the beaker with water	365.1	gms
Weight of the displaced water	65.9	gms
First level		
Initial weight of the beaker	299.2	gms
Final Weight of the beaker with water	427.6	gms
Weight of the displaced water	128.4	gms
Total weight of the displaced water	194.3	gms
Density of water at 70 C	0.998	gm/cm^3
Volume of displaced water= bitumen volume in pores	194.7	cm^3
Bitumen saturation in pores	**90.1**	%
Second level		
Initial weight of the beaker	155.7	gms
Weight of the pipeline	18.6	gms

Final Weight of the beaker with bitumen	171.7	gms
Weight of the beaker after 3 days	161.1	gms
Approximate weight of water in bitumen	10.6	gms
Weight of the displaced bitumen	5.4	gms
Volume of the pipeline	15.1	cm^3
Weight of the pipeline with bitumen	33.4	gms
Weight of bitumen in pipelines remaining	15.0	gms
Density of bitumen at 70 C	0.98	gm/cm^3
Weight of displaced bitumen	35.2	gm
Volume of bitumen displaced	35.91	cm^3
Initial volume of bitumen in the pores	194.7	cm^3
Bitumen volume in pores	158.8	cm^3
Bitumen saturation in pores	**73.5**	%

Third level calculation		
Initial weight of the beaker	272	gms
Weight of the pipeline	0	gms
Final Weight of the beaker with bitumen	284.1	gms
Weight of the displaced bitumen	12.08	gms
Weight displaced at level 2	5.4	gms
Total Weight displaced at level 2 including pipeline	35.19	gms
Weight of the pipeline with bitumen	0	gms
Density of bitumen at 70 C	0.98	gm/cm^3
Weight of bitumen displaced	41.87	gm

Volume of bitumen displaced	42.73	cm^3
Initial volume of bitumen in the pores	194.7	cm^3
Bitumen volume in pores	152	cm^3
Bitumen saturation in pores	**70.4**	%

Fourth level calculation		
Initial weight of the beaker	273.7	gms
Weight of the pipeline	0	gms
Final Weight of the beaker with bitumen	279.1	gms
Weight of the displaced bitumen	5.408	gms
Weight of the bitumen displaced till level 3	41.87	gms
Weight of the pipeline with bitumen	0	gms
Density of bitumen at 70 C	0.98	gm/cm^3
Weight of bitumen displaced till level 4	47.28	gm
Volume of bitumen displaced	48.25	cm^3
Initial volume of bitumen in the pores	194.7	cm^3
Bitumen volume in pores	146.4	cm^3
Bitumen saturation in pores	**68**	%

Fifth level calculation		
Initial weight of the beaker day 1	326.7	gms
Weight of the pipeline	54.3	gms
Final Weight of the beaker with bitumen day 1	329.6	gms

Weight of the displaced bitumen	2.943	gms
Initial weight of beaker day 2	0	gms
Final weight of beaker day 2	0	gms
Weight of the bitumen displaced till level 5	80.34	gms
Weight of the pipeline with bitumen	61	gms
Weight of bitumen in the outlet base (below outlet pipe)	0	gms
Density of bitumen at 70 C	0.98	gm/cm^3
Weight of bitumen displaced till now	89.08	gm
Volume of bitumen displaced	90.9	cm^3
Initial volume of bitumen in the pores	194.7	cm^3
Bitumen volume in pores	103.8	cm^3
Bitumen saturation in pores	**48.1**	%

Appendix 8: Saturation calculation for bitumen, water and nitrogen saturated sands

Total volume of the pores (water saturated pore volume)	216	ml

First level calculation

Saturated bitumen volume in sand pack	194.7	cm^3
Weight of Bitumen from last setup inside the pores	89.08	gm
Density of bitumen at 70 C	0.98	gm/cm^3
Volume of bitumen inside pores in last setup	90.9	cm^3
Start volume of pump	507.3	ml
End volume of pump	400	ml
Total bitumen injected into the system	107.3	ml
Empty weight of the production beaker	135	gm
Weight of beaker with bitumen	143.9	gm
Empty weight of the production line	54.3	gm
Weight of the production line including bitumen	58.6	gm
Weight of water in bitumen	8	gm
Total bitumen ejected out of the system	13.2	gm
Total bitumen sent inside the system	86.1	gm
Present weight of bitumen inside pores	191.7	gm
Present volume of bitumen inside pores	195.6	cm^3
Bitumen saturation in pores	**90.6**	%
Water saturation in pores	**9.4**	%
Nitrogen saturation in pores	**0**	%

Second level calculation

Saturated bitumen volume in sand pack	195.6	cm^3
Empty weight of the production beaker	155.7	gm
Weight of beaker with bitumen	175.6	gm
Empty weight of the production line	50	gm
Weight of the production line including bitumen	77	gm
Weight of displaced volume of bitumen	46.9	gm
Density of bitumen at 70 C	0.98	gm/cm^3
Volume of displaced bitumen= Volume of Nitrogen inside pores	47.86	cm^3
Weight of water in bitumen	20.38	gm
Bitumen saturation in pores	**67.8**	%
NCG saturation in pores	**22.8**	%
Water saturation in pores	**9.4**	%

Third level calculation

Saturated bitumen volume in sand pack	195.6	cm^3
Empty weight of the production beaker with bitumen	155.7	gm
Weight of beaker with bitumen	216	gm
Empty weight of the production line	50	gm
Weight of the production line including bitumen	77	gm
Weight of displaced volume of bitumen till now	60.3	gm

Density of bitumen at 70 C	0.98	gm/cm^3
Volume of displaced bitumen= Volume of Nitrogen inside pores	61.53	cm^3
Weight of water in bitumen	20.38	gm
Bitumen saturation in pores	**62.3**	%
NCG saturation in pores	**28.3**	%
Water saturation in pores	**9.4**	%

Fourth level calculation

Saturated bitumen volume in sand pack	195.6	cm^3
Empty weight of the production beaker with bitumen	155.7	gm
Weight of beaker with bitumen	249.7	gm
Empty weight of the production line	50	gm
Weight of the production line including bitumen	77	gm
Weight of displaced volume of bitumen till now	94	gm
Density of bitumen at 70˚C	0.98	gm/cm^3
Volume of displaced bitumen= Volume of Nitrogen inside pores	95.92	cm^3
Weight of water in bitumen	20.38	gm
Bitumen saturation in pores	**46.0**	%
NCG saturation in pores	**44.6**	%
Water saturation in pores	**9.4**	%

Fifth level calculation

Saturated bitumen volume in sand pack	195.6	cm^3
Empty weight of the production beaker with bitumen	155.7	gm
Weight of beaker with bitumen	278	gm
Empty weight of the production line	50	gm
Weight of the production line including bitumen	77	gm
Weight of displaced volume of bitumen till now	122.3	gm
Density of bitumen at 70˚ C	0.98	gm/cm^3
Volume of displaced bitumen= Volume of Nitrogen inside pores	124.8	cm^3
Weight of water in bitumen	20.38	gm
Bitumen saturation in pores	**32.8**	%
NCG saturation in pores	**57.8**	%
Water saturation in pores	**9.4**	%

Appendix 9: Saturation calculation for bitumen, nitrogen and surfactant saturated sands.

First level calculation

Saturation of Bitumen from last setup inside the pores	**32.8**	%
Saturated bitumen volume in sand pack	**70.8**	cm^3
Density of bitumen at 70˚C	0.98	gm/cm^3
Start volume of pump	466.6	ml
End volume of pump	446.6	ml
Total surfactant injected into the system	20	ml
Empty weight of the production beaker	135	gm
Weight of beaker with bitumen	135	gm
Empty weight of the production line	54.3	gm
Weight of the production line including bitumen	54.3	gm
Volume of water in sand pack	20.38	cm^3
Total bitumen ejected out of the system	0	gm
Present volume of nitrogen inside pores	104.8	cm^3
Nitrogen saturation in pores	**48.5**	%

Results

Bitumen saturation in pores	**32.8**	%
Nitrogen saturation in pores	**48.5**	%
Surfactant solution saturation in pores	**18.7**	%

Second level calculation

Saturation of Bitumen from last setup inside the pores	**32.8**	%
Saturated bitumen volume in sand pack	**70.8**	cm^3
Density of bitumen at 70 C	0.98	gm/cm^3
Start volume of pump	446.6	ml
End volume of pump	426.6	ml
Total surfactant injected into the system	40.0	ml
Empty weight of the production beaker	135	gm
Weight of beaker with bitumen	135	gm
Empty weight of the production line	54.3	gm
Weight of the production line including bitumen	54.3	gm
Volume of water in sand pack	20.38	cm^3
Total bitumen ejected out of the system	0	gm
Present volume of nitrogen inside pores	84.8	cm^3
Nitrogen saturation in pores	**39.3**	%

Results

Bitumen saturation in pores	**32.8**	%
Nitrogen saturation in pores	**39.3**	%
Surfactant solution saturation in pores	**28.0**	%

Third level calculation

Saturation of Bitumen from last setup inside the pores	**32.8**	%
Saturated bitumen volume in sand pack	**70.8**	cm^3
Density of bitumen at 70 C	0.98	gm/cm^3
Start volume of pump	426.6	ml
End volume of pump	406.6	ml
Total surfactant injected into the system	60.0	ml
Empty weight of the production beaker	135	gm
Weight of beaker with bitumen	135	gm
Empty weight of the production line	54.3	gm
Weight of the production line including bitumen	54.3	gm
Volume of water in sand pack	20.38	cm^3
Total bitumen ejected out of the system	0	gm
Present volume of nitrogen inside pores	64.8	cm^3
Nitrogen saturation in pores	**30.0**	%

Results

Bitumen saturation in pores	**32.8**	%
Nitrogen saturation in pores	**30.0**	%
Surfactant solution saturation in pores	**37.2**	%

Fourth level calculation

Saturation of Bitumen from last setup inside the pores	**32.8**	%
Saturated bitumen volume in sand pack	**70.8**	cm^3
Density of bitumen at 70 C	0.98	gm/cm^3
Start volume of pump	406.6	ml
End volume of pump	386.5	ml
Total surfactant injected into the system	80.1	ml
Empty weight of the production beaker	135	gm
Weight of beaker with bitumen	135	gm
Empty weight of the production line	54.3	gm
Weight of the production line including bitumen	54.3	gm
Volume of water in sand pack	20.4	cm^3
Total bitumen ejected out of the system	0	gm
Present volume of nitrogen inside pores	44.7	cm^3
Nitrogen saturation in pores	**20.7**	%

Results

Bitumen saturation in pores	**32.8**	%
Nitrogen saturation in pores	**20.7**	%
Surfactant solution saturation in pores	**46.5**	%

Fifth level calculation

Saturation of Bitumen from last setup inside the pores	**32.8**	%
Saturated bitumen volume in sand pack	**70.8**	cm^3
Density of bitumen at 70 C	0.98	gm/cm^3
Start volume of pump	386.5	ml
End volume of pump	379	ml
Total surfactant injected into the system	87.6	ml
Empty weight of the production beaker	135	gm
Weight of beaker with bitumen	135	gm
Empty weight of the production line	54.3	gm
Weight of the production line including bitumen	54.3	gm
Volume of water in sand pack	20.38	cm^3
Total bitumen ejected out of the system	0	gm
Present volume of nitrogen inside pores	37.2	cm^3
Nitrogen saturation in pores	**17.2**	%

Results

Bitumen saturation in pores	**32.8**	%
Nitrogen saturation in pores	**17.2**	%
Surfactant solution saturation in pores	**50.0**	%

Sixth level calculation

Saturation of Bitumen from last setup inside the pores	**32.8**	%
Saturated bitumen volume in sand pack	**70.8**	cm^3
Density of bitumen at 70 C	0.98	gm/cm^3
Empty weight of the production beaker	139.7	gm
Weight of beaker with displaced product	186	gm
Empty weight of the production line	54.3	gm
Weight of the production line including sample	54.3	gm
Saturation of irreducible water in sand pack	**9.43**	%
Volume of water in sand pack	20.38	cm^3
Total product ejected out of the system	46.3	gm
Bitumen% in product	3	%
Surfactant% in product	97	%
Weight of Bitumen displaced	1.389	gm
Weight of Surfactant displaced	44.91	gm
Density of surfactant (9.4299 lbs/gal @ 25°C)	9.43	lbs/gal
Total surfactant volume ejected out of the system	39.74	cm^3
Total bitumen volume ejected out of the system	1.417	cm^3
Present volume of bitumen inside the pores	69.4	cm^3
Present volume of nitrogen inside pores	86.5	cm^3
Nitrogen saturation in pores	**40.0**	%

Results

Bitumen saturation in pores	**32.1**	%
Nitrogen saturation in pores	**40.0**	%
Surfactant solution saturation in pores	**27.8**	%

Seventh level calculation

Saturation of Bitumen from last setup inside the pores	**32.1**	%
Saturated bitumen volume in sand pack	**69.4**	cm^3
Density of bitumen at 70 C	0.98	gm/cm^3
Weight of the production beaker from last level	186	gm
Weight of beaker with displaced product	217.6	gm
Empty weight of the production line	54.3	gm
Weight of the production line including sample	54.3	gm
Volume of water in sand pack	20.38	cm^3
Total product ejected out of the system	31.6	gm
Bitumen% in product	3	%
Surfactant% in product	97	%
Weight of Bitumen displaced	0.948	gm
Weight of Surfactant displaced	30.65	gm
Density of surfactant (9.4299 lbs/gal @ 25°C)	9.43	lbs/gal
Total surfactant volume ejected out of the system	27.13	cm^3
Total bitumen volume ejected out of the system	0.967	cm^3

Present volume of bitumen inside the pores	68.4	cm^3
Present volume of nitrogen inside pores	100.1	cm^3
Nitrogen saturation in pores	**46.3**	%

Results

Bitumen saturation in pores	**31.7**	%
Nitrogen saturation in pores	**46.3**	%
Surfactant solution saturation in pores	**22.0**	%

Eighth level calculation

Saturation of Bitumen from last setup inside the pores	**31.7**	%
Saturated bitumen volume in sand pack	**68.4**	cm^3
Density of bitumen at 70 C	0.98	gm/cm^3
Weight of the production beaker from last level	217.6	gm
Weight of beaker with displaced product	228.6	gm
Empty weight of the production line	54.3	gm
Weight of the production line including sample	54.3	gm
Volume of water in sand pack	20.38	cm^3
Total product ejected out of the system	11	gm
Bitumen% in product	1	%
Surfactant% in product	99	%
Weight of Bitumen displaced	0.11	gm

Weight of Surfactant displaced	10.89	gm
Density of surfactant (9.4299 lbs/gal @ 25°C)	9.43	lbs/gal
Total surfactant volume ejected out of the system	9.637	cm^3
Total bitumen volume ejected out of the system	0.112	cm^3
Present volume of bitumen inside the pores	68.3	cm^3
Present volume of nitrogen inside pores	117.7	cm^3
Nitrogen saturation in pores	**54.5**	%

Results

Bitumen saturation in pores	**31.6**	%
Nitrogen saturation in pores	**54.5**	%
Surfactant solution saturation in pores	**13.9**	%

Appendix 10: LoggerNet software raw file

TOA5	CR1000	CR1000	91635	CR1000.Std.32.03	CPU:tpsys v0908-2.CR1	30531	RawData			
TIMESTAMP	RECORD	Exp_Id	Re	time	I_heat	U_sen	U_cold	Pt_1000	T_hot	T_cold
TS	RN		Ohm/m	Sec	A	mV	mV	Deg C	Deg C	
		Smp	Smp	Smp	Smp	Smp	Smp	Smp	Smp	Smp
55:25.5	52807	644	84.28	-20	0	0.13	1.13	124	154.9	151.49
2019-12-04 20:55	52808	644	84.28	-19.5	-6.68E-08	0.13	1.13	124	154.9	151.5
55:26.5	52809	644	84.28	-19	-6.68E-08	0.13	1.13	124	154.9	151.53
2019-12-04 20:55	52810	644	84.28	-18.5	0	0.13	1.13	124	154.9	151.48
55:27.5	52811	644	84.28	-18	-6.68E-08	0.13	1.13	124	154.9	151.48
2019-12-04 20:55	52812	644	84.28	-17.5	0	0.13	1.13	124	154.9	151.48
55:28.5	52813	644	84.28	-17	0	0.13	1.12	124	154.9	151.48
2019-12-04 20:55	52814	644	84.28	-16.5	0	0.13	1.13	124	154.9	151.47
55:29.5	52815	644	84.28	-16	-6.68E-08	0.13	1.13	124	154.9	151.47
2019-12-04 20:55	52816	644	84.28	-15.5	0	0.13	1.12	124	154.9	151.46
55:30.5	52817	644	84.28	-15	0	0.13	1.12	124	154.9	151.47
2019-12-04 20:55	52818	644	84.28	-14.5	0	0.13	1.12	124	154.9	151.46
55:31.5	52819	644	84.28	-14	-6.68E-08	0.13	1.12	124	154.9	151.46
2019-12-04 20:55	52820	644	84.28	-13.5	0	0.13	1.12	124	154.9	151.46
55:32.5	52821	644	84.28	-13	0	0.13	1.12	124	154.9	151.46
2019-12-04 20:55	52822	644	84.28	-12.5	-6.68E-08	0.13	1.12	124	154.9	151.46

TOA5	CR1000	CR1000	91635	CR1000.Std.32.03	CPU:tpsysv0908-2.CR1	30531	RawData			
TIMESTAMP	RECORD	Exp_Id	Re	time	I_heat	U_sen	U_cold	Pt_1000	T_hot	T_cold
TS	RN		Ohm/m	Sec	A	mV	mV	Deg C	Deg C	
		Smp	Smp	Smp	Smp	Smp	Smp	Smp	Smp	Smp
55:33.5	52823	644	84.28	-12	0	0.13	1.12	124	154.9	151.46
2019-12-04 20:55	52824	644	84.28	-11.5	-6.68E-08	0.13	1.12	124	154.9	151.48
55:34.5	52825	644	84.28	-11	0	0.13	1.12	124	154.9	151.46
2019-12-04 20:55	52826	644	84.28	-10.5	-6.68E-08	0.13	1.12	124	154.9	151.46
55:35.5	52827	644	84.28	-10	0	0.14	1.13	124	154.9	151.49
2019-12-04 20:55	52828	644	84.28	-9.5	0	0.13	1.12	124	154.9	151.46
55:36.5	52829	644	84.28	-9	0	0.13	1.12	124.1	155	151.57
2019-12-04 20:55	52830	644	84.28	-8.5	0	0.13	1.12	124	154.9	151.46
55:37.5	52831	644	84.28	-8	0	0.13	1.12	124	154.9	151.46
2019-12-04 20:55	52832	644	84.28	-7.5	0	0.13	1.12	124	154.9	151.46
55:38.5	52833	644	84.28	-7	-6.68E-08	0.13	1.13	124	154.9	151.49
2019-12-04 20:55	52834	644	84.28	-6.5	0	0.13	1.12	124	154.9	151.46
55:39.5	52835	644	84.28	-6	-6.68E-08	0.13	1.12	124	154.9	151.46
2019-12-04 20:55	52836	644	84.28	-5.5	0	0.13	1.12	124	154.9	151.46
55:40.5	52837	644	84.28	-5	-6.68E-08	0.13	1.12	124.1	155	151.58
2019-12-04 20:55	52838	644	84.28	-4.5	-6.68E-08	0.13	1.12	124	154.9	151.46
55:41.5	52839	644	84.28	-4	0	0.13	1.12	124	154.9	151.46
2019-12-04 20:55	52840	644	84.28	-3.5	-6.68E-08	0.13	1.12	124	154.9	151.46
55:42.5	52841	644	84.28	-3	-6.68E-08	0.13	1.12	124	154.9	151.49

TOA5	CR1000	CR1000	91635	CR1000.Std.32.03	CPU:tpsysv0908-2.CR1	30531	RawData			
TIMESTAMP	RECORD	Exp_Id	Re	time	I_heat	U_sen	U_cold	Pt_1000	T_hot	T_cold
TS	RN		Ohm/m	Sec	A	mV	mV	Deg C	Deg C	
		Smp	Smp	Smp	Smp	Smp	Smp	Smp	Smp	Smp
2019-12-04 20:55	52842	644	84.28	-2.5	-6.68E-08	0.13	1.12	124	154.9	151.46
55:43.5	52843	644	84.28	-2	-6.68E-08	0.13	1.12	124	154.9	151.46
2019-12-04 20:55	52844	644	84.28	-1.5	-6.68E-08	0.13	1.12	124	154.9	151.46
55:44.5	52845	644	84.28	-1	0	0.13	1.12	124.1	155	151.58
2019-12-04 20:55	52846	644	84.28	-0.5	0	0.13	1.12	124	154.9	151.46
55:45.5	52847	644	84.28	0	0	0.13	1.12	124	154.9	151.46
2019-12-04 20:55	52848	644	84.28	0.5	-0.09708	0.13	1.12	124	154.9	151.5
55:46.5	52849	644	84.28	1	-0.09708	0.14	1.12	124	155	151.49
2019-12-04 20:55	52850	644	84.28	1.5	-0.09708	0.14	1.12	124	155.1	151.5
55:47.5	52851	644	84.28	2	-0.09708	0.14	1.12	124	155.1	151.49
2019-12-04 20:55	52852	644	84.28	2.5	-0.09708	0.14	1.12	124	155.1	151.49
55:48.5	52853	644	84.28	3	-0.09708	0.14	1.12	124.1	155.2	151.6
2019-12-04 20:55	52854	644	84.28	3.5	-0.09708	0.14	1.12	124	155.1	151.5
55:49.5	52855	644	84.28	4	-0.09708	0.14	1.12	124	155.2	151.48
2019-12-04 20:55	52856	644	84.28	4.5	-0.09708	0.14	1.12	124	155.2	151.5
55:50.5	52857	644	84.28	5	-0.09715	0.14	1.13	124	155.2	151.51
2019-12-04 20:55	52858	644	84.28	5.5	-0.09708	0.14	1.12	124	155.2	151.5
55:51.5	52859	644	84.28	6	-0.09711	0.14	1.12	124	155.2	151.49

TOA5	CR1000	CR1000	91635	CR1000.Std.32.03	CPU:tpsysv0908-2.CR1	30531	RawData			
TIMESTAMP	RECORD	Exp_Id	Re	time	I_heat	U_sen	U_cold	Pt_1000	T_hot	T_cold
TS	RN		Ohm/m	Sec	A	mV	mV	Deg C	Deg C	
		Smp	Smp	Smp	Smp	Smp	Smp	Smp	Smp	Smp
2019-12-04 20:55	52860	644	84.28	6.5	-0.09715	0.14	1.12	124	155.2	151.49
55:52.5	52861	644	84.28	7	-0.09715	0.14	1.13	124.1	155.3	151.59
2019-12-04 20:55	52862	644	84.28	7.5	-0.09715	0.14	1.12	124	155.2	151.49
55:53.5	52863	644	84.28	8	-0.09715	0.14	1.12	124	155.2	151.49
2019-12-04 20:55	52864	644	84.28	8.5	-0.09715	0.14	1.12	124.1	155.3	151.6
55:54.5	52865	644	84.28	9	-0.09715	0.14	1.12	124	155.2	151.46
2019-12-04 20:55	52866	644	84.28	9.5	-0.09715	0.14	1.12	124	155.2	151.49
55:55.5	52867	644	84.28	10	-0.09715	0.14	1.12	124	155.2	151.48
2019-12-04 20:55	52868	644	84.28	10.5	-0.09715	0.14	1.13	124	155.2	151.49
55:56.5	52869	644	84.28	11	-0.09715	0.14	1.12	124	155.2	151.49
2019-12-04 20:55	52870	644	84.28	11.5	-0.09715	0.14	1.12	124	155.2	151.49
55:57.5	52871	644	84.28	12	-0.09715	0.14	1.13	124	155.2	151.49
2019-12-04 20:55	52872	644	84.28	12.5	-0.09715	0.14	1.13	124	155.2	151.49
55:58.5	52873	644	84.28	13	-0.09715	0.14	1.13	124	155.2	151.49
2019-12-04 20:55	52874	644	84.28	13.5	-0.09715	0.14	1.13	124.1	155.3	151.6
55:59.5	52875	644	84.28	14	-0.09715	0.14	1.13	124	155.2	151.48
2019-12-04 20:56	52876	644	84.28	14.5	-0.09715	0.14	1.13	124	155.2	151.49
56:00.5	52877	644	84.28	15	-0.09715	0.14	1.13	124	155.2	151.48

TOA5	CR1000	CR1000	91635	CR1000.Std.32.03	CPU:tpsysv0908-2.CR1	30531	RawData			
TIMESTAMP	RECORD	Exp_Id	Re	time	I_heat	U_sen	U_cold	Pt_1000	T_hot	T_cold
TS	RN		Ohm/m	Sec	A	mV	mV	Deg C	Deg C	
		Smp	Smp	Smp	Smp	Smp	Smp	Smp	Smp	Smp
2019-12-04 20:56	52878	644	84.28	15.5	-0.09715	0.14	1.13	124	155.2	151.49
56:01.5	52879	644	84.28	16	-0.09715	0.14	1.13	124	155.2	151.48
2019-12-04 20:56	52880	644	84.28	16.5	-0.09715	0.14	1.13	124	155.2	151.49
56:02.5	52881	644	84.28	17	-0.09715	0.14	1.13	124	155.2	151.48
2019-12-04 20:56	52882	644	84.28	17.5	-0.09715	0.14	1.13	124	155.2	151.48
56:03.5	52883	644	84.28	18	-0.09715	0.14	1.13	124	155.2	151.48
2019-12-04 20:56	52884	644	84.28	18.5	-0.09715	0.14	1.13	124	155.2	151.48
56:04.5	52885	644	84.28	19	-0.09715	0.14	1.13	124.1	155.3	151.59
2019-12-04 20:56	52886	644	84.28	19.5	-0.09715	0.14	1.13	124	155.2	151.48
56:05.5	52887	644	84.28	20	-0.09715	0.14	1.13	124	155.2	151.47